Modern human brain growth and development.

Contribution to brain evolution in hominids.

Dissertation

zur

Erlangung der naturwissenschaftlichen Doktorwürde

(Dr. sc. nat.)

vorgelegt der

Mathematisch-naturwissenschaftlichen Fakultät

der

Universität Zürich

-

Muséum National d'Histoire Naturelle, Paris, France

von

Fernando Ventrice

von/aus

Argentinien

Promotionskomitee

Prof. Dr. Christoph P. E. Zollikofer

Dr. Fernando V. Ramírez-Rozzi

Dr. Dean Falk

Dr. Katerina Semendeferi

Zürich, 2011

To my wife and the little child she carries.

Acknowledgments

Following my schematic way of thinking, I will mention in a possibly strange order all the people that supported and helped me so much in the realization of this PhD thesis.

My two directors... Fernando Ramírez-Rozzi, my "heterochronic mentor", helped me to develop my ideas and mature them into this work. He also contacted me with Christoph Zollikofer, who assisted me with the difficult task of understanding geometric morphometrics and introduced me to the programming world.

My wife... Ana Tropea, because she was the person that suffered and enjoyed (but mostly suffered) with me all these years through the thesis construction, and always offered me all her support.

At Paris... I am very grateful to my workmates of the laboratory UPR 2147: "Dynamique de l'Évolution Humaine", who gave me a very stimulating place to work and think. Especially to Anne-Marie Guihard-Costa, who trusted me and helped me in every possible way through all the comings and goings of these years.

At Zurich... All my workmates of the Anthropological Institute made me feel at home. I enjoyed stimulating discussions in every meal with my laboratory mates of the University

of Zurich. In particular, Renaud Lebrun helped me with his algorithm implementations on the MorphoTools software.

At Buenos Aires... I am very thankful to the staff of the nonprofit organization: "Fundación para la Lucha contra las Enfermedades Neurológicas de la Infancia" (FLENI) in Argentina for letting me access to the Computed Tomographic (CT) and Magnetic Resonance (MR) Scanner, for their permission to work with FLENI's medical image data base, and for their constant support in every technical aspect regarding the specific data bases constructed in this PhD. Silvia Vazquez made all this possible by her faith in my work. I musk thank Carolina Tropea, who worked very hard to transform the initial thesis manuscript in an almost painless English readable text.

The Alβan programme... And finally, this thesis could not have been done without the financial support awarded by the Alβan programme during these years of hard work.

Contents

List of Figures

List of Tables

Abstract

Human phylogenetic history is directly related to brain evolution. But many biologic processes related to the appearance of this complex organ are unknown, mainly due to the fact that it is an organ composed of soft tissue, which is not sensitive to the fossilization processes. Hence, to infer human brain evolution it is essential to study the indirect evidences it leaves in the cranial bones, such as the endocranial size (cranial capacity) and shape. In this sense, the hominid fossil record has an important cranial representation in relation to other bones. However, in order to interpret the information the cranium provides about the brain it shelter and infer evolutive theories, it is vital to understand the relationship between the brain and the endocranial vault.

In this PhD, modern human endocranium and brain growth and development will be characterized from a morphometric point of view, with the aim of defining how these two structures interact and correlate throughout maturation from birth to adulthood. This body of knowledge will be applied to enlighten our interpretations of the different indirect evidences we have about the human brain evolution. In this way, the present thesis research will not only contribute to our understanding of brain evolution in the human lineage, but it will also assist future medical research that investigate human brain and cranial growth and development trajectories.

In order to answer these questions two data bases were created: one of them consisting

of computed tomographic (CT) images to study bone structure maturation, and the other one consisting of magnetic resonance (MR) images to quantify ontogenetic changes in the soft brain tissue. These data bases contain individuals in a range from birth to the age of 31. The data was analysed by means of geometric morphometric techniques, which allow the statistic separation of size and shape changes throughout ontogeny, in this particular case.

The results showed that the brain and endocranium present a close ontogenetic relationship from birth to the first adolescence (approximately to the age of 10 in females and 12.5 in males). From this time onwards the brain starts loosing volume (mainly gray matter due to neuronal rearrangements), and therefore, the close relationship between brain cortex and endocranial vault gradually diminishes, at the same time that the brain modifies its shape. For this reason, brain shape changes from adolescence onwards are not reflected in endocranial regions. An important contribution was the construction of accurate and precise brain / endocranial volume (BV/ECV) ratio formulas dependent of sex, age and endocranial size, which may serve to extract better information from cranial data. A third main subject of this PhD was the study of asymmetric patterns in both brain and endocranium. In this sense, it was shown that the brain macroscopic asymmetries and the endocranial petal pattern are not the same for the different periods analysed, and they even change their trajectories through ontogeny. Hence, the adult asymmetric patterns are not the same than in the sub-adults. Finally, sexual dimorphism was investigated in both structures, and the characterization of growth and development divergences between females and males could be done through heterochonic processes.

Growth and development of the brain and its surrounding bony endocranial tissue

could be characterized in the human species, with the aid of 3D medical images and new geometric morphometric techniques specially developed for this study. New information about the ontogenetic relationship between these two structures was discovered, constituting an important tool that will enlighten human studies about brain evolution.

Chapter 1

Introduction

The human brain is a very complex organ that presents several unsolved enigmas, its evolution being perhaps the most intriguing one. This topic is deeply related to the evolution of our own species, and that is the reason why several paleoanthropologists are trying at present to understand the process that gave origin to human brain. Unfortunately, this organ is formed by soft tissue, which is not sensitive to the fossilization process. Therefore, we must deal with indirect evidences to infer brain evolution from the fossil record: the well known cranial capacity; the *impressiones gyrorum* of the different brain gyri and sulci (*i.e.* lunate sulcus, perisylvian asymmetries); the petalia patterns; and the anatomical compared studies on brains of extant primates (Holloway, 1996; Semendeferi et al., 1997; Falk, 2006; Schoenemann, 2006). Consequently, the fossil record provides only endocranial information. To better understand the clues provided by this information on human brain evolution, it is essential to determine the existing relationship between the brain and the endocranium, and how this relationship develops throughout the maturation process in our species.

The debate about the amount of information that could be extracted from endocast

examination was initiated by Symington (1916). He prepared and studied a great number of endocranial, endodural, arachnoid, and brain casts of recent man to ascertain the extent to which the inner surface of the cranial wall is moulded by the underlying surface of the brain. His conclusions were precise and absolute: "... a cast may considerably differ both in size and form from the brain itself. (...) the simplicity or complexity of the cerebral fissures and convolutions cannot be determined with any degree of accuracy from endocranial casts, even on complete skulls, much less on reconstructions from imperfect skulls." In his work he criticized as highly speculative and fallacious the conclusions about brain anatomy from endocast examination reached in several contemporary studies (Dubois, 1899; Boule and Anthony, 1911; Anthony, 1913; Smith, 1913). Clark et al. (1936) also investigated this question through the analysis of chimpanzee endocasts. The authors constructed endocasts from skulls and compared them with the corresponding chimpanzee brains, and arrived at equally pessimistic conclusions regarding the reliability of chimpanzee endocasts as replicators of sulcal patterns: "The preceding account shows that very little information about sulcal pattern can be extracted from the majority of our endocranial casts of the chimpanzee." Connolly (1950) also compared endocasts with their corresponding ape and human brains and he also concluded that endocasts do not reproduce many details of hominoid sulcal patterns. Finally, Falk (1980), who frequently used latex endocasts to investigate sulcal patterns of primates and fossil anthropoids, stated that: "... latex endocasts prepared from selected prosimian and monkey skulls reproduce clear sulcal patterns; endocasts prepared from pongid and human skulls (even if carefully selected) do not." This poor reproduction of brain surface features observed in pongid and human endocasts was explained by Holloway (1974), who hypothesized

that the relatively thick meningeal structures situated between the brain and the skull of hominoids could be the cause of this information loss. Nowadays, this debate was left aside and in many studies endocranial landmarks are used as indicators of brain structures (Bruner, 2004, 2008; Bruner and Holloway, 2010; Bruner, 2010). In a recent work (Neubauer et al., 2010) it was stated that: "Endocasts - imprints of the brain and the surrounding tissues into the internal table of cranial bones - can serve as proxies for brain morphology". Although this approach might be the only possible one to address hominid brain evolutionary questions, brain and endocranial relationship must be better characterized and understood to determine the information the bony endocranium can provide about the brain. For this reason, in this thesis five main questions about this relationship will be investigated in the human species: First, (1) the relationship between brain and endocranial volume will be studied; to be able to measure this relationship, (2) brain and endocranial growth curves will be defined; then (3) the shape covariation between brain and endocranium throughout development will be established; next, (4) the asymmetric patterns in both structures will be described; and finally, (5) the dimorphic differences between sexes for all these parameters will be quantified.

Brain / endocranial volume relationship (BV / ECV)

One of the most studied and well known indirect evidences of hominid brain evolution is cranial capacity. The pattern followed by this parameter throughout the fossil record shows that there was an absolute increment of the ECV in the last 3 millions years (Holloway et al., 2004; Schoenemann, 2006; Falk, 2006). Considering the different hominid species as different branches of a complex evolutive bush (Stringer, 2001), it is evident that this ECV increase was not an isolated phenomenon, but arose in different terminal

branches (Elton et al., 2001). This would imply that the encephalization phenomenon was not specific to our own lineage; it may have occurred independently in different hominid species, under distinct selective pressures. However, it is important to be cautious and these allegations should be put in relief, because we are referring to an increase in absolute ECV, with no correction for total body size (Jerison, 1973). Although this discussion about absolute and relative ECV measurements is still an open debate (Holloway, 1966; Kappelman, 1996; Ruff et al., 1997; Rightmire, 2004; Spocter and Manger, 2007), it has been claimed that at a behavioral level the absolute ECV *per se* can be much more relevant within a closely related lineage (Schoenemann, 2006). Another aspect that deserves some attention is the fact that we are measuring ECV and not the actual BV. The latter is much smaller than the former, due to fluids, vessels, blood and the connective tissue membranes (meninges) that cover the brain. Hofman (1983) stated that BV equals 95% of ECV; however, this ratio was criticized and it was suggested that cerebrospinal fluid represents almost 12% of ECV (Peters et al., 1998), with the BV representing in consequence less than 88% of the ECV. Another obstacle is the fact that we ignore the BV/ECV ratio in other non-human primates. This ratio is thought to be inversely correlated to the total cranium size (Connolly, 1950); hence, smaller species with smaller crania will have larger BV/ECV ratios. For this reason, it is essential to reevaluate the BV/ECV relation in humans in order to understand better the ECV values found in the hominid fossil record. However, to be able to analyse ECV and BV relationship through maturation, their normal growth curves must be first well established.

Brain maturation growth curves

The first studies about brain growth date back to the '80s and focused on the qualitative description of gray and white matter during the first 2 years of life (Levene et al., 1982; Johnson and Bydder, 1984; Holland, 1986; McArdle et al., 1987; Barkovich et al., 1988). During the first 6 months, using conventional sequences of magnetic resonance (MR) imaging techniques, the intensities of gray and white matter are inverted with respect to the adult pattern (that is to say, the gray matter appears clearer than the white matter). From 6 to 12 months old a gradual transition is developed towards the adult pattern, during which it is not possible to differentiate between gray and white matter. This phenomenon is thought to be related to water loss in both tissues, followed by the development of the macromolecular mielin precursors and the mielin itself (Inder and Huppi, 2000; Paus et al., 2001). The general growth pattern found consists of the white matter volume (WMV) increasing and the gray matter volume (GMV) decreasing throughout maturation (Jernigan and Tallal, 1990; Reiss et al., 1996; Schaefer et al., 1990). A more recent study (Giedd et al., 1999) analysed individuals from 4 to 22 years old and confirmed the almost lineal WMV increment, but demonstrated non-lineal changes for the GMV. The latter followed an "inverted U" growth curve, with different maximum peaks for the different brain lobules. On the other hand, the total brain volume (BV) reaches 90% of its maximum value approximately at an age of 5 (Lenroot and Giedd, 2006) and 95% at the age of 6, with a maximum peak at 14.5 years old for males and 11.5 years old for females (Giedd et al., 1999). This information is consistent with previous studies based on postmortem data (Dekaban and Sadowsky, 1978). It is clear that brain growth is very well characterized and studied; this is not the case for the endocranial growth.

Endocranial maturation growth curves

Many studies reviewed by DeSilva and Lesnik (2006) showed that the endocranium grows 29% of its final adult size inside the uterus. Three other studies present precise ECV information for the period from birth to adulthood (Sgouros et al., 1999; Neubauer et al., 2009; Kamdar et al., 2009); and it is relevant to mention that from these three works, only one one of them (Kamdar et al., 2009) presents differential growth curves for males and females. Sgouros et al. (1999) studied a small sample of 24 children during the first 3 years of life obtained from MR imaging data, and found that in the first few months of life ECV averages 900 cm3 for males and 600 cm3 for females, increasing to 1500 and 1300 cm3 by the age of 15, respectively. The authors found that 77% of endocranial growth was achieved during the first 2 years after birth. Neubauer et al. (2009) studied dried crania of 48 subadult and 60 adult specimens, but they could not include adolescents in their study. They also found that endocranial size increases dramatically in the first 2 postnatal years. Thereafter, growth rate decelerate with increasing age and endocranial size increases slightly after deciduous dentition is completed. They reported that 90-95% of adult ECV is achieved at about 7-8 years old. A more complete study that focused on the first 6 years after birth was that of Kamdar et al. (2009), which included 123 healthy children. They reported a growth curve showing a doubling of the ECV from birth to 9 months old and a tripling of the ECV by the age of 6. Moreover, growth was shown to be more rapid from birth to 12 months old, and continue more slowly during the following 5 years. Based on these considerations, it is evident that although some studies addresses ontogenetic endocranial growth, they used very small samples or do not present a complete and continuous data set.

Brain and endocranial developmental relationship (shape covariation)

One of the first studies that investigated the relationship between brain and endocranium was that of Virchow (1856). He found that certain compensation takes place in skulls; an increase in brain size leads to an increase in the skull size at the point of minimal resistance. The resistance depends on the influence of the facial and basilar elements and on the degree of muscular development. According to this view, the brain would be the only structure controlling the size of the skull. In 1930, Pickering (1930) found that approximately 30% of the cranium shape is controlled by the brain, with the remaining 70% being under control of other factors, such as growth and development of face and cranial muscles. In fact, the proper coordination between brain and endocranial precursors, as well as other specialized soft tissues that constitutes the organs of the head, allows the correct development of the embryonic skull (Richtsmeier et al., 2006). For example, the mesenchyme that gives rise to the neurocranial vault is arranged first as a capsular membrane around the developing brain. This membrane is composed of an inner layer of endomeninx, which primarily originates from neural crest cells, and an outer ectomeninx, which originates from neural crest cells and paraxial mesoderm. The endomeninx forms the pia mater and the arachnoid, and differentiates into the inner dura mater, which covers the brain and remains unossified. The ectomeninx ossified in a intramembranous manner over the expanding dome of the brain, forming the cranial vault (Sperber, 2001) (Figure 1.1). Once formed, both the brain and the cranium are related to the head shape, although these relationships are poorly understood (Richtsmeier et al., 2006). In 1960, Moss and Young (1960) found that the neurocranium is a relatively linear system, where growth (size change) is mainly related to brain expansion, while development (shape

change) is associated to meningeal connective tensors. Consequently, the brain and the connective tensors conduct the neurocraneal morphogenesis, inducing the neurocranial bones to suffer structural rearrangements in their external and internal surface due to deposition and absorption (Enlow, 1990); this mechanism is possibly mediated by transduction signals in the suture limits (Ogle et al., 2004). The first studies that combined medical computed tomographic (CT) images and magnetic resonance (MR) images to analyse brain and cranium relationships came from Richtsmeier's team (Aldridge et al., 2005; Richtsmeier et al., 2006), who found strong and positive associations between the brain, meninges and cranium, and demonstrated that these structures interact in a coordinated and integrated way with the closing suture pattern. From these reviewed studies it can be inferred that there is a certain uncoupling between growth (size change) and development (shape change) of the brain and the cranium. Bastir et al. (2006) also found an existing dissociation between size and shape changes during cranium maturation. The authors described how the different neurocranial components mature. In terms of shape, the earliest structure to mature was the midline cranial base, followed by the lateral cranial floor and the midline neurocranium. However, in terms of size, the maturation of the lateral cranial floor occurred first, followed by the middle cranial base and finally the middle neurocranium. Therefore, they confirmed the ontogenetic dissociation between size and shape maturation of the cranium midline base and lateral floor. Based on this line of evidence, it may be important to define the relationship between the brain and endocranium with respect to their ontogenetic changes in size and shape. In order to characterize better such relationship, growth and developmental curves will be obtained in this thesis by means of the separate study of shape and size for brain and endocranium.

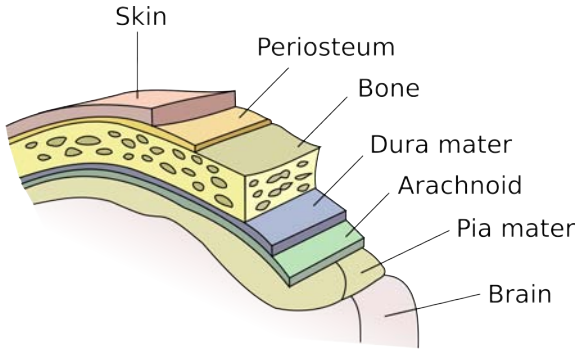

Figure 1.1: **Endocranial meninges.** Schema of the meninges, a system of membranes which envelops the central nervous system. The meninges consist of three layers: the dura mater, the arachnoid mater, and the pia mater.

Brain and endocranial macroscopic and perisylvian asymmetries

Another important source of indirect evidence presented by the endocranial bone is the macroscopic asymmetry. This feature is thought to correspond to brain asymmetries. Although in humans both brain hemispheres are similar in weight and volume, the tissue distribution considerably differs between them. First, the right hemisphere protrudes more anteriorly, while the left hemisphere extends more posteriorly than its contralateral one. A second characteristic is that in the frontal region, the right hemisphere is frequently broader than the left one; this relationship being reverted in the occipital region (Toga and Thompson, 2003) (Figure 1.2). These asymmetries, also called Yakovlevian anticlockwise torque (LeMay, 1976), produce marks in the inner endocranial bone, known as petalias. Given that important behavioral aspects are asymmetrically organized in the brain (Corballis, 1989; Bradshaw, 1991; Annett, 2002; Tommasi, 2009), it would be interesting to search for these cortical asymmetries in the fossil record, as a possible tool to predict behavioral aspects of the extinct species. Holloway and Costelareymondie (1982) addressed this issue and found that only hominids (*Australopithecus* sp., *Homo erectus*, *Homo sapiens*, and *Homo neanderthalensis*) consistently presented right-frontal and left-

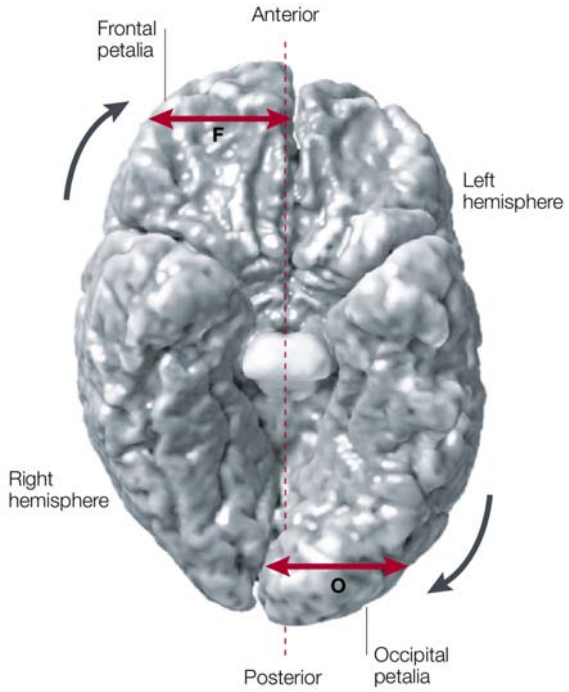

Figure 1.2: **Brain adult asymmetries.** Figure 2 from Toga and Thompson (2003). Three-dimensional rendering of the inferior surface of a human brain derived from a magnetic resonance (MR) imaging scan to illustrate prominent asymmetries found in the gross anatomy of the two brain hemispheres.

occipital petalia patterns, while other pongids showed petalias with different patterns. Falk et al. (1990) studied cercopithecoids (*Macaca mulatta*) and demonstrated the presence of right-frontal petalias but not left-occipital ones. Although it was stated that in humans the mentioned petalia pattern is already present at birth (Toga and Thompson, 2003), no scientific studies have demonstrated to the moment that the infant asymmetric pattern is the same as in adults, and at present it is poorly understood the way this pattern arises and develops throughout ontogeny.

Following these same type of evidences, endocranial imprints corresponding to two specific brain regions have been largely investigated: the Broca's area (Brodmann's area 44 and 45, or *pars opercularis* and *pars triangularis*) and the Wernicke's area (Brodmann area 21, 22 and, in a broader sense, 37, 39 and 40, or Heschl's *gyrus* and *planum tem-*

porale) (Garey, 1994) (see also Appendix A). In modern humans these two areas have an important role in language generation and in language comprehension, respectively (Broca, 1861; Wernicke, 1874; Price, 2000). These regions develop asymmetrically and as they are located closely to the Sylvian fissure, they are called perisylvian asymmetries; they have been described since the XIX century (Eberstaller, 1884; Cunningham, 1892). Promptly it was demonstrated that the *planum temporale* presented a conspicuous leftward volume asymmetry (Fleschig, 1908), which was recently detected with MR images as well. Additionally, the *pars opercularis* showed the same type of asymmetry, while there was no significant volume asymmetry of the *pars triangularis* (Keller et al., 2007). The *planum temporale*, which constitutes the major part of the classical anatomical Wernicke's area, received a particular attention, as it is considered the most likely anatomical correlate of language lateralization. This hypothesis was included in a complex and influential model of cerebral lateralization that was called the Geschwind/Galaburda theory (Geschwind and Levitsky, 1968; Galaburda et al., 1978; Geschwind and Galaburda, 1985a,b,c; McManus and Bryden, 1991). Some postulates of this model are at present under debate. For example, there were contradictory evidences about the relationship between handedness and cerebral asymmetries. Chiu and Damasio (1980) showed that they are independent variables, whereas Habib et al. (1995) found a significant larger leftward asymmetry in right-handers. One possible explanation for this disagreement could be the fact that Chiu and Damasio (1980) measured frontal and occipital petalias on the bony endocranium, while in Habib et al. (1995) brain volumes were quantified. On the other hand, similarly to Wernicke's area, the Broca's area of the left hemisphere has a larger volume than its contralateral Falzi et al. (1982); Amunts et al. (1999). All these

perisylvian asymmetries were recognized on the bony endocranium of several hominids (*Australopithecus* sp., *Homo habilis*, *Homo erectus* y *Homo neanderthalensis*) (Holloway, 1980; LeMay, 1976; Tobias, 1987). Although at first the presence of these asymmetries were considered as a proof of complex language capabilities, and even of spoken language, these speculations have lost significance at present due a recent finding: these same perisylvian asymmetries were also found on chimpanzees (Gannon et al., 1998; Cantalupo and Hopkins, 2001; Gannon et al., 2001). This could imply that the Wernicke's and the Broca's areas were already asymmetric and equipotential in the common ancestor of humans and chimpanzees, and then evolved independently in both lineages. Therefore, although the presence or absence of these asymmetries may not imply direct language capabilities, they are related to brain lateralization, which is broadly widespread among vertebrates (Vallortigara et al., 1999), and may have been of importance on human brain evolution (Calvin, 1982; Holloway and Costelareymondie, 1982; Toth, 1985; Falk, 1987; Bradshaw, 1991). For this reason, we consider it crucial to determine at which ontogenetic period these asymmetries arise and how they develop both in the brain and the endocranium.

Brain and endocranium sexual dimorphism

Since Raisman and Field (1971) demonstrated that the brain could be a sexually dimorphic structure, this issue has been extensively addressed in several studies (DeLacoste-Utamsing and Holloway, 1982; Ankney, 1992; Rushton, 1993; Lynn, 1994). However, this was not always done from an objective point of view (Swaab and Hofman, 1984; Hofman and Swaab, 1991), and frequently abusive conclusions were drawn about differences in intelligence between sexes based on morphological evidences. This discussion will not be

addressed in this thesis. Instead, we will analyse the question of where these dimorphic morphologies reside and how they develop. Ankney (1992) investigated this matter and found that there is an absolute volumetric (size) dimorphism between sexes. He showed that even when large data sets are corrected after covariance adjustment for body size, female brain is in average 100 g lighter and 110 cm^3 smaller than men brain. However, Goldstein et al. (1999, 2001), who studied different cortical and subcortical brain regions through volumetric imaging techniques, found that the adult brain, although presenting a generally larger volume in males, has several regions proportionately larger in females. These areas include: the caudate nucleus, hippocampus, some prefrontal cortical areas, the superior temporal gyrus, and some white matter structures such as the anterior commissure. Proportionately larger regions in the adult male brain include the hypothalamus, *stria terminalis*, cerebral ventricles, and the *splenium* and *genu* of the *corpus callosum*. From these studies together with those that located the distribution of neuronal receptors in other non-human animals (Pfaff and Keiner, 1973; MacLusky et al., 1987; Clark et al., 1988; Sibug et al., 1991), it can be asserted that there is a greater sexual dimorphism in brain areas that are homologous with those showing greater levels of sex steroid receptors during critical periods of brain development in non-human animals. A recent study in rats showed that pubertal hormones contribute to the postnatal preservation of sexual dimorphisms through sex-specific modulation of new cell addition to sexually dimorphic brain regions (Ahmed et al., 2008). This evidence could imply that similar processes occur in other mammals and specifically in humans. Hence, the brain dimorphism recognized in adults may develop at some intermediate period, and not necessarily be already expressed before birth. Therefore, in this thesis we will investigate the time during ontogeny

in which these dimorphic differences in size and shape arise and how they develop.

The endocranial dimorphism in humans has been studied mainly by measuring and comparing its volume between sexes, and mostly in adult samples (Stewart, 1934; Ricklan and Tobias, 1986; Rushton, 1992, 1994). These studies have shown that there is an absolute volumetric (size) dimorphism between sexes, and even after covariance adjustment for the effects of stature and weight, large data sets show that female ECV is in average 110 cm^3 lower than men ECV (Rushton, 1992). In this thesis we will focus on how this difference develops and during which ontogenetic period it arises. It is important to mention that to the moment no studies have specifically answered the question about the existence of sexual dimorphism in endocranial vault shape, and when it is expressed. As Shea (1992) stated, sexual dimorphism is the result of allometric and heterochronic trajectories (Gould, 1977; Alberch et al., 1979; Klingenberg, 1998; Gould, 2000) (see Appendix C). In this sense, the comprehension of the dimorphic timings and patterns of growth and development followed by the brain and endocranium will allow us to investigate the heterochronic processes that may explain brain and endocranium sexual differences.

The main importance of this study lies on the present lack of information about the relationship between the growing brain and its surrounding endocranial bone. The knowledge of this relationship throughout ontogeny may help to determine what information the bone can give us about the brain and consequently to understand better the evolution of the brain in our species. Five main questions about this matter will be investigated in this PhD, with the consequent testing of their five respective hypotheses, which will be described in the next chapter.

Chapter 2

Objectives & Hypotheses

The main objective of this PhD is to characterize, from a morphometric point of view, growth and development of modern human endocranium and brain from birth to the age of 31, in order to determine how these two structures interact and correlate throughout maturation. This study will focus on the correlation between the endocranial vault and the cortical brain. This body of knowledge will be applied to enlighten our interpretations of the indirect evidences available about human brain evolution.

The following specific questions, with their respective hypothesis, will be addressed throughout this thesis:

What kind of growth and development curve has endocranial vault and cortical brain?

H_1: The cortical brain and endocranial vault maturation curves are linear and constant.

What relationship has the cranial capacity measured from the bony endocranium with the brain volume?

H_2: The larger the endocranium, the lower will be the percentage of the volume occupied by the brain within the cranial vault. In other words, there is an inverse relationship between the endocranium size and the volume percentage occupied by the brain within the cranial vault.

What degree of covariation exists between endocranial and brain shape?

H_3: There is no covariation between endocranial vault and cortical brain.

When do endocranial petal patterns and brain macroscopic asymmetries grow and develop?

H_4: Macroscopic brain asymmetries and endocranial petal patterns are already present at birth.

Is there sexual dimorphism throughout endocranium and brain growth and development?

H_5: There is no sexual dimorphism throughout endocranial vault and cortical brain growth and development.

Chapter 3

Theoretical / methodological framework

The theoretical / methodological framework under which this thesis will be performed is the "Gould-Mosimann School", defined by Klingenberg (1998). This mathematical and theoretical framework provides a mode for the analysis of size and shape based on geometric similarity, with size and shape being independent variables that together characterise the form of a structure. Based on this framework, we can define several concepts that will be used throughout the present thesis. First, the concept of "ontogeny" will be understood as all the changes that an individual experience throughout his life, from conception to death. Second, the concept of "growth" will be strictly defined as ontogenetic size changes. Third, "development" will be interpreted as ontogenetic shape modifications. And finally, the concept of "maturation" will be understood as the sum of "growth" and "development"; or, equally, as the sum of ontogenetic size and shape changes, also known as ontogenetic "form" changes. All these definitions are summarized in the following schema:

In this way, the maturation of a specific structure will be quantified through its form

Maturation	=	Growth	+	Development
=		=		=
ΔForm	=	ΔSize	+	ΔShape

Table 3.1: Maturation can be defined as two different processes summed together: growth and development.

modifications, its growth through its size changes, and its development by means of its shape changes throughout ontogeny.

Chapter 4

Materials

For the purpose of this PhD two data bases were constructed at the nonprofit organization Fundación para la Lucha contra las Enfermedades Neurológicas de la Infancia (FLENI), Buenos Aires, Argentina. One data base consists of head computed tomographic (CT) images, which will provide information about bony cranial tissue; and the other one corresponds to head magnetic resonance (MR) images, to examine soft brain tissue. These two imaging techniques have different physics principles and therefore provide complementary information (Ventrice, 2010). The basic physics principle of CT scanning is that different projections based on X-rays emissions towards an object from different angles, allow the reconstruction of the internal structure of that object. Different structures present a variety of absorption rates depending on its constituent tissues. For this reason, when all projections are integrated, CT images are much sharper than X-rays, showing a higher definition not only in bone structures but also in soft tissues (Hsieh, 2009). Hence, in a head CT image the bone appears white and very clear because it absorbs large quantities of X-rays; grease and other soft tissues absorb less quantities of X-rays and appear in a gray scale; and finally, the air absorbs very little radiation, hollow structures appearing

black (Figure 4.1). The MR physics principle is based on the resonance capacity of certain atoms, particularly the protons. When an object is exposed to a strong magnetic field, the small magnetic fields produced by the protons get positioned in a particular direction. After a radio-frequency pulse application, an exciting and relaxing response of the protons is obtained. This response is called resonance, and can be measured and quantified to determine the type of tissue that is being analyzed (Brown and Semelka, 2003). In the human body, the molecule responsible for most of this kind of resonance is water (H_2O), since it contains two protons and is present in the tissues in a high percentage. Thus, in a head MR image the bone structures are shown black because of their lack of water, but the soft tissues of the brain can be clearly recognized with high detail: gray matter, white matter and cerebrospinal fluid (Figure 4.2). As it was shown, CT and MR scanning techniques offer valuable and complementary information on the different structures that constitute the studied object. However, as they are solely imaging procedures, they do not provide quantified data; to obtain this, it is necessary to apply complementary techniques, such as geometric morphometrics, which are described in Methods.

The two data bases were constructed from different individuals. The CT data base consisted of 154 CT image stacks belonging to healthy individuals raging from 0 to 31 years old (Table 4.1), and scanned with a General Electric Light Speed RT16. Normally, at FLENI medical institute, head CT scans are performed following a protocol that provides 16 axial images of the skull. This number of images is sufficient for medical observation, but it is inadequate to make three dimension (3D) reconstructions. Therefore, to achieve this purpose and to reduce the individual exposure to X-rays, two new CT scan protocols were specifically developed: the protocol (1) for individuals ranging from 0 to 15 years old,

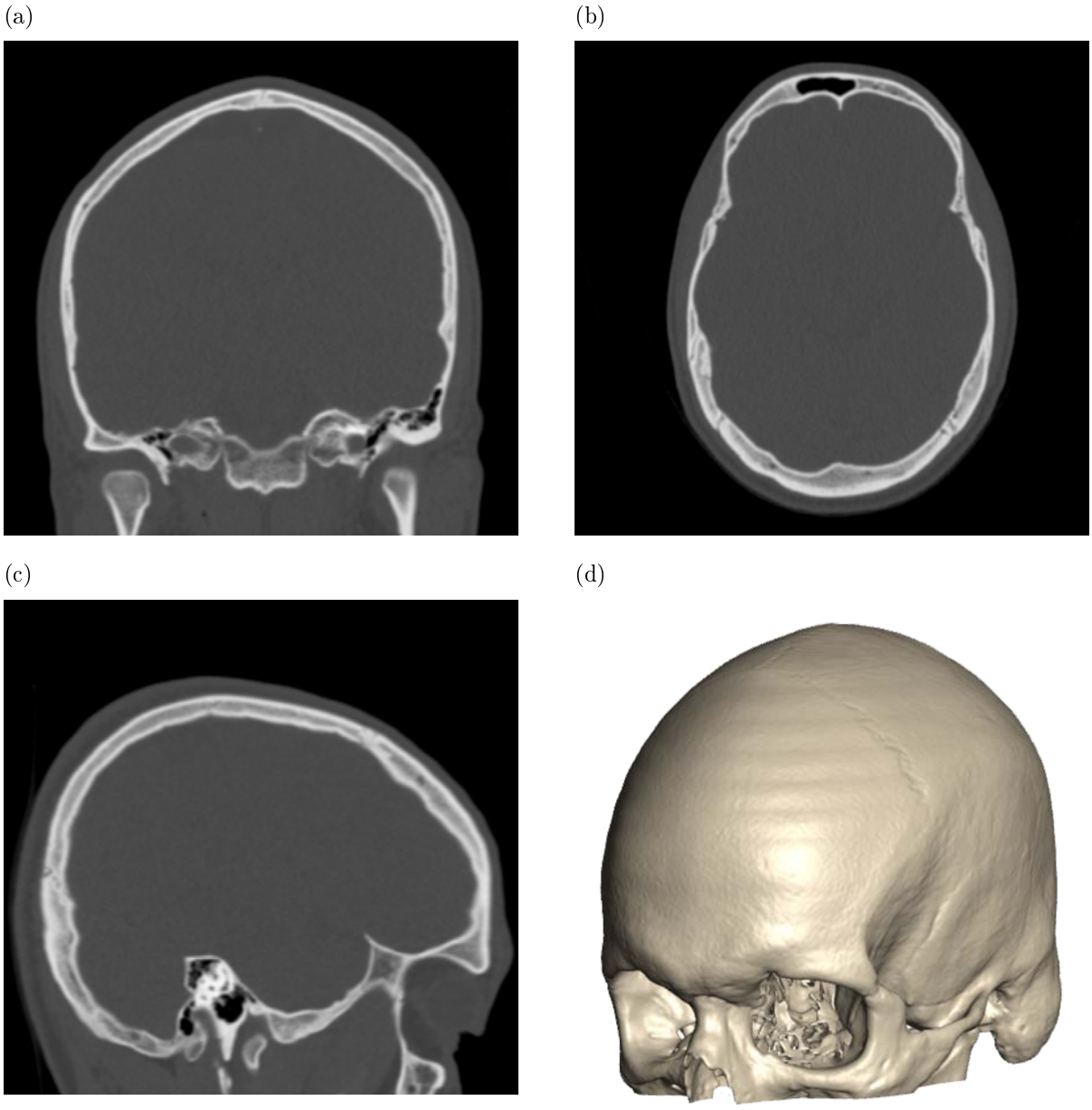

Figure 4.1: **CT cranium images and 3D reconstruction. (a)** Coronal view of a CT cranium image. **(b)** Horizontal view of a CT cranium image. **(c)** Sagittal view of a CT cranium image. **(d)** 3D reconstruction of CT cranium image (see Figure 5.1 for description of how to construct 3D from 2D images through segmentation).

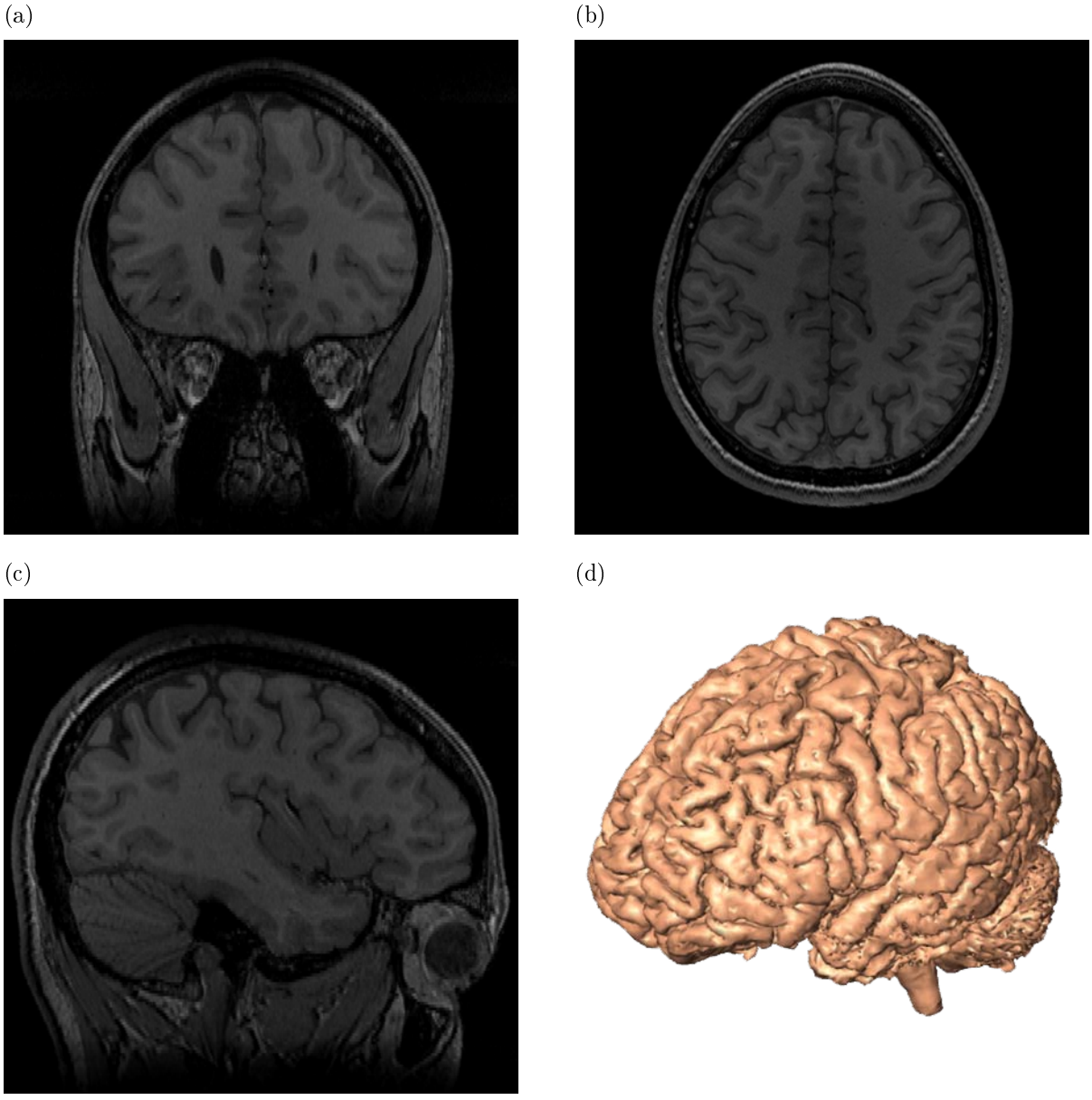

Figure 4.2: **MR brain images and 3D reconstruction.** **(a)** Coronal view of a MR brain image. **(b)** Horizontal view of a MR brain image. **(c)** Sagittal view of a MR brain image. **(d)** 3D reconstruction of MR brain image (see Figure 5.2 for description of how to construct 3D from 2D images through segmentation).

and the protocol (2) for individuals ranging from 16 to 31 years old. In this way, taking advantage of their reduced bone thickness, children, juveniles and young adolescents had a specific protocol with less exposure to X-rays. The protocol (1) was performed as follows: scanned in axial mode, 150 mA[1] of current, 120 kVp[2] of accelerating voltage, and a gantry/detector tilt positioned in 0.0° that produced 275 axial (resolution: 512 x 512 pixel) CT images with a voxel[3] size equal to 0.449 x 0.449 x 0.625 mm. The protocol (2) was performed as follows: scanned in axial mode, 200 mA, 120 kVp, gantry/detector tilt position at 0.0° which gave 275 axial (resolution: 512 x 512 pixel) CT images with a voxel size equal to 0.449 x 0.449 x 0.625 mm.

The MR data base consisted of 252 MR image stacks belonging to healthy individuals ranging from 0 to 31 years old (Table 4.2), scanned with a General Electric Signa Excite 1.5T. To construct this MR data base the FLENI's patient information bank was used. A simple algorithm was used to search through this data base and select patients from 0 to 31 years old with MR brain images. A total of 1843 patient medical reports were obtained, each of which was analysed looking for subjects with no brain diseases or injuries. 252 persons met these characteristics, with good MR images suitable for 3D reconstruction. This group of images consisted of four different types of MR stacks, which were performed with the same scanner but had different orientation and voxel size. The latter does not represent a problem as the images will be converted to 3D for further analyses (see Methods). The four types of MR stacks are: (1) MR acquisition type: T1 axial 3D fSPGR-

[1]The tube current determines the number of electrons hitting the anode, and therefore the total amount of X-rays. The X-ray intensity is then directly proportional to the tube current (mili Amperes = 1/1000 Amperes).

[2]The accelerating kilovolts peak (kVp) voltage applied in an X-ray tube is determined by the highest instantaneous voltage between the cathode and anode, corresponding to the highest X-ray energy emitted.

[3]A digital image is composed of a finite number of elements, each of which has a particular location and value; the picture elements of a 2D image are named pixels. In the case of 3D images, the volume elements are called voxels.

IRprep (T1-weighted fast spoiled gradient echo inversion recovery prepared), 12.956 ms TR[1], 6.1 ms TE[2], 400 ms TI[3], 15° flip angle[4], 256 x 256 acquisition matrix that gave image stacks of 120 axial (resolution: 512 x 512 pixel) images with voxel size equal to 0.469 x 0.469 x 1.6 mm; (2) MR acquisition type: T1 sagittal 3D fSPGR-IRprep, 12.1 ms TR, 5.21 ms TE, 300 ms TI, 20° flip angle, 256 x 256 acquisition matrix that gave image stacks of 120 sagittal 256 x 256 pixel images with a voxel size of 0.938 x 0.938 x 1.5 mm; (3) MR acquisition type: T1 coronal 3D fSPGR-IRprep, 10.91 ms TR, 5.08 ms TE, 400 ms TI, 15° flip angle, 256 x 256 acquisition matrix that gave image stacks consisting of 120 coronal 512 x 512 pixel images with a voxel size of 0.469 x 0.469 x 1.6 mm; and (4) MR acquisition type: T1 coronal 3D fSPGR-IRprep, 5.5 ms TR, 1.4 ms TE, 300 ms TI, 20° flip angle, 256 x 256 acquisition matrix that gave image stacks of 120 coronal 256 x 256 pixel images a with voxel size equal to 0.938 x 0.938 x 1.5 mm. The 252 MR image data base consisted of 4 individuals with the first type of axial MR image stack, 5 with the second sagittal one, 79 with the third coronal stack, and 164 with the fourth one.

[1]The repetition time (TR) is the lapse of time that exists between successive pulse sequences applied to the same slice.

[2]The echo time (TE) represents the time in milliseconds between the application of the 90° pulse and the peak of the echo signal.

[3]The inversion time (TI) is the time lapse between the 180° inversion pulse and the 90° excitation pulse in an inversion recovery pulse sequence.

[4]The angle to which the net magnetization is rotated or tipped relative to the main magnetic field direction via the application of an excitatory pulse.

Table 4.1: **CT image data base.** List of normal individuals appertaining to the computed tomographic (CT) cranial data base. This data base is composed 154 individuals: 7 females and 12 males from 0-71 months, 12 females and 17 males from 72-143 months, 16 females and 14 males from 144-215 months, and 53 females and 23 males from 216-379 months.

#	Name	Sex	Age (months)	Age (years)	Age group
1	00F-001	female	5	0.42	infant-child
2	01F-004	female	7	0.58	infant-child
3	01F-005	female	11	0.92	infant-child
4	03F-012	female	38	3.17	infant-child
5	04F-015	female	44	3.67	infant-child
6	04F-016	female	50	4.17	infant-child
7	06F-018	female	69	5.75	infant-child
8	00M-002	male	3	0.25	infant-child
9	00M-003	male	6	0.50	infant-child
10	01M-006	male	7	0.58	infant-child
11	01M-007	male	7	0.58	infant-child
12	01M-008	male	7	0.58	infant-child
13	01M-009	male	12	1.00	infant-child
14	01M-010	male	14	1.17	infant-child
15	01M-011	male	17	1.42	infant-child
16	03M-013	male	31	2.58	infant-child
17	03M-014	male	35	2.92	infant-child
18	05M-017	male	61	5.08	infant-child
19	06M-019	male	67	5.58	infant-child
20	07F-021	female	83	6.92	juvenile
21	09F-029	female	103	8.58	juvenile
22	09F-030	female	104	8.67	juvenile
23	09F-031	female	106	8.83	juvenile
24	09F-032	female	112	9.33	juvenile
25	10F-036	female	120	10.00	juvenile
26	10F-037	female	123	10.25	juvenile
27	11F-156	female	127	10.58	juvenile
28	11F-042	female	129	10.75	juvenile
29	11F-043	female	131	10.92	juvenile
30	11F-044	female	132	11.00	juvenile
31	12F-047	female	138	11.50	juvenile
32	06M-020	male	72	6.00	juvenile
33	07M-022	male	79	6.58	juvenile
34	07M-023	male	80	6.67	juvenile
35	07M-024	male	84	7.00	juvenile
36	07M-025	male	85	7.08	juvenile
37	07M-026	male	86	7.17	juvenile
38	08M-027	male	91	7.58	juvenile
39	08M-155	male	92	7.67	juvenile

Table 4.1 (continued)

#	Name	Sex	Age (months)	Age (years)	Age group
40	08M-028	male	95	7.92	juvenile
41	09M-033	male	105	8.75	juvenile
42	09M-034	male	109	9.08	juvenile
43	09M-035	male	110	9.17	juvenile
44	10M-038	male	116	9.67	juvenile
45	10M-040	male	122	10.17	juvenile
46	10M-041	male	125	10.42	juvenile
47	11M-045	male	135	11.25	juvenile
48	11M-046	male	138	11.50	juvenile
49	12F-153	female	146	12.17	adolescent
50	13F-049	female	151	12.58	adolescent
51	13F-050	female	156	13.00	adolescent
52	13F-051	female	156	13.00	adolescent
53	14F-054	female	168	14.00	adolescent
54	14F-055	female	169	14.08	adolescent
55	14F-056	female	174	14.50	adolescent
56	15F-059	female	181	15.08	adolescent
57	15F-060	female	182	15.17	adolescent
58	15F-061	female	183	15.25	adolescent
59	16F-063	female	187	15.58	adolescent
60	16F-064	female	188	15.67	adolescent
61	16F-065	female	190	15.83	adolescent
62	16F-066	female	192	16.00	adolescent
63	16F-067	female	198	16.50	adolescent
64	17F-071	female	208	17.33	adolescent
65	12M-151	male	144	12.00	adolescent
66	12M-048	male	149	12.42	adolescent
67	13M-052	male	151	12.58	adolescent
68	13M-053	male	157	13.08	adolescent
69	14M-057	male	165	13.75	adolescent
70	14M-058	male	170	14.17	adolescent
71	15M-062	male	178	14.83	adolescent
72	16M-068	male	190	15.83	adolescent
73	16M-069	male	191	15.92	adolescent
74	16M-070	male	198	16.50	adolescent
75	17M-072	male	200	16.67	adolescent
76	17M-073	male	201	16.75	adolescent
77	17M-074	male	202	16.83	adolescent
78	17M-075	male	204	17.00	adolescent
79	18F-077	female	218	18.17	adult
80	19F-079	female	233	19.42	adult
81	20F-080	female	236	19.67	adult
82	20F-081	female	243	20.25	adult

Table 4.1 (continued)

#	Name	Sex	Age (months)	Age (years)	Age group
83	21F-084	female	247	20.58	adult
84	21F-085	female	248	20.67	adult
85	21F-086	female	252	21.00	adult
86	22F-089	female	263	21.92	adult
87	22F-090	female	268	22.33	adult
88	22F-091	female	268	22.33	adult
89	23F-096	female	273	22.75	adult
90	23F-097	female	277	23.08	adult
91	23F-098	female	282	23.50	adult
92	23F-099	female	282	23.50	adult
93	24F-101	female	286	23.83	adult
94	24F-102	female	289	24.08	adult
95	24F-103	female	290	24.17	adult
96	24F-104	female	293	24.42	adult
97	25F-106	female	294	24.50	adult
98	25F-107	female	296	24.67	adult
99	25F-108	female	296	24.67	adult
100	25F-109	female	297	24.75	adult
101	25F-154	female	301	25.08	adult
102	25F-110	female	302	25.17	adult
103	25F-111	female	302	25.17	adult
104	26F-115	female	307	25.58	adult
105	26F-116	female	312	26.00	adult
106	26F-117	female	314	26.17	adult
107	26F-118	female	317	26.42	adult
108	26F-119	female	318	26.50	adult
109	27F-123	female	319	26.58	adult
110	27F-124	female	321	26.75	adult
111	27F-152	female	325	27.08	adult
112	27F-125	female	326	27.17	adult
113	27F-126	female	326	27.17	adult
114	27F-150	female	329	27.42	adult
115	27F-127	female	330	27.50	adult
116	28F-128	female	330	27.50	adult
117	28F-130	female	332	27.67	adult
118	28F-131	female	336	28.00	adult
119	28F-132	female	337	28.08	adult
120	28F-157	female	337	28.08	adult
121	28F-133	female	341	28.42	adult
122	29F-135	female	342	28.50	adult
123	29F-136	female	346	28.83	adult
124	29F-137	female	350	29.17	adult
125	29F-138	female	351	29.25	adult

Table 4.1 (continued)

#	Name	Sex	Age (months)	Age (years)	Age group
126	29F-139	female	353	29.42	adult
127	30F-142	female	357	29.75	adult
128	30F-143	female	364	30.33	adult
129	30F-144	female	364	30.33	adult
130	31F-146	female	367	30.58	adult
131	31F-147	female	372	31.00	adult
132	18M-078	male	216	18.00	adult
133	20M-082	male	236	19.67	adult
134	20M-083	male	244	20.33	adult
135	21M-087	male	249	20.75	adult
136	21M-088	male	255	21.25	adult
137	22M-092	male	267	22.25	adult
138	22M-093	male	267	22.25	adult
139	22M-094	male	269	22.42	adult
140	22M-095	male	270	22.50	adult
141	23M-100	male	273	22.75	adult
142	24M-105	male	288	24.00	adult
143	25M-112	male	295	24.58	adult
144	25M-113	male	303	25.25	adult
145	25M-114	male	303	25.25	adult
146	26M-120	male	308	25.67	adult
147	26M-121	male	310	25.83	adult
148	26M-122	male	318	26.50	adult
149	28M-134	male	334	27.83	adult
150	29M-140	male	345	28.75	adult
151	29M-141	male	345	28.75	adult
152	30M-145	male	366	30.50	adult
153	31M-148	male	368	30.67	adult
154	32M-149	male	379	31.58	adult

Table 4.2: **MR image data base.** List of normal individuals appertaining to the magnetic resonance (MR) brain data base. This data base is composed 252 individuals: 5 females and 7 males from 0-71 months, 25 females and 37 males from 72-143 months, 42 females and 39 males from 144-215 months, and 55 females and 42 males from 216-382 months.

#	Name	Sex	Age (months)	Age (years)	Age group
1	04F-005	female	42	3.50	infant-child
2	05F-009	female	55	4.58	infant-child
3	05F-007	female	59	4.92	infant-child
4	05F-010	female	62	5.17	infant-child
5	05F-008	female	65	5.42	infant-child
6	01M-001	male	12	1.00	infant-child
7	02M-003	male	28	2.33	infant-child
8	02M-004	male	29	2.42	infant-child
9	04M-006	male	54	4.50	infant-child
10	05M-011	male	61	5.08	infant-child
11	06M-016	male	66	5.50	infant-child
12	06M-015	male	69	5.75	infant-child
13	06F-014	female	72	6.00	juvenile
14	06F-012	female	74	6.17	juvenile
15	06F-013	female	77	6.42	juvenile
16	07F-020	female	80	6.67	juvenile
17	07F-021	female	80	6.67	juvenile
18	07F-017	female	84	7.00	juvenile
19	07F-019	female	87	7.25	juvenile
20	07F-018	female	88	7.33	juvenile
21	07F-022	female	89	7.42	juvenile
22	08F-035	female	96	8.00	juvenile
23	08F-034	female	97	8.08	juvenile
24	08F-033	female	101	8.42	juvenile
25	09F-041	female	103	8.58	juvenile
26	09F-042	female	112	9.33	juvenile
27	09F-040	female	113	9.42	juvenile
28	10F-052	female	118	9.83	juvenile
29	10F-051	female	120	10.00	juvenile
30	10F-050	female	124	10.33	juvenile
31	10F-053	female	125	10.42	juvenile
32	11F-068	female	126	10.50	juvenile
33	11F-067	female	128	10.67	juvenile
34	11F-070	female	133	11.08	juvenile
35	11F-066	female	134	11.17	juvenile
36	12F-085-070	female	140	11.67	juvenile
37	12F-081	female	143	11.92	juvenile
38	07M-030	male	78	6.50	juvenile
39	07M-026	male	79	6.58	juvenile

Table 4.2 (continued)

#	Name	Sex	Age (months)	Age (years)	Age group
40	07M-032	male	80	6.67	juvenile
41	07M-027	male	82	6.83	juvenile
42	07M-024	male	84	7.00	juvenile
43	07M-023	male	86	7.17	juvenile
44	07M-029-006	male	87	7.25	juvenile
45	07M-025	male	88	7.33	juvenile
46	07M-028	male	90	7.50	juvenile
47	08M-038	male	97	8.08	juvenile
48	08M-037	male	99	8.25	juvenile
49	08M-036	male	102	8.50	juvenile
50	09M-046	male	105	8.75	juvenile
51	09M-045	male	107	8.92	juvenile
52	09M-049	male	108	9.00	juvenile
53	09M-043	male	109	9.08	juvenile
54	09M-044	male	110	9.17	juvenile
55	09M-047-032	male	110	9.17	juvenile
56	09M-048	male	111	9.25	juvenile
57	10M-061	male	116	9.67	juvenile
58	10M-057	male	117	9.75	juvenile
59	10M-058	male	118	9.83	juvenile
60	10M-059	male	118	9.83	juvenile
61	10M-065	male	118	9.83	juvenile
62	10M-062	male	119	9.92	juvenile
63	10M-056	male	120	10.00	juvenile
64	10M-063	male	124	10.33	juvenile
65	10M-060	male	125	10.42	juvenile
66	11M-078	male	129	10.75	juvenile
67	11M-071	male	131	10.92	juvenile
68	11M-075	male	131	10.92	juvenile
69	11M-073	male	132	11.00	juvenile
70	11M-074	male	132	11.00	juvenile
71	11M-077	male	132	11.00	juvenile
72	11M-072	male	134	11.17	juvenile
73	11M-079	male	136	11.33	juvenile
74	11M-080	male	138	11.50	juvenile
75	12F-084	female	144	12.00	adolescent
76	12F-086	female	145	12.08	adolescent
77	12F-087	female	147	12.25	adolescent
78	12F-082-068	female	149	12.42	adolescent
79	12F-083	female	149	12.42	adolescent
80	12F-088-123	female	149	12.42	adolescent
81	13F-093	female	152	12.67	adolescent
82	13F-092	female	153	12.75	adolescent

Table 4.2 (continued)

#	Name	Sex	Age (months)	Age (years)	Age group
83	13F-094	female	153	12.75	adolescent
84	13F-091	female	154	12.83	adolescent
85	13F-095	female	155	12.92	adolescent
86	13F-097	female	157	13.08	adolescent
87	14F-106	female	162	13.50	adolescent
88	14F-110	female	163	13.58	adolescent
89	14F-107	female	167	13.92	adolescent
90	14F-105	female	169	14.08	adolescent
91	14F-109	female	170	14.17	adolescent
92	14F-108	female	173	14.42	adolescent
93	15F-129	female	178	14.83	adolescent
94	15F-128	female	181	15.08	adolescent
95	15F-130	female	181	15.08	adolescent
96	15F-131	female	182	15.17	adolescent
97	15F-126	female	183	15.25	adolescent
98	15F-127	female	183	15.25	adolescent
99	15F-124	female	185	15.42	adolescent
100	16F-146	female	189	15.75	adolescent
101	16F-145	female	190	15.83	adolescent
102	16F-147	female	190	15.83	adolescent
103	16F-141	female	193	16.08	adolescent
104	16F-143	female	193	16.08	adolescent
105	16F-144	female	195	16.25	adolescent
106	16F-148	female	195	16.25	adolescent
107	16F-149	female	195	16.25	adolescent
108	16F-142	female	196	16.33	adolescent
109	17F-163	female	198	16.50	adolescent
110	17F-160	female	203	16.92	adolescent
111	17F-158	female	205	17.08	adolescent
112	17F-159	female	205	17.08	adolescent
113	17F-161	female	205	17.08	adolescent
114	17F-162	female	205	17.08	adolescent
115	18F-171	female	212	17.67	adolescent
116	18F-170	female	215	17.92	adolescent
117	12M-089	male	147	12.25	adolescent
118	12M-090	male	150	12.50	adolescent
119	13M-102	male	151	12.58	adolescent
120	13M-100	male	155	12.92	adolescent
121	13M-099	male	160	13.33	adolescent
122	13M-103	male	160	13.33	adolescent
123	13M-098	male	161	13.42	adolescent
124	13M-101	male	162	13.50	adolescent
125	14M-117	male	162	13.50	adolescent

Table 4.2 (continued)

#	Name	Sex	Age (months)	Age (years)	Age group
126	14M-113	male	164	13.67	adolescent
127	14M-118	male	167	13.92	adolescent
128	14M-116	male	169	14.08	adolescent
129	14M-112	male	170	14.17	adolescent
130	14M-111	male	171	14.25	adolescent
131	14M-121	male	173	14.42	adolescent
132	15M-133	male	177	14.75	adolescent
133	15M-135	male	177	14.75	adolescent
134	15M-139	male	181	15.08	adolescent
135	15M-138	male	182	15.17	adolescent
136	15M-136	male	184	15.33	adolescent
137	15M-134	male	185	15.42	adolescent
138	15M-137	male	185	15.42	adolescent
139	15M-140	male	186	15.50	adolescent
140	16M-152	male	187	15.58	adolescent
141	16M-153	male	189	15.75	adolescent
142	16M-154	male	192	16.00	adolescent
143	16M-150-098	male	195	16.25	adolescent
144	16M-151	male	197	16.42	adolescent
145	16M-155	male	197	16.42	adolescent
146	16M-157	male	197	16.42	adolescent
147	17M-169	male	202	16.83	adolescent
148	17M-165	male	205	17.08	adolescent
149	17M-167	male	205	17.08	adolescent
150	17M-166	male	207	17.25	adolescent
151	17M-168	male	210	17.50	adolescent
152	18M-178	male	210	17.50	adolescent
153	18M-177	male	213	17.75	adolescent
154	18M-175	male	214	17.83	adolescent
155	18M-174	male	215	17.92	adolescent
156	18F-173	female	218	18.17	adult
157	18F-172	female	220	18.33	adult
158	19F-179	female	224	18.67	adult
159	19F-181	female	225	18.75	adult
160	19F-180	female	230	19.17	adult
161	20F-188	female	240	20.00	adult
162	20F-189-182	female	245	20.42	adult
163	21F-197	female	247	20.58	adult
164	21F-199	female	249	20.75	adult
165	21F-200-168	female	251	20.92	adult
166	21F-204	female	252	21.00	adult
167	21F-201	female	253	21.08	adult
168	21F-198	female	254	21.17	adult

Table 4.2 (continued)

#	Name	Sex	Age (months)	Age (years)	Age group
169	21F-202	female	254	21.17	adult
170	21F-203	female	258	21.50	adult
171	22F-214	female	261	21.75	adult
172	22F-213	female	264	22.00	adult
173	22F-212	female	268	22.33	adult
174	22F-211	female	269	22.42	adult
175	23F-220	female	271	22.58	adult
176	23F-219	female	275	22.92	adult
177	23F-218-202	female	279	23.25	adult
178	24F-228	female	286	23.83	adult
179	24F-230	female	286	23.83	adult
180	24F-226	female	288	24.00	adult
181	24F-224	female	290	24.17	adult
182	24F-223	female	291	24.25	adult
183	24F-225	female	291	24.25	adult
184	24F-229	female	292	24.33	adult
185	24F-227	female	293	24.42	adult
186	25F-236	female	295	24.58	adult
187	25F-237	female	298	24.83	adult
188	26F-244	female	308	25.67	adult
189	26F-243	female	310	25.83	adult
190	26F-245	female	317	26.42	adult
191	27F-251	female	321	26.75	adult
192	27F-255	female	322	26.83	adult
193	27F-253	female	326	27.17	adult
194	27F-254	female	328	27.33	adult
195	27F-252	female	330	27.50	adult
196	28F-259	female	337	28.08	adult
197	28F-257	female	342	28.50	adult
198	29F-263	female	344	28.67	adult
199	29F-260	female	345	28.75	adult
200	29F-262	female	345	28.75	adult
201	29F-261	female	349	29.08	adult
202	29F-264	female	352	29.33	adult
203	30F-267	female	355	29.58	adult
204	30F-270	female	359	29.92	adult
205	30F-268	female	365	30.42	adult
206	30F-269	female	366	30.50	adult
207	31F-274	female	367	30.58	adult
208	31F-273	female	369	30.75	adult
209	31F-275	female	375	31.25	adult
210	32F-277	female	382	31.83	adult
211	18M-176	male	218	18.17	adult

Table 4.2 (continued)

#	Name	Sex	Age (months)	Age (years)	Age group
212	19M-186	male	223	18.58	adult
213	19M-184	male	225	18.75	adult
214	19M-185	male	227	18.92	adult
215	19M-187	male	229	19.08	adult
216	19M-183	male	231	19.25	adult
217	20M-190	male	235	19.58	adult
218	20M-191	male	236	19.67	adult
219	20M-193	male	242	20.17	adult
220	20M-195	male	242	20.17	adult
221	20M-196	male	245	20.42	adult
222	20M-192	male	246	20.50	adult
223	21M-208	male	246	20.50	adult
224	21M-207	male	248	20.67	adult
225	21M-205	male	249	20.75	adult
226	21M-209	male	251	20.92	adult
227	21M-210	male	251	20.92	adult
228	22M-215	male	262	21.83	adult
229	22M-217-195	male	267	22.25	adult
230	22M-216	male	269	22.42	adult
231	23M-221	male	277	23.08	adult
232	23M-222	male	277	23.08	adult
233	24M-235	male	285	23.75	adult
234	24M-233	male	286	23.83	adult
235	24M-234	male	287	23.92	adult
236	24M-231	male	288	24.00	adult
237	24M-232	male	292	24.33	adult
238	25M-241	male	296	24.67	adult
239	25M-238	male	297	24.75	adult
240	25M-240	male	299	24.92	adult
241	25M-242	male	302	25.17	adult
242	26M-248	male	306	25.50	adult
243	26M-249	male	306	25.50	adult
244	26M-246	male	307	25.58	adult
245	26M-250	male	311	25.92	adult
246	26M-247	male	314	26.17	adult
247	27M-256	male	325	27.08	adult
248	29M-265	male	344	28.67	adult
249	29M-266-247	male	346	28.83	adult
250	30M-272	male	358	29.83	adult
251	30M-271	male	360	30.00	adult
252	31M-276-271	male	371	30.92	adult

Chapter 5

Methods

To better discriminate shape modifications throughout the ontogenetic period analyzed, individuals from the two different data bases were separated in groups according to age: infant-child: 0-71 months old (0-5 years old), juvenile: 72-143 months old (6-11 years old), adolescent: 144-215 months old (12-17 years old), and adult: 216+ months old (18+ years old). These age categories were established based on the known human tooth eruption pattern (Smith, 1994), which marks the eruption of the first molar (M1) at 6 years old, the second molar (M2) at 12 years old, and the third molar (M3) at 18 years old. The construction of these age groups offers two advantages: first, it allows *a posteriori* comparisons with other developmental studies that do not provide age information but use tooth eruption as a proxy (Bastir and Rosas, 2004; Bastir et al., 2006; Sardi and Rozzi, 2007). Second, it prevents the masking and no detection of small shape modifications occurring in one period due to larger shape changes arising in another period, which could occurred if the individuals were analyzed all together.

The CT and MR image stacks from each data base were transformed from DICOM format (Digital Imaging and Communications in Medicine format) to Analyze format for

compatibility reasons; during this procedure images became anonymous with the program MIPAV (Medical Image Processing, Analysis and Visualization) (McAuliffe et al., 2001). The endocranium and the brain will be extracted from these volumetric CT and MR Analyze image stacks by means of segmentation techniques. Segmentation is a type of image processing which partitions an image into regions, which represent the different objects in the image. There are two main segmentation algorithms categories for gray-scale image processing: one based on the concept of discontinuity, which refers to the abrupt changes between the objects and the background in an image; and the other category based on the concept of similarity, which describes the uniformity and homogeneity within a given object or region in an image; therefore, a region is formed by a connected set of pixels having more or less the same homogeneous characteristics (Gonzalez and Woods, 2002; Acharya and Ray, 2005). The first approach involves the detection of points, lines and edges in an image, whereas segmentation methods based on the second property include thresholding, region growing, and region splitting and merging. In the case of endocranial segmentation from CT stacks, the thresholding segmentation technique was used. This technique only relies on the point or pixel values of the image. Gray-level thresholding segments an image based on the value at each point relative to a specified threshold value; in this case, the value is the bone tissue minimal intensity, so that every pixel presenting a larger intensity value will be selected. In this way, we obtain a segmented 3D skull from the whole CT stack. To obtain the endocranium from this 3D image, some manual edition must be performed slice by slice. First, holes and foramens (*i.e. foramen magnum*, *foramen ovale*, carotid canal, jugular fossa, etc.) connecting the internal part of cranium with the external skull must be manually filled in. Then the internal part of

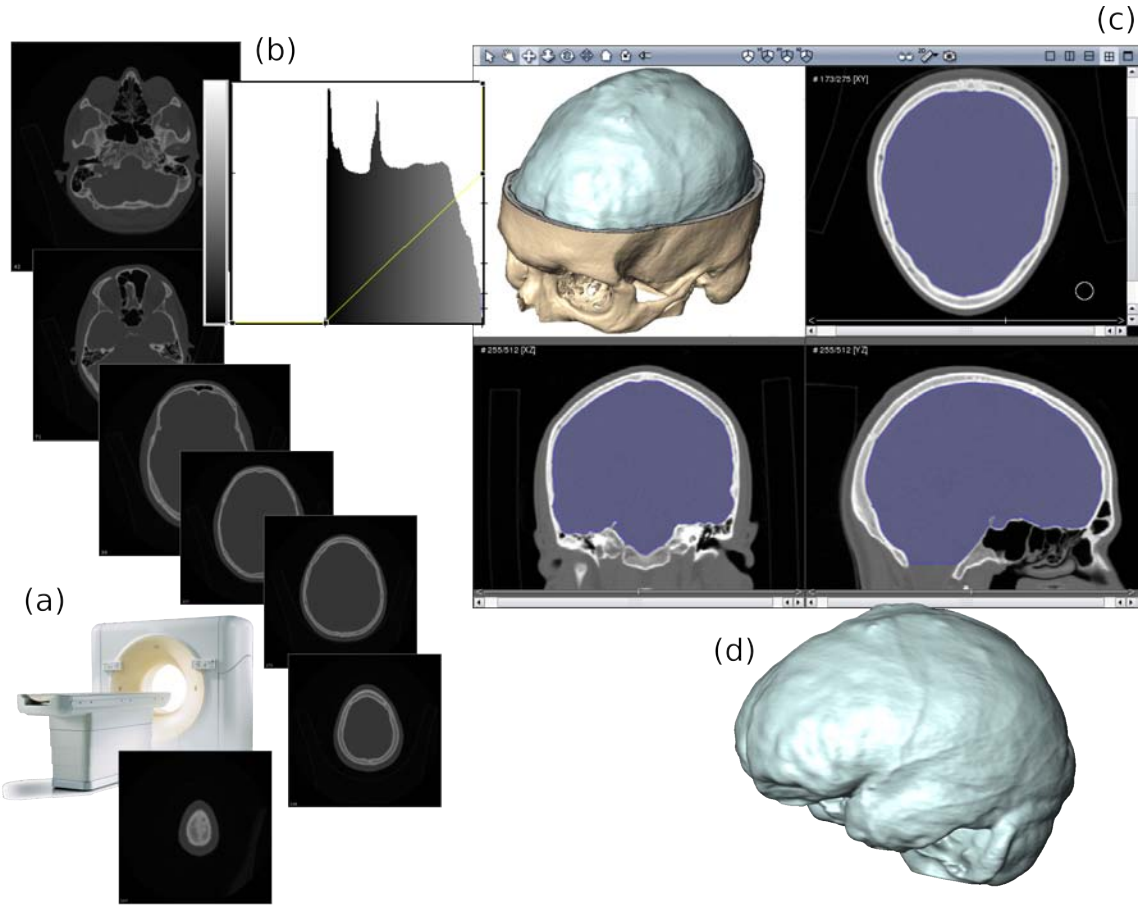

Figure 5.1: **Semi-automated method for endocranial segmentation.** **(a)** Images are obtained through CT scanning techniques. **(b)** Through automated gray-level thresholding bone tissue is recognized and a 3D reconstruction of the skull is made. **(c)** Holes and foramens which connect the internal endocranium with the exterior of the skull are filled by manual editing. **(d)** Finally the internal endocast is filled with a growing tool and that selected group of voxels are used to construct a 3D endocranium.

the cranium, completely isolated now from the external skull, can be filled and selected to make the endocranial 3D reconstruction. This procedure was entirely performed with the program Amira and is schematically and briefly explained in Figure 5.1. Once the endocranial 3D reconstruction was obtained, endocranial capacities were measured for each individual.

In the case of MR image stacks, they were segmented by means of two different methodologies, which are complex and present several stages; hence, they can not be included in the discontinuity or the similarity concept segmentation groups. In fact, they both have stages that belong to one or the other category. The first methodology is the brain extraction tool (BET) algorithm (Smith, 2002) implemented in the FMRIB Software Library (FSL) (Smith et al., 2004); and the second one is the voxel based morphometry (VBM) segmentation algorithm (Ashburner and Friston, 2000) within the Statistical Parametric Mapping (SPM) software (Friston et al., 2006). These two algorithms are almost entirely automated except for some variables that can be specified. The BET algorithm was mainly applied to obtain a good 3D reconstruction of the brain cortex, but could not be used to obtain volumetric information because it usually fails to extract correctly internal and basal brain structures (which did not affect this study because brain landmarks were located at the cortex, see below). The volumetric information was obtained through the VBM segmentation algorithm, which segments the brain into gray matter, white matter and cerebrospinal fluid. Hence, to get the whole brain volume (BV), gray (GMV) and white matter volumes (WMV) must be added. A simple schema of these two procedures is depicted in Figure 5.2. At this point GMV, and WMV were measured and BV was calculated for each individual.

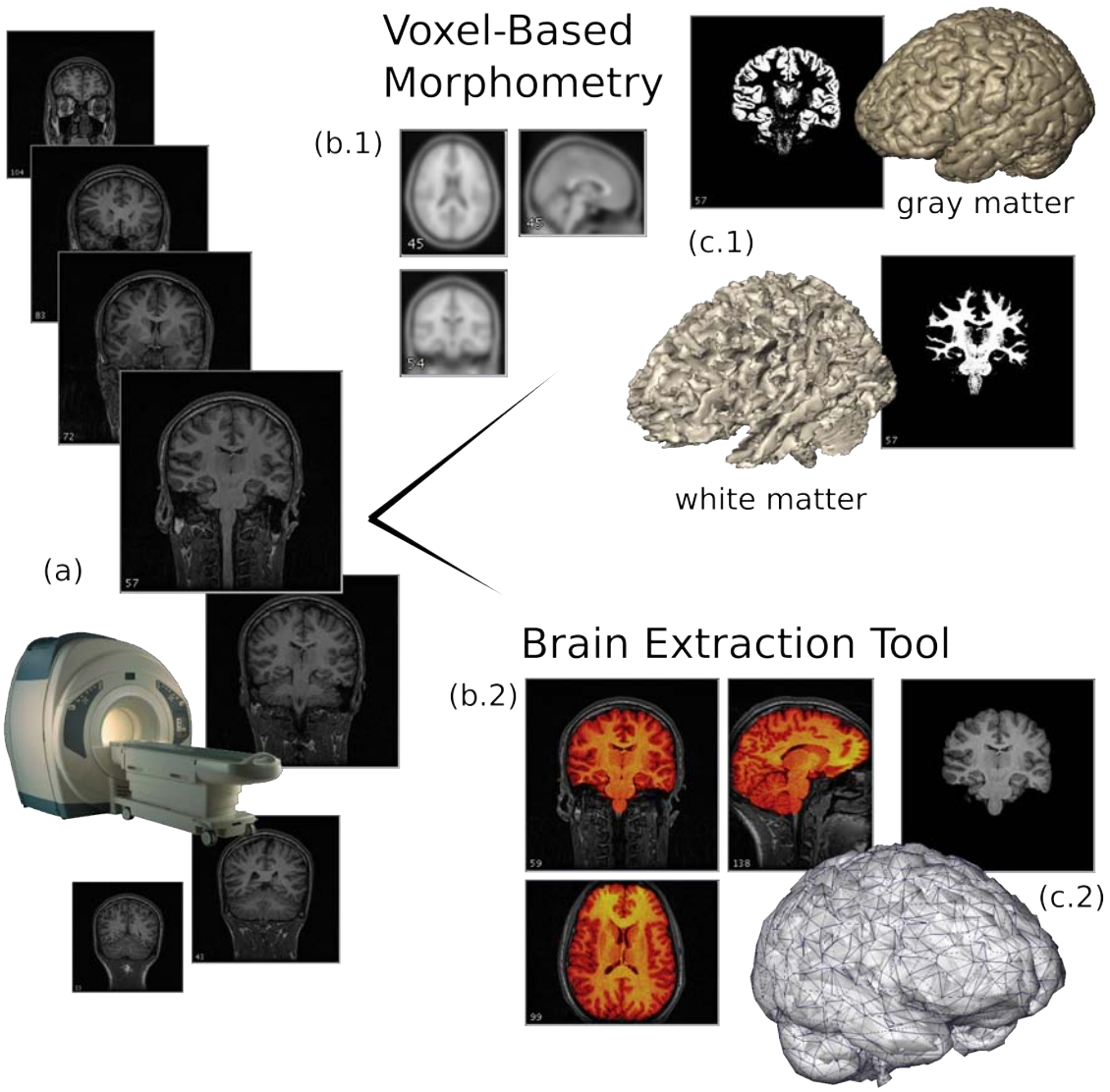

Figure 5.2: **Automated methods for brain segmentation: Voxel-Based Morphometry (VBM) and Brain Extraction Tool (BET). (a)** Images are obtained through MR scanning techniques. **(b.1)** VBM starts with spatial normalisation, which involves registering the individual MR images to the same template image. This template consists of the average of a large number of MR images that have been registered in the same stereotactic space. **(c.1)** The spatially normalised images are then segmented into gray matter and white matter. This is achieved by combining a priori probability maps or "Bayesian priors", which encode the knowledge of the spatial distribution of different tissues in normal subjects, with a mixture model cluster analysis which identifies voxel intensity distributions of particular tissue types (Mechelli et al., 2005). **(b.2)** BET is a fast and robust brain extraction technique which, first, calculates the robust image intensity minimum and maximum. From these values the center of gravity is calculated, where a spherical tessellated surface is initially centered. **(c.2)** Each vertex in the tessellated surface is updated by estimating where best that vertex should move to, to improve the surface; and finally arriving to a brain surface mesh (Smith, 2002).

Geometric morphometrics

Throughout this thesis general and specific geometric morphometric (GM) analyses will be used to assess the different questions and hypothesis presented. Therefore, to clarify the following descriptions of the specific procedures used to evaluate each of these questions, the general basis of GM studies will be described. But first it is important to explain why GM analysis was chosen over other methodologies. There are at least two other different ways of extracting and quantifying shape information from an object apart from GM methods: (1) measuring angles between specific landmarks, and (2) calculating ratios from distances between landmarks. These two techniques impose certain restrictions: they can not provide a graphical representation of shape modifications; and they solely provide specific and local shape quantification, which means that several ratios and/or angles in different parts of the object must be measured to obtain a complete quantification of the object shape. Also, there must be some previous hypothesis to select which ratios and/or angles are measured, while in the case of GM analyses the quantification of shape is made from the whole set of landmarks with no *a priory* ideas about the possible location of shape changes. Moreover, GM is a multivariate technique that allows the statistic dissociation of shape and size information from a group of objects. Shape can be understood as the proportional relationships among landmarks defined on different parts of an object. A more precise and mathematically useful definition is the one proposed by Kendall (1977): shape is all the geometrical information that remains when location, scale and rotational effects are filtered out from an object. This is to say that if we have a very precise wooden replica of an African elephant in our desk, it will have the same shape of a real elephant living in the Savannah, which presents a different scale, location and rotational

information (of course if you don't happen to have a real one in your desk!). This definition is mathematically useful because it expresses exactly what GM analysis does through a generalized least squares Procrustes superimposition analysis (GPA) (Rohlf, 1990). But first, the group of objects to be studied must be resumed and simplified into numerical landmark matrices. To achieve this, homologous landmarks should be defined and placed on the object of interest so that its form is recognized in those landmarks. Also, the defined landmarks must provide some meaningful information, like a particular biological significance or certain important aspects of the structure form (Zelditch et al., 2004). Once we have our set of objects transformed into a set of numerical landmark matrices, a GPA can be performed. As it was mentioned above, GPA resembles the definition of shape, because it normalizes scale, translational, and rotational differences between the landmark configurations of the data set (Rohlf and Bookstein, 1990). GPA returns as output Procrustes residuals, which are coordinates of a landmark configuration obtained by a Procrustes superimposition. They are residuals in the sense that they indicate the deviation of each specimen from the mean (Zelditch et al., 2004). Centroid size (CS) values for each specimen or object are given as a secondary output[1]. CS is a measure of geometric scale, calculated as the square root of the addition of squared distances between each landmark and the centroid of the landmark configuration. The Procrustes residuals can be used in several ways depending on the question that is being assessed. For example, a simple way to analyse the shape variation of a sample that is associated with a given variable (*e.g.* CS) would be to perform a principal component analysis[2] (PCA) on these

[1]It is called *secondary output*, because they are actually calculated before the GPA and are used within it to scale the landmark configurations to unit centroid size by dividing each coordinate of each landmark by the centroid size of that configuration (Zelditch et al., 2004)

[2]The central idea of the principal component analysis (PCA) is to reduce the dimensionality of a data set consisting of a large number of interrelated variables, while retaining as much as possible of the variation present in it. This is achieved by transforming the data set into a new set of variables, the

Procrustes residuals (Dryden and Mardia, 1998), and to evaluate which of the different principal components (PCs) have a significant regression with that given variable by means of a multivariate regression. Other specific GM methods will be described below. All GM analyses were performed using Morphologika software (O'Higgins and Jones, 1998), MorphoTools (Specht et al., 2007) and R (Team, 2010).

Landmarks

Landmarks are discrete anatomical loci that can be recognized as the same loci in all specimens / objects under study (Zelditch et al., 2004). In this thesis, the main objective is to elucidate the relationship between the bony endocranium and the brain soft tissue through the maturation process. Consequently, we chose those anatomical landmarks that best describe this relationship. Therefore, landmarks were placed at the surface of the brain cortex and along the endocranial vault of each individual using Amira. The relationship between the cranial base and the brain base was not evaluated as it was not possible to find representative landmarks at this brain region (Maudgil et al., 1998). 14 endocranial landmarks describing the endocranial vault were chosen (Howells, 1978; McCarthy, 2001; Aiello and Dean, 2002; Bruner et al., 2003; Lieberman et al., 2007; Balzeau et al., 2009) (Table 5.1, Figure 5.3), and 28 brain landmarks delineating the brain cortex surface were determined (Maudgil et al., 1998; Free et al., 2001; Aldridge et al., 2005; Richtsmeier et al., 2006) (Table 5.2, Figure 5.4). Landmark precision was evaluated by taking all 14 endocranial landmarks of one individual of the CT data base five different times, and the same procedure was performed for all 28 brain landmarks of one individual

principal components (PCs), which are uncorrelated, and ordered so that the first few retain most of the variation present in all the original variables (Jolliffe, 2002).

of the MR data base. In both cases the average standard deviation of all landmarks was calculated and compared with the average distance among all landmarks to assay the error percentage; if this error percentage is equal or lower than 3% the accuracy of the landmark positioning is accepted (Corner et al., 1992; von Cramon-Taubadel N., 2007). Landmark collections of each individual were standardised by symmetry using the sagittal plane to obtain symmetric individuals. To evaluate if this procedure augmented the explanatory variance of the shape analyses reinforcing the signal, but without loosing information, results of non standardized individuals were compared with those of symmetric ones. For the search of asymmetries this last procedure of symmetrization was not applied, and the raw data were used.

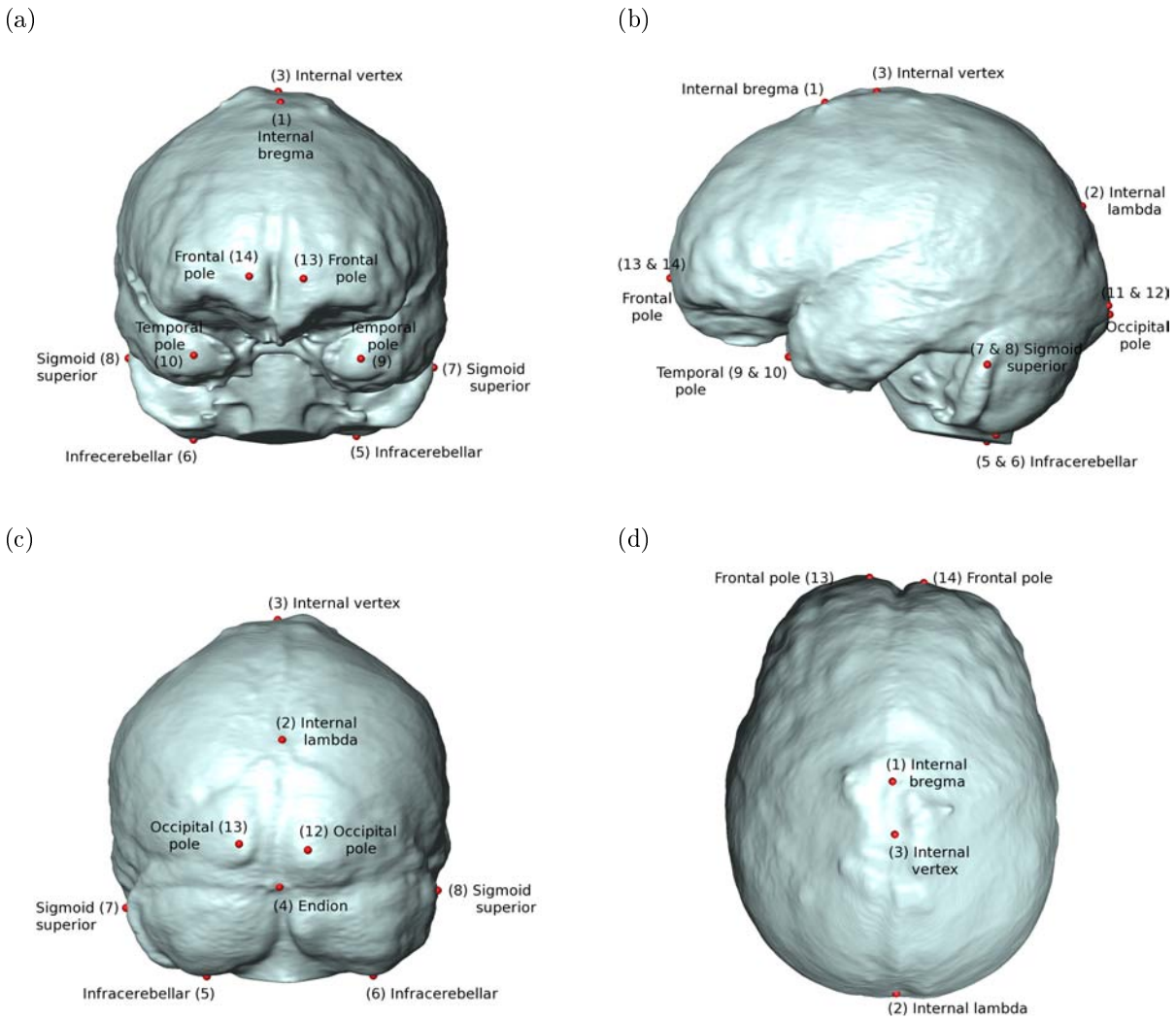

Figure 5.3: **Endocranial Landmarks.** See Table 5.1 for description of landmarks. **(a)** Coronal anterior view. **(b)** Sagital right view. **(c)** Coronal posterior view. **(d)** Horizontal superior view.

Table 5.1: **Endocranial landmarks.** List of anatomical landmarks placed in the 3D reconstructions of the endocranial vault. See Figure 5.3 for graphical representation of these landmarks in a 3D endocranial vault.

#	Name	Description
1	Internal bregma	The internal point at which the sagittal and coronal sutures meet.
2	Internal lambda	The internal point at which the lambdoid and sagittal sutures meet.
3	Internal vertex	The superior internal point of the cranium in the midsagittal contour when the skull is in Frankfurt Horizontal.
4	Endinion	Point in the median plane at the junction of the sagittal and lateral sinuses.
5	Infracerebellar (left)	Most inferior point on cerebella (not on the transverse sinus), left side.
6	Infracerebellar (right)	Most inferior point on cerebella (not on the transverse sinus), right side.
7	Sigmoid superior (left)	Most superior point on the sigmoid sinus, left side.
8	Sigmoid superior (right)	Most superior point on the sigmoid sinus, right side.
9	Temporal pole (left)	Most anterior prominent point on the temporal lobe, left side.
10	Temporal pole (right)	Most anterior prominent point on the temporal lobe, right side.
11	Occipital pole (left)	Most posterior prominent point on the occipital lobe, left side.
12	Occipital pole (right)	Most posterior prominent point on the occipital lobe, right side.
13	Frontal pole (left)	Most anterior prominent point on the frontal lobe, left side.
14	Frontal pole (right)	Most anterior prominent point on the frontal lobe, right side.

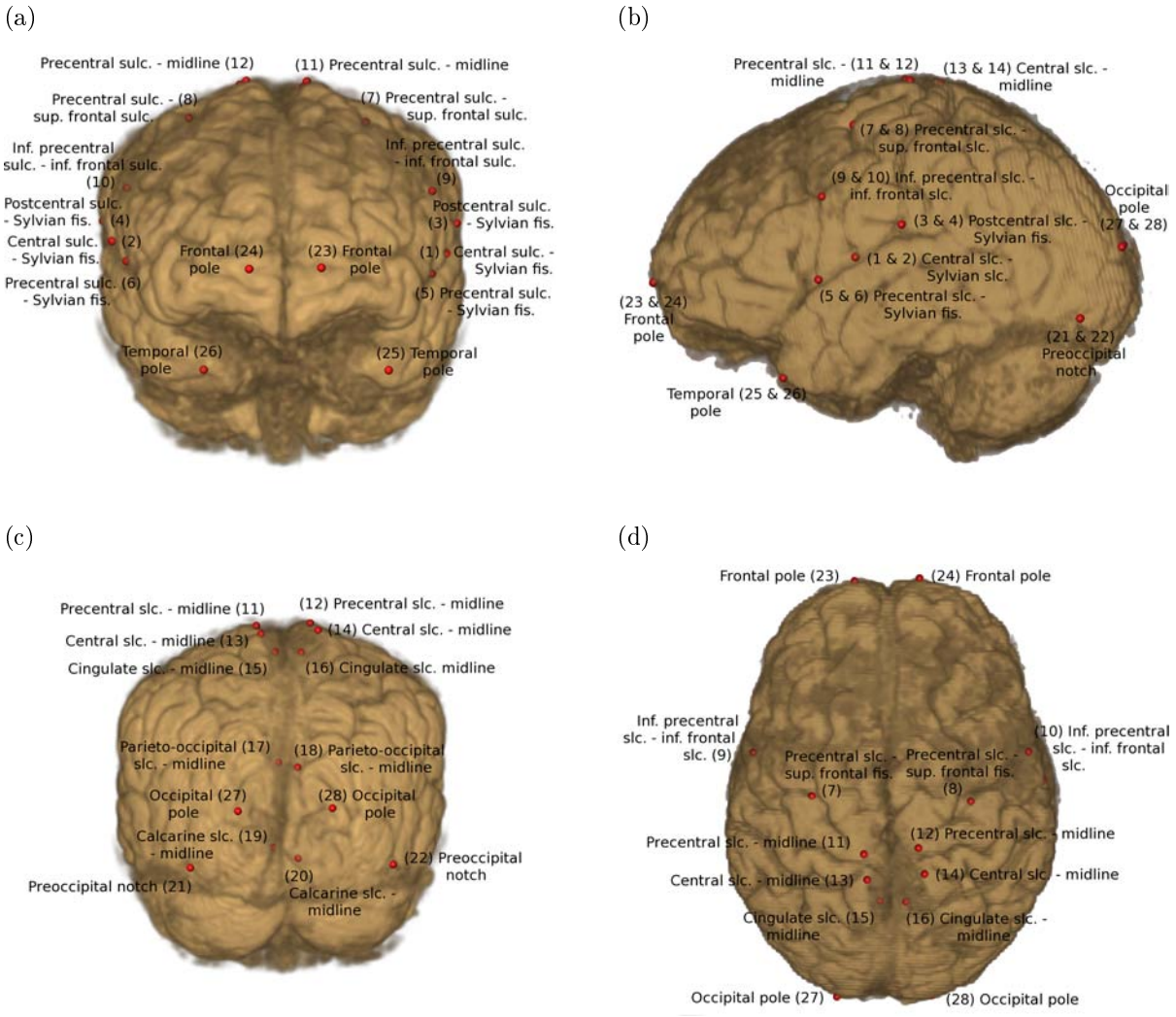

Figure 5.4: **Brain landmarks.** See Table 5.2 for description of landmarks. **(a)** Coronal anterior view. **(b)** Sagital right view. **(c)** Coronal posterior view. **(d)** Horizontal superior view.

Table 5.2: **Brain landmarks.** List of anatomical landmarks placed in the 3D reconstructions of the brain cortex. See Figure 5.4 for graphical representation of these landmarks in a 3D brain.

#	Description
1	Central sulcus intersection with the Sylvian fissure, left hemisphere.
2	Central sulcus intersection with the Sylvian fissure, right hemisphere.
3	Postcentral sulcus intersection with the Sylvian fissure, left hemisphere.
4	Postcentral sulcus intersection with the Sylvian fissure, right hemisphere.
5	Precentral sulcus intersection with the Sylvian fissure, left hemisphere.
6	Precentral sulcus intersection with the Sylvian fissure, right hemisphere.
7	Precentral sulcus intersection with the superior frontal sulcus, left hemisphere.
8	Precentral sulcus intersection with the superior frontal sulcus, right hemisphere.
9	Inferior precentral sulci with inferior frontal sulci, left hemisphere.
10	Inferior precentral sulci with inferior frontal sulci, right hemisphere.
11	Precentral sulcus to the midline, left hemisphere.
12	Precentral sulcus to the midline, right hemisphere.
13	Central sulcus to the midline, left hemisphere.
14	Central sulcus to the midline, right hemisphere.
15	Termination of cingulate sulcus at the midline, left hemisphere.
16	Termination of cingulate sulcus at the midline, right hemisphere.
17	Parieto-occipital sulcus to the midline, left hemisphere.
18	Parieto-occipital sulcus to the midline, right hemisphere.
19	Calcarine sulcus to the midline, left hemisphere.
20	Calcarine sulcus to the midline, right hemisphere.
21	Preoccipital notch, left hemisphere.
22	Preoccipital notch, right hemisphere.
23	Frontal pole, or the anterior end of the hemisphere, left hemisphere.
24	Frontal pole, or the anterior end of the hemisphere, right hemisphere.
25	Temporal pole, or the anterior end of the temporal lobe, left hemisphere.
26	Temporal pole, or the anterior end of the temporal lobe, right hemisphere.
27	Occipital pole, or the posterior end of the hemisphere, left hemisphere.
28	Occipital pole, or the posterior end of the hemisphere, right hemisphere.

What kind of growth and development curve has the endocranium and the brain?

Graphs quantifying growth and development of endocranial vault and cortical brain were constructed to determine what kind of curve described them best. Growth was quantified by means of size changes and development by means of shape changes according to the

theoretical framework chosen. Size can be quantified through the CS value given by the GM analysis described above, or through the volume of the structure being analysed. This last variable describe more exhaustively the size of a determined structure as it does not depend on the landmarks chosen and resumes the whole entity size. For this reason, and because this volumetric information was available in 3D imaging data, the size of the brain was expressed in terms of the BV (GMV plus WMV); and the endocranium size was determined by the endocranial volume (ECV). On the other hand, brain and endocranial degree of shape differentiation is a much more complicated variable to quantify; it was measured using two different approaches. For the first one, the Procrustes residuals of the sample had to be calculated through a GPA, a PCA had to be performed on those residuals, and finally the shape trajectory that followed the ontogenetic sample displaying the first three PCs had to be evaluated. The second methodology also started from a GPA for the whole sample, obtaining the Procrustes distances[1], the conventional measure of a morphometric distance in geometric morphometrics (Marcus et al., 1996). The sample was divided into seven groups (0 to 35, 36-71, 72-107, 108-143, 144-179, 180-215, and 216 or more months old), and the degree of development of each individual was quantified through the measuring of the morphometric Procrustes distances between each individual and the average of the previous subgroup; for the first subgroup the distances were calculated in relation to the five youngest individuals (Zelditch et al., 2003). Then individuals were regrouped to calculate the means and standard error of the means (SEM) of the original four groups (infant-child, juvenile, adolescent and adult).

[1]The distance between two landmark configurations in the linear space tangent to Kendall's shape space (*i.e.* the tangent space) when centroid size of one is allowed to vary in order to minimize the distance between the shapes rather than fixed to unit size (Zelditch et al., 2004).

What relationship has the cranial capacity measured from the bony endocranium with the brain volume?

To distinguish how the relationship between the bony endocranium and brain volume modifies throughout the ontogenetic period analyzed, mean BV and mean ECV were measured for each year. Individuals from 0 to 4 years old were excluded from the analysis because the scarce data available for those ages prevented the comparisons between data sets. A simple ratio was calculated as the division between the BV and ECV means (mean BV / mean ECV), obtaining in this way a score that expressed the percentage occupied by the brain inside the endocranium for each year. It is important to mention that this procedure was followed because the CT data base and the MR data base were built from different individuals (see Materials for details); otherwise, it would have been sufficed to calculate the relationship between each individual BV and ECV, and analyse how it varies through the sample.

What degree of covariation exists between endocranial and brain shape?

To answer this question an indirect methodology must be used because of the same reason mentioned above (the two data bases come from different individuals). Therefore, the age was used as a proxy to compare both structures. Shape changes that were positively correlated with aging throughout the ontogenetic period analysed were quantified for brain and endocranial vault. Hence, we could evaluate the modifications associated with a certain age transition (*e.g.* from youth to adolescence) for both structures, and search for the presence of a common pattern; this common pattern was evaluated visually from the graphical GM results. Then, to quantify shape GM analyses were performed; in all

cases both data sets were separated into three age subgroups (infant-child and juveniles, juveniles and adolescents, and adolescents and adults), in order to obtain a better resolution of shape changes. The GM analysis was performed using MorphoTools software, and consisted of three main steps: (1) a general Procrustes analysis (GPA); (2) a regression of the Procrustes coordinates versus age, yielding regression coefficients; and, using these coefficients, (3) the construction of one single morphometric vector that accounts for all the shape changes that positively correlate with age. This morphometric vector is called common chronological shape vector (CCSV) and resumes all the shape changes that are related to aging for the analysed sample. For this GM analysis a strong correlation P (< 0.001) was used because it was found that this kind of study always results in a morphometric vector, even if the changes that such vector summarizes are not significantly correlated to age. For this reason, is more adequate to use a P lower than the usual one to ensure that the morphological vector is of interest.

When do endocranial petal patterns and brain macroscopic asymmetries grow and develop?

In order to quantify macroscopic asymmetries of endocranial vault and brain two different procedures were applied. The first one consisted of measuring the Procrustes distance between each individual and its reflection (also known as mirror image). This provided an overall value of asymmetry but it did not show in which region the asymmetries resided. The second procedure, performed with the aid of the MorphoTools software, consisted of: (1) a GPA between individual landmark configurations and their reflections; (2) for each pair of individual - individual mirror, delta vectors were calculated from bilateral landmarks; (3) asymmetric residuals were calculated with these vectors; and (4) a regres-

sion between the asymmetric residuals and age was performed to calculate the regression coefficients, which were normalized to obtain a regression axis (Mardia et al., 2000; Kent and Mardia, 2001). This regression axis, named common chronological asymmetric shape vector (CCASV), depicts all the shape changes associated with ageing for each group analysed. This methodology highlighted which asymmetric components were correlated to ageing, and it allowed the comparison between endocranial vault and brain patterns to search for covariation evidence. However, a phenomenon that must be taken into account when evaluating asymmetric patterns is the fact that in a normal sample of individuals, if the common and more frequent pattern of asymmetry is described, for example, in a left-right direction, there is always a minority that expresses the same pattern in the contrary direction (right-left). Consequently, this phenomenon obscures the more frequent asymmetric pattern by partially cancelling its signal with the contrary pattern of the minority. Therefore, to avoid this problem a maximization of the directional asymmetry was performed by an iterative procedure, called directional asymmetric optimization (DAO). This procedure rotates each specimen, one by one, until it reaches a local maximum so that the individuals that express an asymmetric pattern which is contrary to that of the majority are flipped. In this way, the asymmetric patterns were enhanced. The CCASV was calculated both with and without the application of this iterative optimization process, the results being compared at the end of the analysis.

Is there sexual dimorphism throughout endocranium and brain growth and development?

Concerning sexual dimorphism throughout growth and development of endocranial vault and brain, sexes were identified in each analysis described above, making it possible to

quantify sexual dimorphism. Analyses of covariance (ANCOVA) were performed with the aid of R software (Team, 2010), to detect differences between sexes eliminating the age effect.

Chapter 6

Results

After brain and endocranium 3D reconstruction, landmarks were placed and their accuracy was evaluated. This evaluation resulted satisfactory since landmark data sets of both endocranial vault and brain presented an average standard deviation that did not exceed 3% of the average distance calculated between landmarks (Corner et al., 1992; von Cramon-Taubadel N., 2007). It is important to mention that endocranial landmarks were much more precise, presenting an average standard deviation equal to 0.41%, while brain landmarks had a standard deviation of 1.05%.

What kind of growth and development curve has the endocranium and the brain?

The endocranial growth curve is depicted by ECV changes versus age in Figure 6.1. On the other hand, to depict brain growth four different graphs were arranged: (1) Figure 6.2 presenting GMV changes throughout the data set analysed; (2) Figure 6.3 for WMV changes; (3) Figure 6.4 presenting the relationship between WMV and GMV; and (4) Figure 6.5 presenting the sum of these two (BV), which shows the size variations that suffer the whole brain through the period analysed. These growth curves were divided

into ontogenetic periods to obtain linear regressions for males and females that could be evaluated with statistical methods (such as ANCOVA) to quantify sexual dimorphism. ECV presents high growth rates and follows a logarithmic-type curve from birth to approximately 30 months old, then the rate diminishes and arrives to a plateau. Females reach this plateau approximately at an age of 10 and males at an age of 15 (Figure 6.1). ECV showed sexual dimorphism in all the analysed periods, with male endocranial capacity being always larger than female one (Tables B.1, B.2, B.3). GMV presents an "inverted U" type curve, with a high growth rate before arriving to its maximum peak (this maximum peak occurs earlier in females than in males), and then decreasing slowly. In the last period it is evident that the GMV growth rate decreases more sharply in males than in females (Figure 6.2). On the other hand, WMV grows following lineal curves throughout the whole period analysed, with different rates in the different sub-periods. When reaching young adulthood, the WMV growth rate seems to increase in males compared to females (Figure 6.2). The ratio GMV / WMV decreases throughout the whole ontogenetic period analysed, with both sexes presenting very similar decaying rates until adulthood, when females show a lower rate compared to males (Figure 6.4). Finally, BV growth trajectory is similar to that of GMV, an "inverted U" curve with its characteristic maximum peak. Once more, females arrive first to this peak and in the last period analysed the growth rate decreases much more sharply for males than for females (Figure 6.5). In the case of GMV, WMV and BV, sexual dimorphism was also found throughout the ontogenetic periods analysed, with males presenting always larger volumes than females (Tables B.4, B.5, B.6, B.7, B.8, B.9, B.10, B.11, B.12). Even though this difference was significant in all periods, the P value was much more significant for the juvenile to ado-

lescent and adolescent to adult groups ($P \ll 0.0001$) than for the infant-child to juvenile group ($0.0005 < P < 0.05$). Regarding the ratio GMV / WMV, sexual dimorphism was only found in the last period, from adolescent to adult ($P < 0.05$) (Figure 6.4.d, Tables B.13, B.14, B.15).

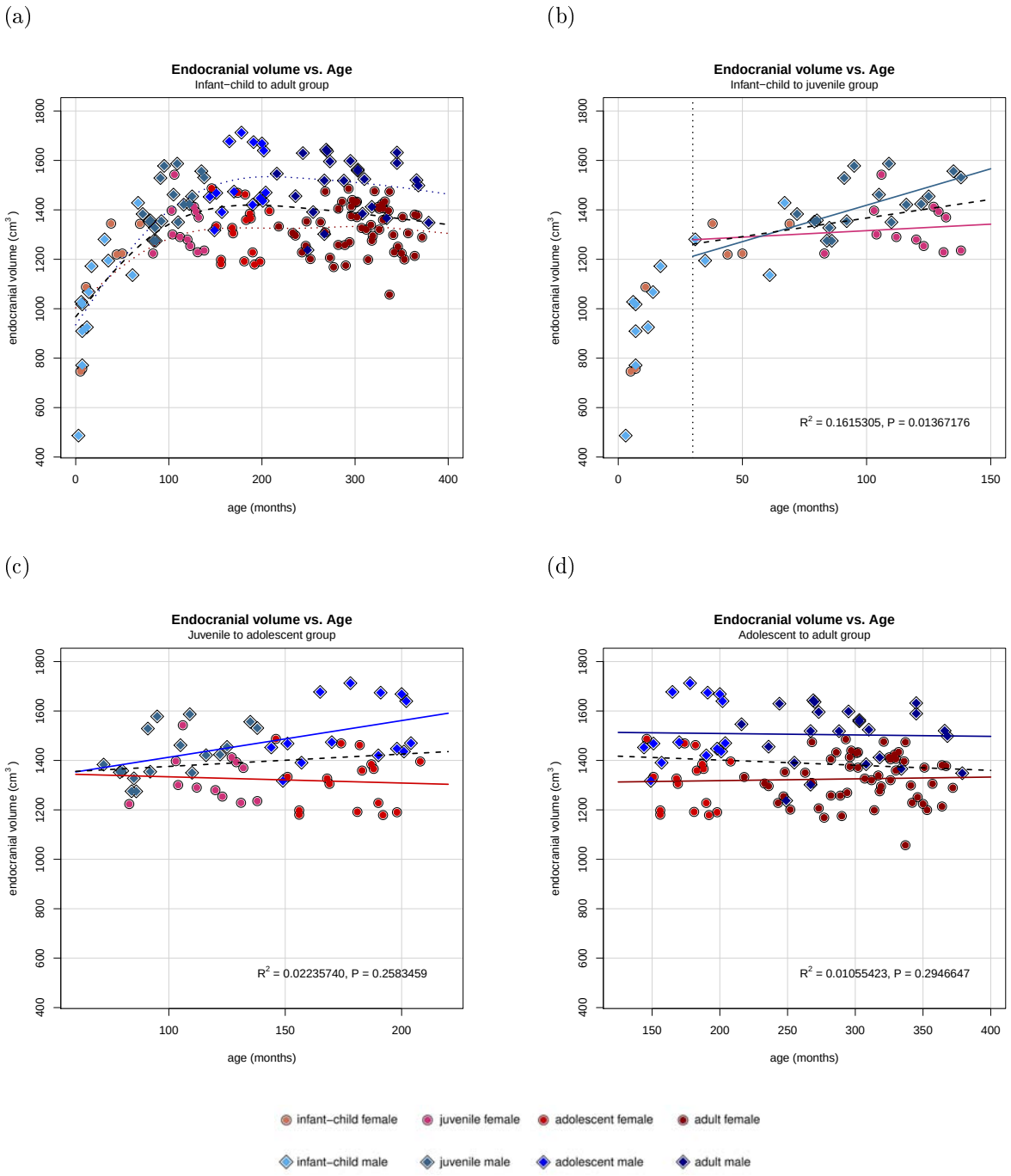

Figure 6.1: **Endocranial growth vs. age.** **(a)** All individuals (infant-child to adult group). Curve legends: dashed black curve: smooth spline for all individuals; dotted red curve: smooth spline for females; dotted blue curve: smooth spline for males. **(b)** Infant-child to juvenile group. Curve legends: dashed black line: lineal regression for individuals from 30 to 143 months; solid red line: lineal regression for females from 30 to 143 months; solid blue line: lineal regression for males from 30 to 143 months. Dimorphism was found between sexes ($P < 0.005$) (see Table B.1 for ANCOVA details). **(c)** Juvenile to adolescent group. Curve legends (valid for *(c)* and *(d)*): dashed black line: lineal regression for all individuals of the group; solid red line: lineal regression for all group females; solid blue line: lineal regression for all group males. Dimorphism was found between sexes ($P \ll 0.0001$) (Table B.2). **(d)** Adolescent to adult group. Dimorphism was found between sexes ($P \ll 0.0001$) (Table B.3).

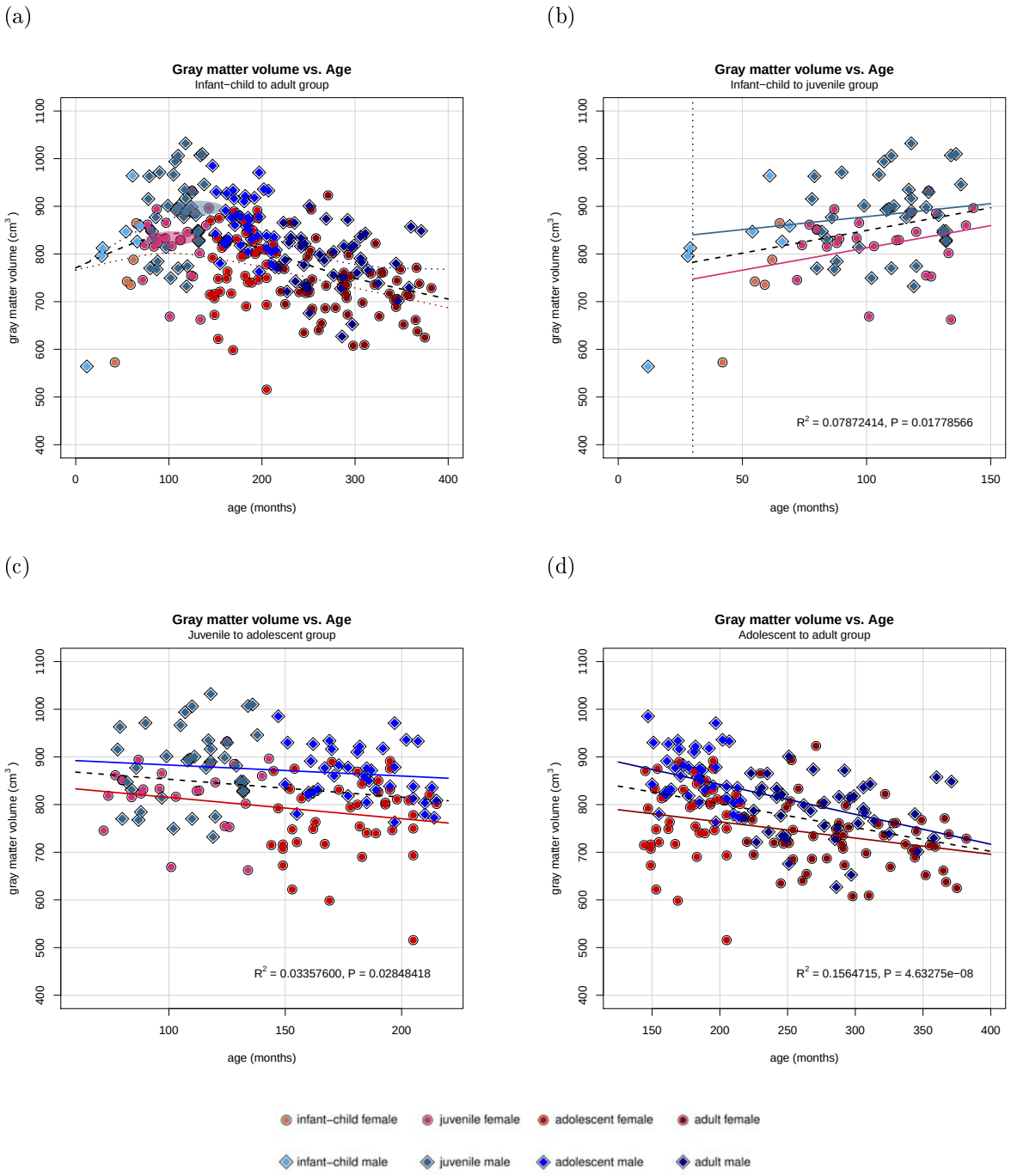

Figure 6.2: **Gray matter growth vs. age. (a)** All individuals (infant-child to adult group). Curve legends: dashed black curve: smooth spline for all individuals; dotted red curve: smooth spline for females; dotted blue curve: smooth spline for males. **(b)** Infant-child to juvenile group. Curve legends: dashed black line: lineal regression for individuals from 30 to 143 months; solid red line: lineal regression for females from 30 to 143 months; solid blue line: lineal regression for males from 30 to 143 months. Dimorphism was found between sexes ($P < 0.001$) (see Table B.4 for ANCOVA details). **(c)** Juvenile to adolescent group. Curve legends (valid for *(c)* and *(d)*): dashed black line: lineal regression for all individuals of the group; solid red line: lineal regression for all group females; solid blue line: lineal regression for all group males. Dimorphism was found between sexes ($P \ll 0.0001$) (Table B.5). **(d)** Adolescent to adult group. Dimorphism was found between sexes ($P \ll 0.0001$) (Table B.6).

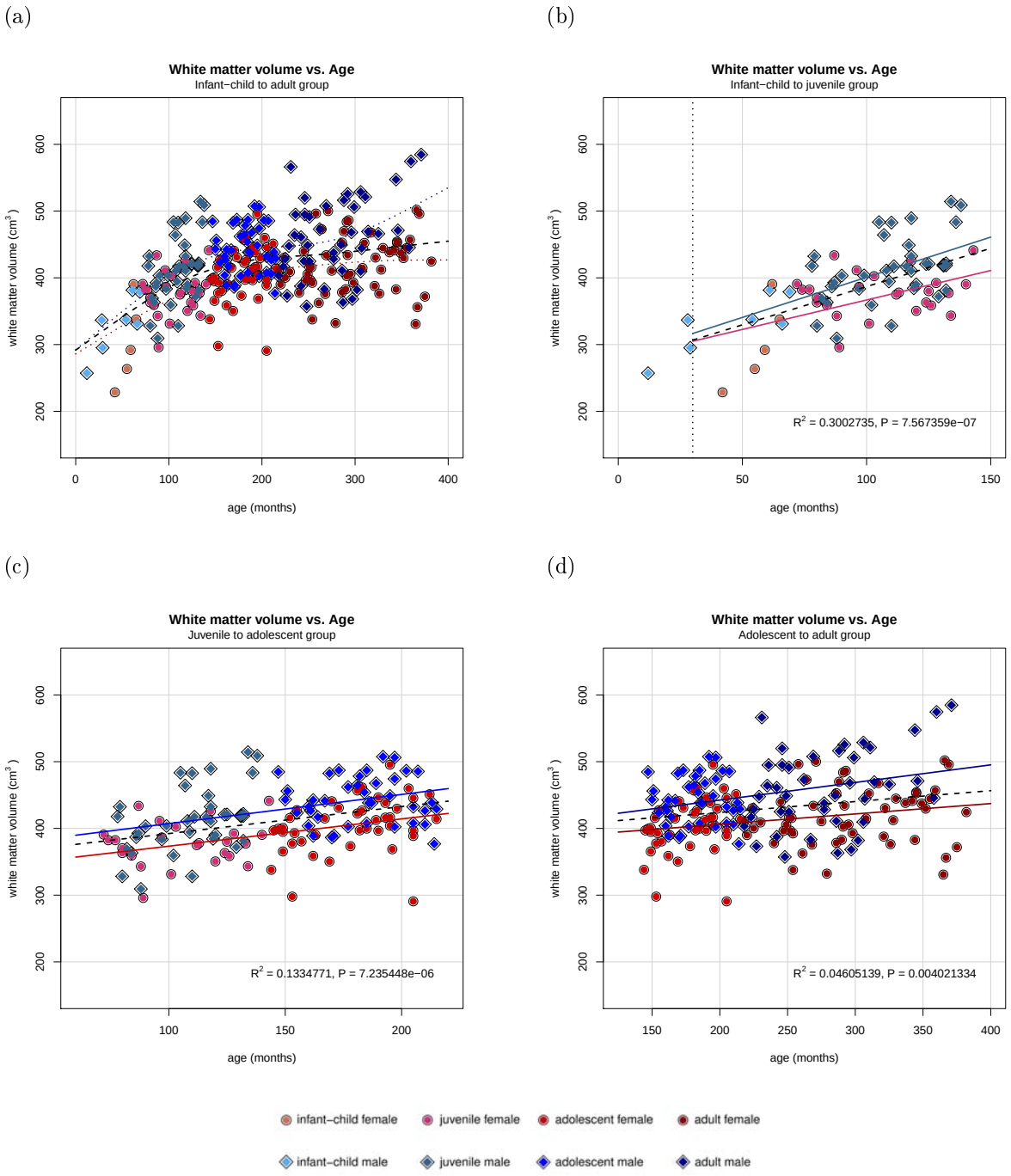

Figure 6.3: **White matter growth vs. age. (a)** All individuals (infant-child to adult group). Curve legends: dashed black curve: smooth spline for all individuals; dotted red curve: smooth spline for females; dotted blue curve: smooth spline for males. **(b)** Infant-child to juvenile group. Curve legends: dashed black line: lineal regression for individuals from 30 to 143 months; solid red line: lineal regression for females from 30 to 143 months; solid blue line: lineal regression for males from 30 to 143 months. Dimorphism was found between sexes ($P < 0.005$) (see Table B.7 for ANCOVA details). **(c)** Juvenile to adolescent group. Curve legends (valid for *(c)* and *(d)*): dashed black line: lineal regression for all individuals of the group; solid red line: lineal regression for all group females; solid blue line: lineal regression for all group males. Dimorphism was found between sexes ($P \ll 0.0001$) (Table B.8). **(d)** Adolescent to adult group. Dimorphism was found between sexes ($P \ll 0.0001$) (Table B.9).

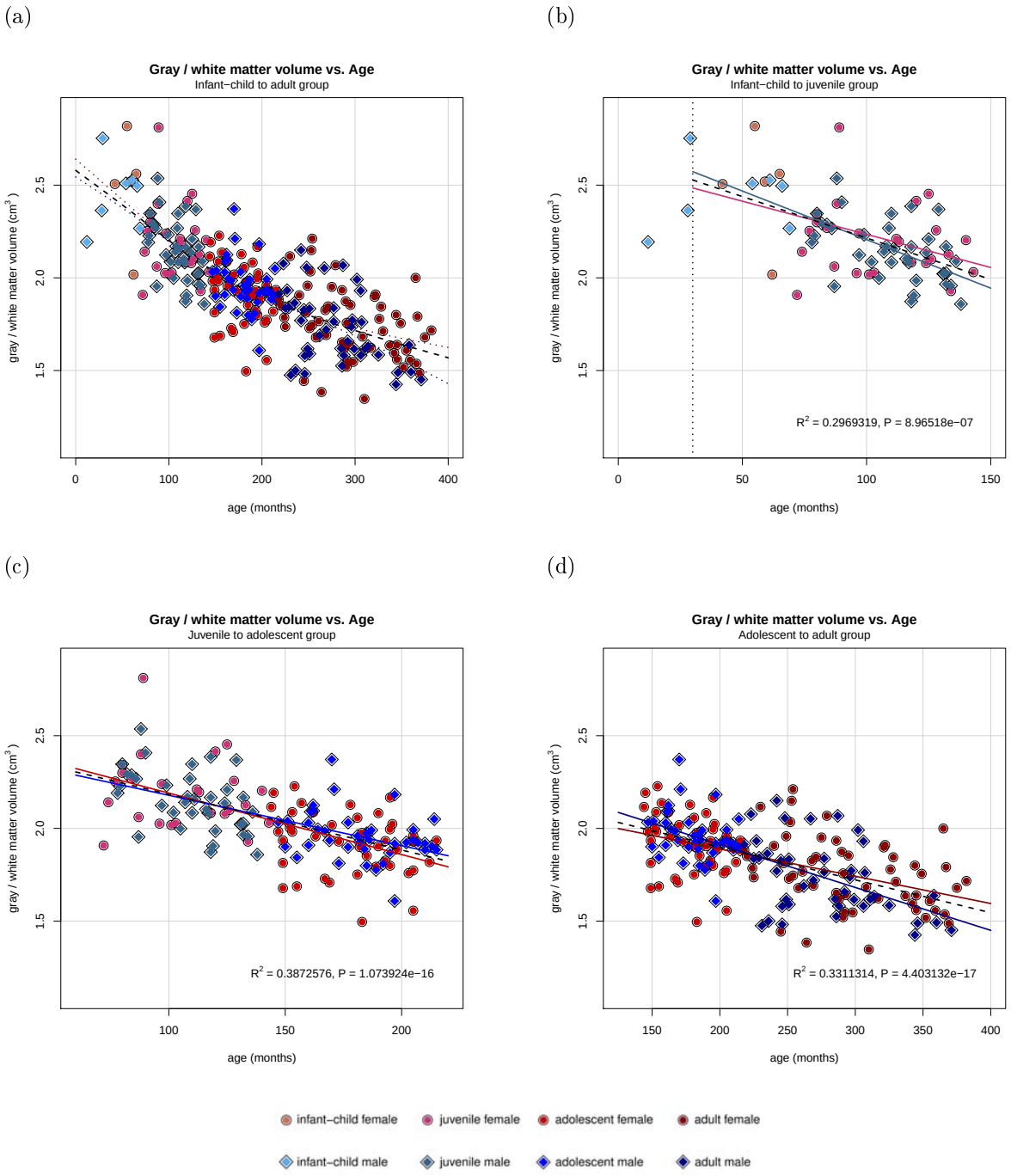

Figure 6.4: **White and grey matter growth relation vs. age. (a)** All individuals (infant-child to adult group). Curve legends: dashed black curve: smooth spline for all individuals; dotted red curve: smooth spline for females; dotted blue curve: smooth spline for males. **(b)** Infant-child to juvenile group. Curve legends: dashed black line: lineal regression for individuals from 30 to 143 months; solid red line: lineal regression for females from 30 to 143 months; solid blue line: lineal regression for males from 30 to 143 months. Dimorphism was no found between sexes ($P > 0.1$) (see Table B.13 for ANCOVA details). **(c)** Juvenile to adolescent group. Curve legends (valid for *(c)* and *(d)*): dashed black line: lineal regression for all individuals of the group; solid red line: lineal regression for all group females; solid blue line: lineal regression for all group males. Dimorphism was no found between sexes ($P > 0.5$) (Table B.14). **(d)** Adolescent to adult group. Dimorphism was found between sexes ($P < 0.05$) (Table B.15).

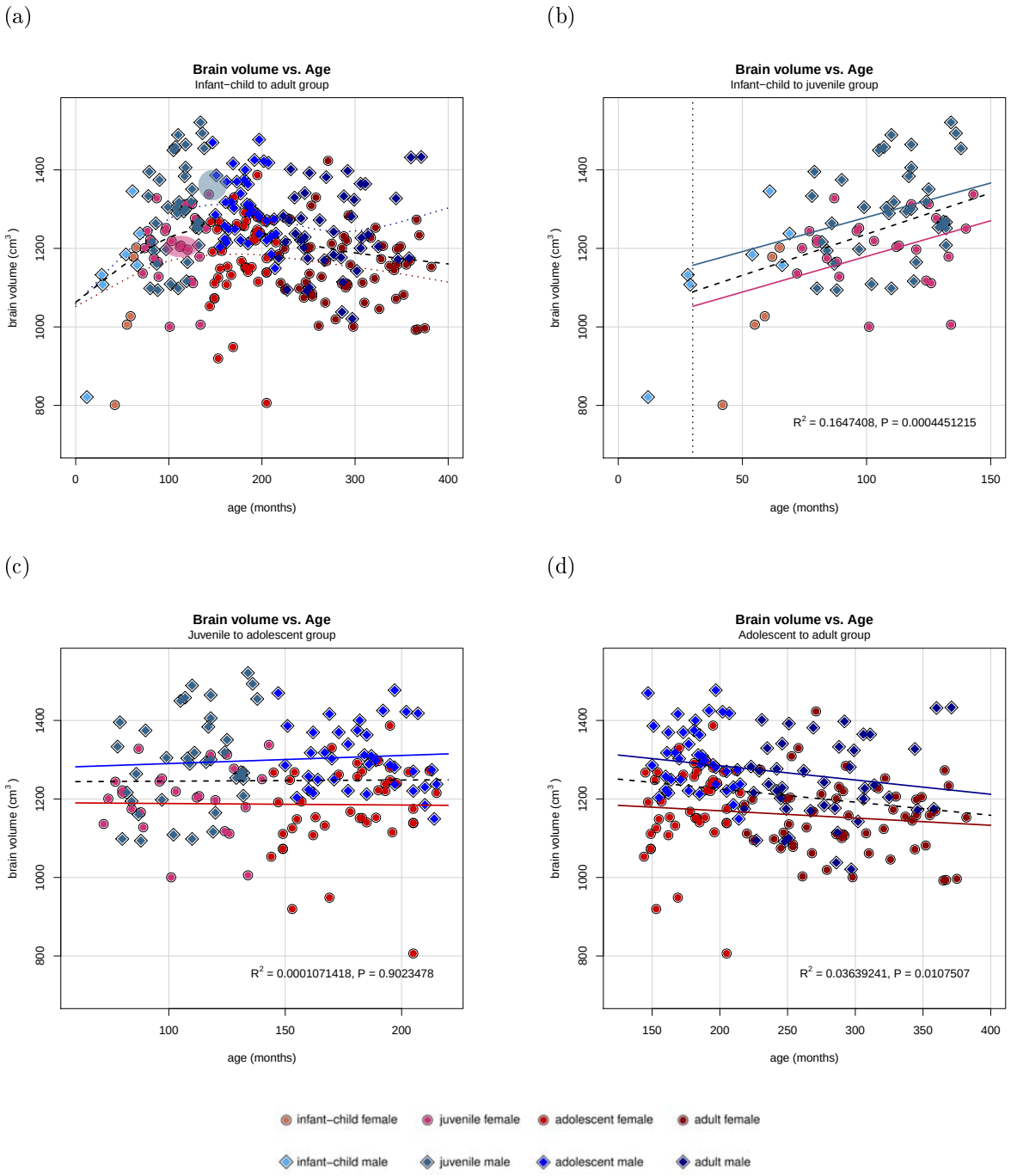

Figure 6.5: **Brain growth vs. age. (a)** All individuals (infant-child to adult group). Curve legends: dashed black curve: smooth spline for all individuals; dotted red curve: smooth spline for females; dotted blue curve: smooth spline for males. **(b)** Infant-child to juvenile group. Curve legends: dashed black line: lineal regression for individuals from 30 to 143 months; solid red line: lineal regression for females from 30 to 143 months; solid blue line: lineal regression for males from 30 to 143 months. Dimorphism was found between sexes ($P < 0.001$) (see Table B.10 for ANCOVA details). **(c)** Juvenile to adolescent group. Curve legends (valid for *(c)* and *(d)*): dashed black line: lineal regression for all individuals of the group; solid red line: lineal regression for all group females; solid blue line: lineal regression for all group males. Dimorphism was found between sexes ($P \ll 0.0001$) (Table B.11). **(d)** Adolescent to adult group. Dimorphism was found between sexes ($P \ll 0.0001$) (Table B.12).

The endocranial shape trajectory described by the first three PCs is shown in Figures 6.6 and 6.7; while brain shape trajectories described by the first three PCs are shown in Figure 6.8 and 6.9.

The endocranial vault shape trajectory presents a linear curve, with the first period (from infant-child to juvenile) being the most distant trajectory (Figure 6.6). When moving from a negative PC1 value (dashed wireframe in Figure 6.7.a) to a positive one (solid wireframe in Figure 6.7.a) several proportional shape changes can be described: elongation of internal vertex - internal lambda distance; a great shortening of internal vertex - internal bregma distance; and the elongation of sigmoid superior - temporal pole distance. These changes imply a proportional elongation of the parietal region in a ventral-dorsal direction and also a proportional elongation of the temporal region in an anterior-posterior direction. The comparison of PC2 negative values with positive ones (Figure 6.7.b) denotes the following proportional shape changes: elongation of vault height, mainly through internal vertex - internal lambda distance elongation; and the reduction of the vault width, with an occipital region protrusion. And finally, when moving from a negative PC3 value to a positive one (Figure 6.7.c) the most important proportional shape changes observed are: the elongation of endion - sigmoid superior - temporal pole distances, which denotes a temporal region widening; and the reduction of the vault height together with a localized widening of sigmoid superior left-right landmarks distance.

The brain shape trajectory described by the first three PCs shows a non linear curve; the first period (from infant-child to juvenile) is relatively short, while the last one (from adolescent to adult) presents the longest distance (Figure 6.8). When moving from a neg-

ative PC1 value (dashed wireframe in Figure 6.9.a) to a positive one (solid wireframe in Figure 6.9.a) several proportional shape changes can be described: elongation of calcarine sulcus - occipital pole and parieto-occipital sulcus - cingulate sulcus distances, which implies an important elongation of the parieto-occipital region in a dorso-ventral direction; and a posterior depression of frontal and parietal poles, with a proportional reduction of the brain length. When comparing PC2 negative values with positive ones (Figure 6.9.b) the following proportional shape changes are detected: strong protrusion of the occipital region, mainly of the occipital poles; and prefrontal narrowing along the entire precentral sulcus. When moving from a negative PC3 value to a positive one (Figure 6.9.c) the following proportional shape changes arise: elongation of calcarine sulcus - preoccipital notch distance, while preoccipital notch displaced anteriorly; elongation of cingulate sulcus - parieto-occipital sulcus distance; reduction of distance between hemispheres and backwards extension of Sylvian fissure, while widening of temporal lobes takes place.

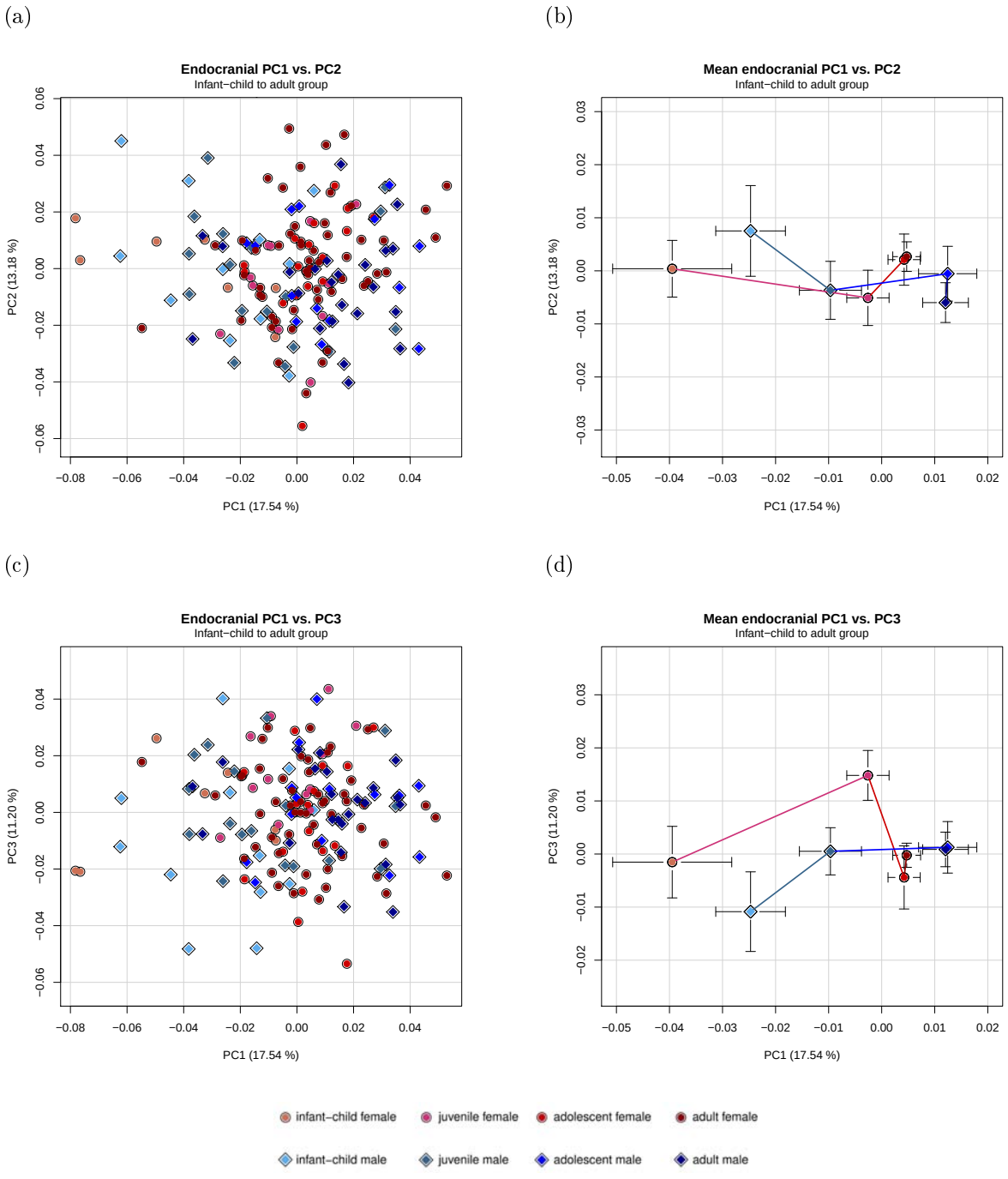

Figure 6.6: **Endocranial PCs shape trajectory (continued on next page).** **(a)** Endocranial PC1 vs. PC2. **(b)** Mean age group endocranial PC1 vs. PC2 scores with their respective standard error of the mean (SEM). **(c)** Endocranial PC1 vs. PC3. **(d)** Mean age group endocranial PC1 vs. PC3 scores with their respective SEM.

(e)

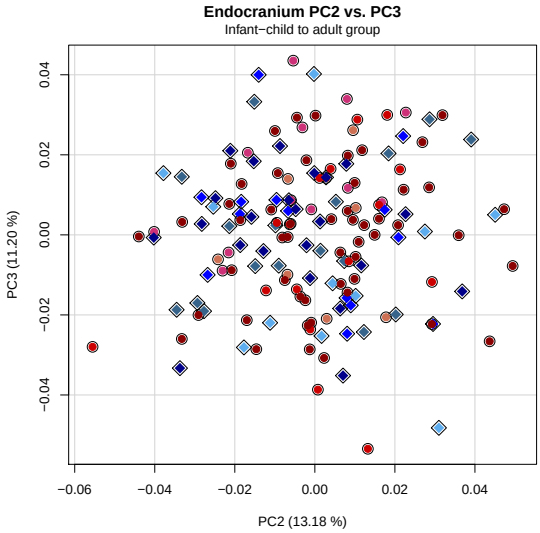

(f)

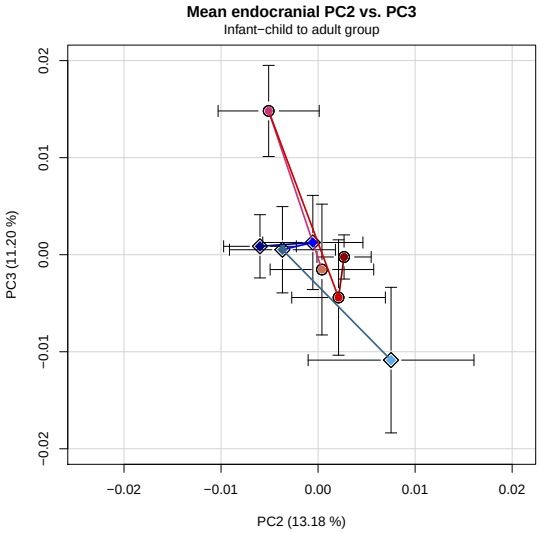

Figure 6.6: **Endocranial PCs shape trajectory (continued). (e)** Endocranial PC2 vs. PC3. **(f)** Mean age group endocranial PC2 vs. PC3 scores with their respective SEM.

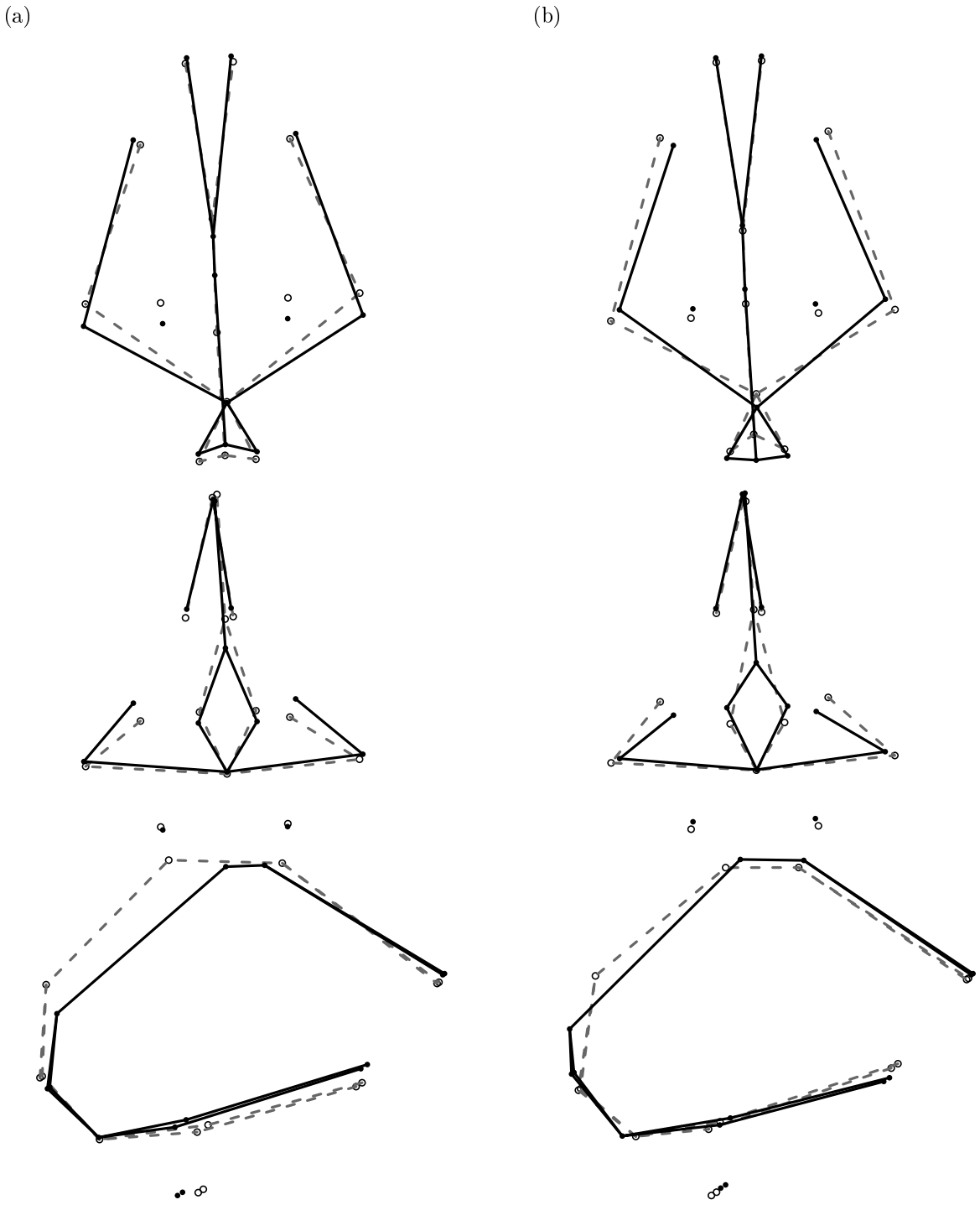

Figure 6.7: **Edocranial PCs shape deformations (continued on next page). (a)** Endocranial shape changes deformations from a negative PC1 value (dashed wireframe) to a positive one (solid wireframe). **(b)** Endocranial shape changes deformations from a negative PC2 value (dashed wireframe) to a positive one (solid wireframe).

(c)

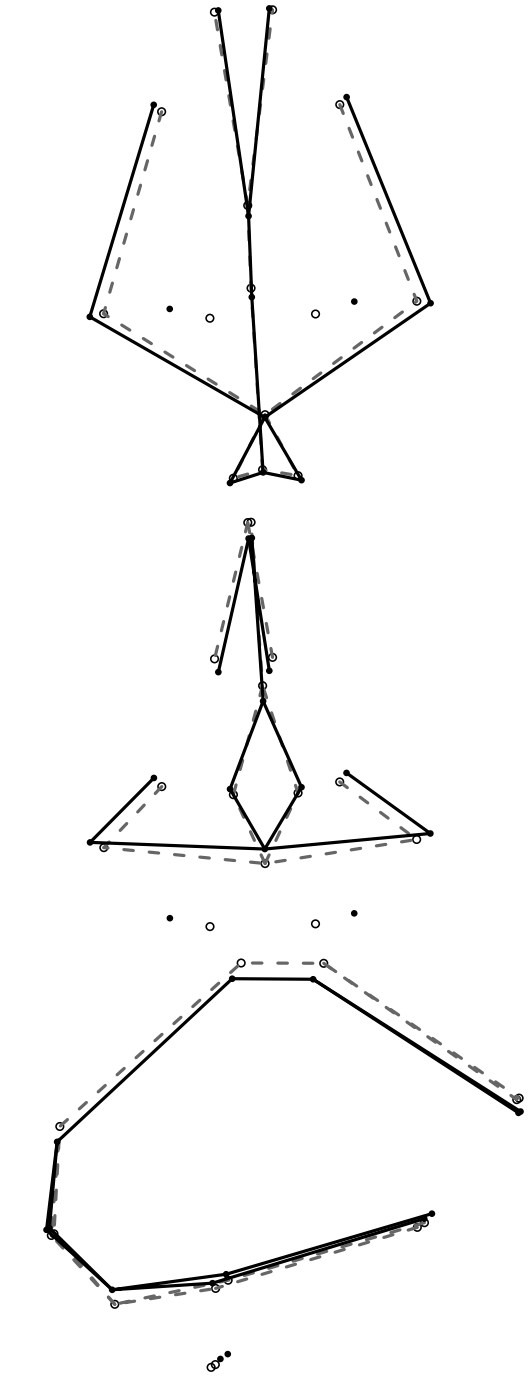

Figure 6.7: **Edocranial PCs shape deformations (continued). (c)** Endocranial shape changes deformations from a negative PC3 value (dashed wireframe) to a positive one (solid wireframe).

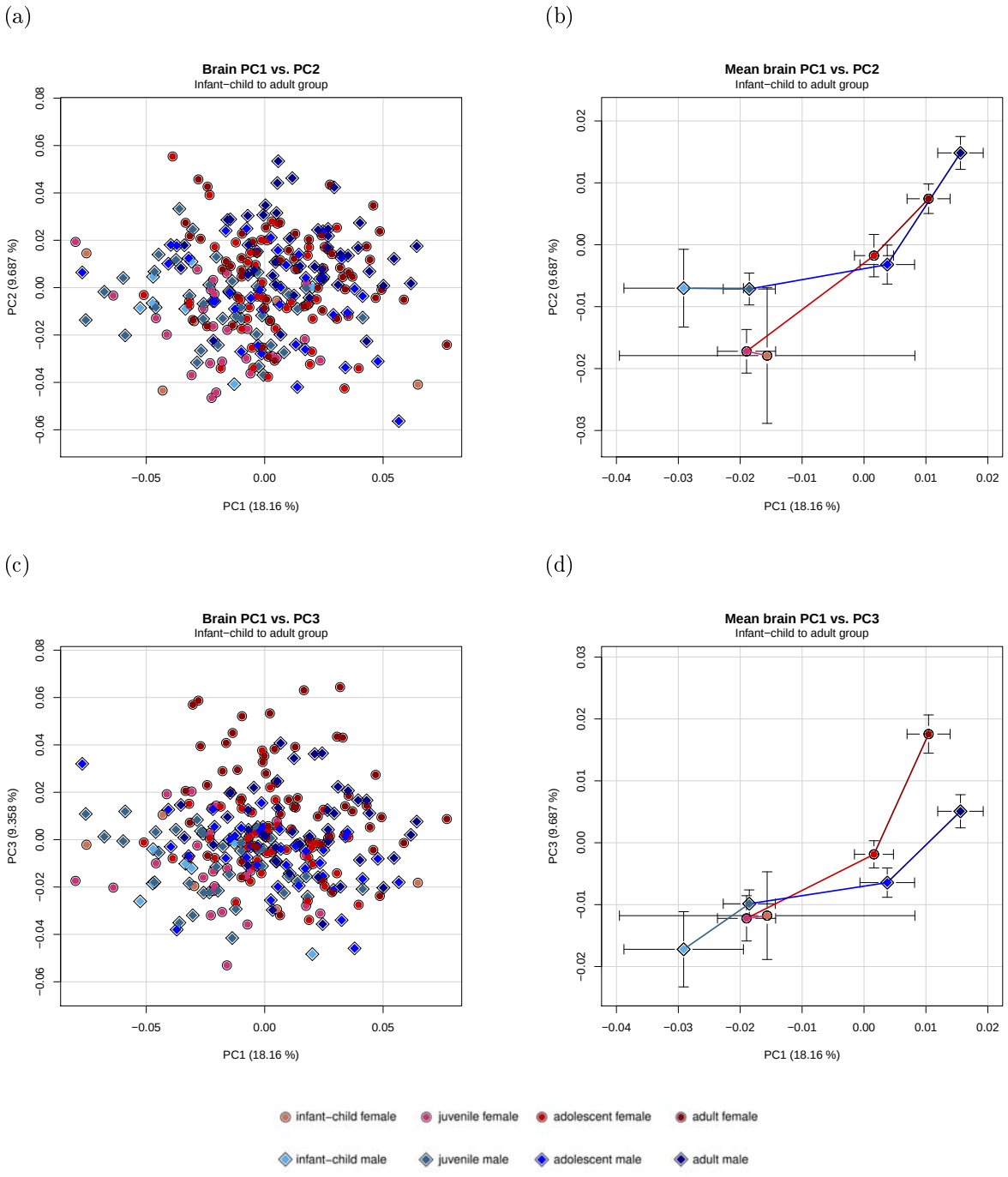

Figure 6.8: **Brain PCs shape trajectory (continued on next page).** **(a)** Brain PC1 vs. PC2. **(b)** Mean age group brain PC1 vs. PC2 scores with their respective standard error of the mean (SEM). **(c)** Brain PC1 vs. PC3. **(d)** Mean age group brain PC1 vs. PC3 scores with their respective SEM.

(e)

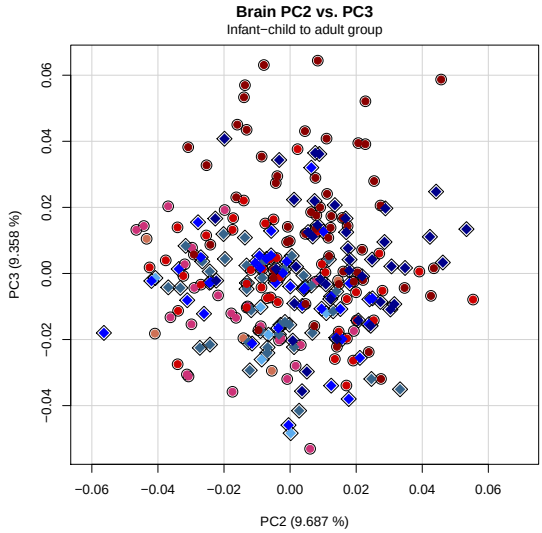

(f)

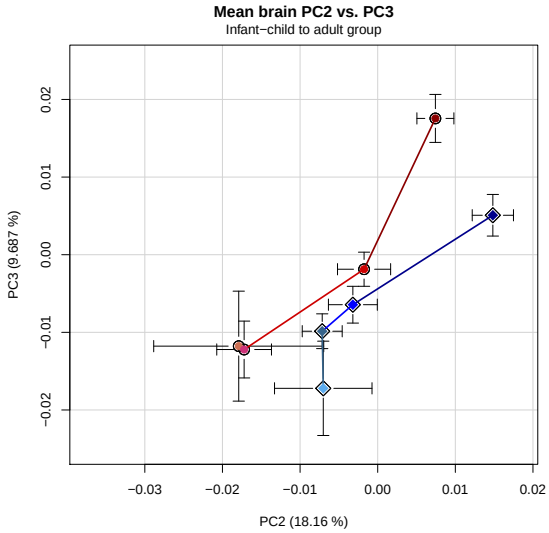

Figure 6.8: **Brain PCs shape trajectory (continued).** **(e)** Brain PC2 vs. PC3. **(f)** Mean age group brain PC2 vs. PC3 scores with their respective SEM.

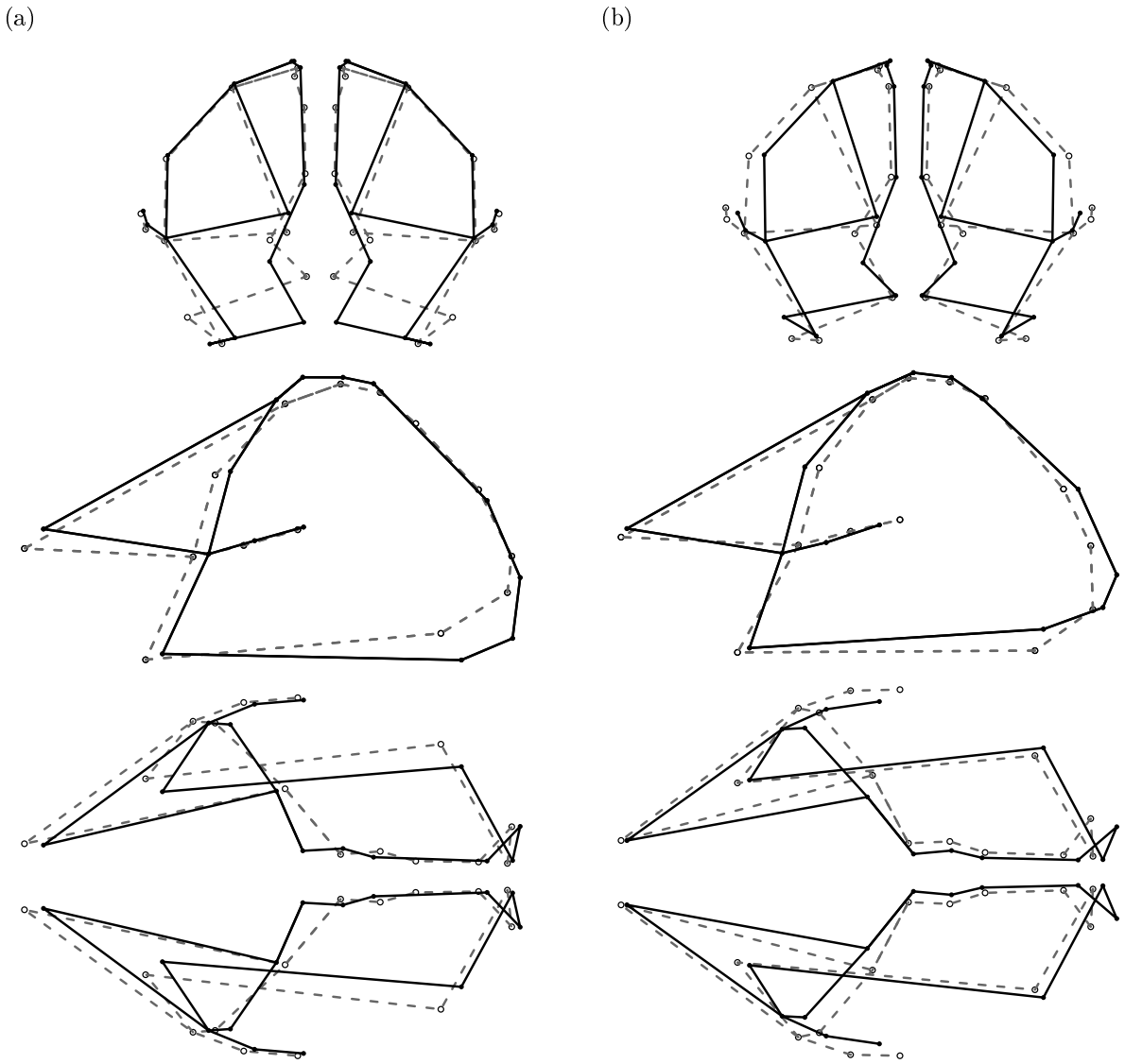

Figure 6.9: **Brain PCs shape deformations (continued on next page). (a)** Brain shape changes deformations from a negative PC1 value (dashed wireframe) to a positive one (solid wireframe). **(b)** Brain shape changes deformations from a negative PC2 value (dashed wireframe) to a positive one (solid wireframe).

(c)

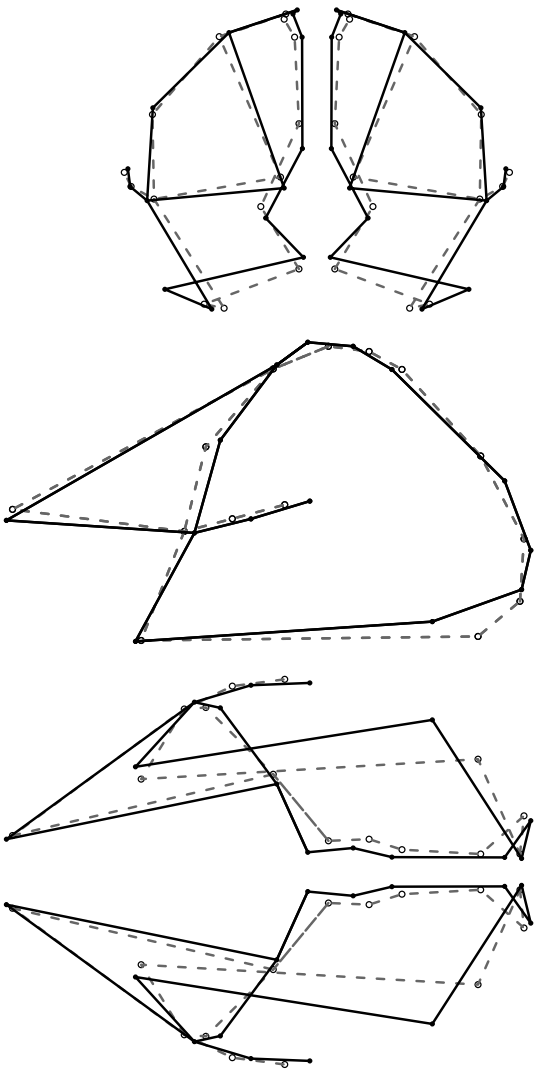

Figure 6.9: **Brain PCs shape deformations (continued). (c)** Brain shape changes deformations from a negative PC3 value (dashed wireframe) to a positive one (solid wireframe).

The development curves of the endocranial vault and the brain, which were quantified by the Procrustes distances, are shown in Figure 6.10 and Figure 6.11. The endocranial vault presents a high development rate in the first period, which is considerably reduced afterwards. On the contrary, the brain development rate seems to augment significantly from adolescence onwards, presenting also a high value in the first period.

(a) (b)

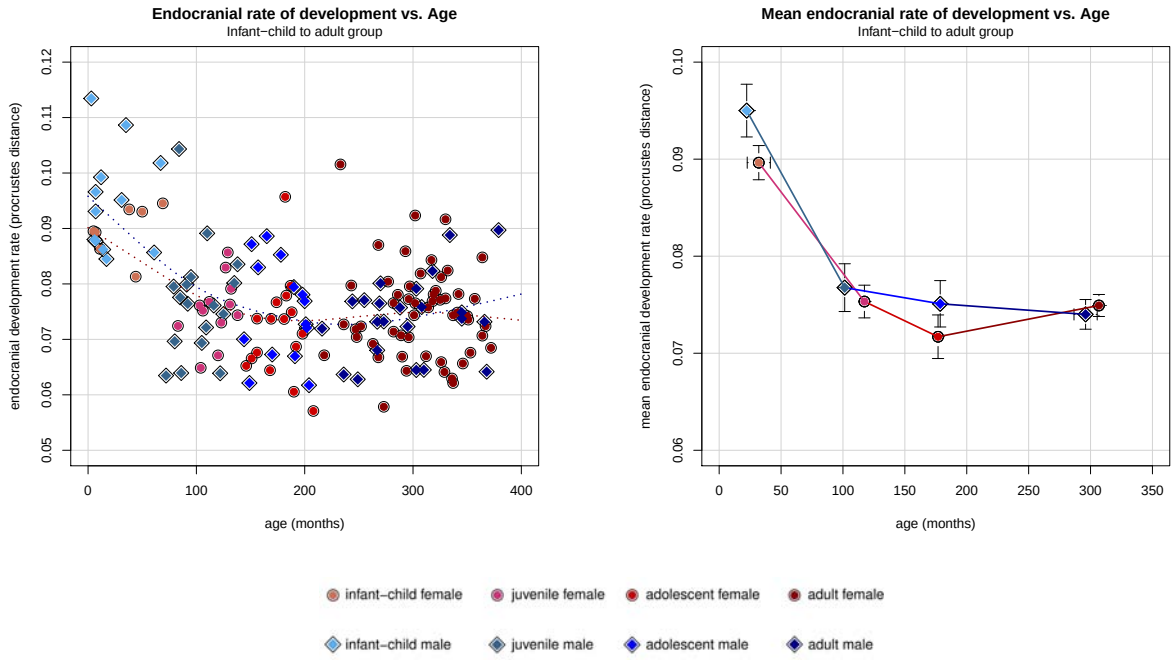

Figure 6.10: **Endocranial rate of development.** The sample is divided into seven groups (0 to 35 months, 36-71, 72-107, 108-143, 144-179, 180-215, and 216 or more months), and the degree of development of each individual is quantified by measuring the morphometric Procrustes distance between each individual and the average of the previous subgroup, for the first subgroup the distances were calculated to the youngest five individuals. Then individuals are regrouped to calculate the means and standard error of the means (SEM) from the original four groups (infant-child, juvenile, adolescent, and adult). **(a)** Legends: dotted red curve: smooth spline for females; dotted blue curve: smooth spline for males. **(b)** Mean age groups with their respective SEM.

(a) (b)

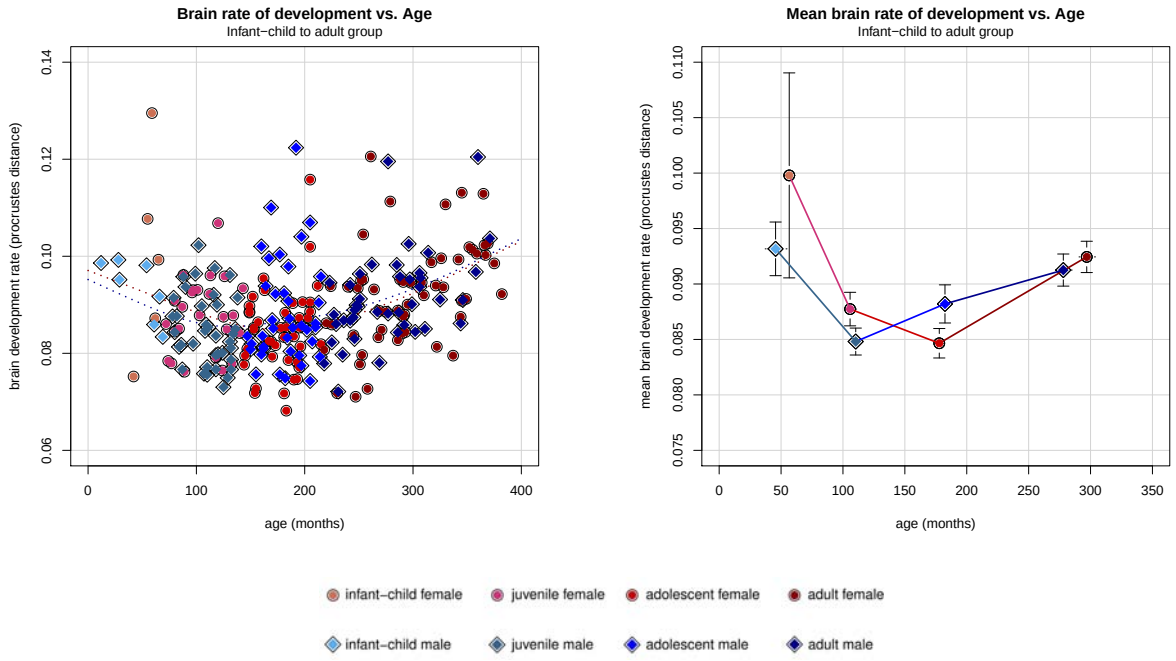

Figure 6.11: **Brain rate of development.** The sample is divided into seven groups (0 to 35 months, 36-71, 72-107, 108-143, 144-179, 180-215, and 216 or more months), and the degree of development of each individual is quantified by measuring the morphometric Procrustes distance between each individual and the average of the previous subgroup, for the first subgroup the distances were calculated to the youngest five individuals. Then individuals are regrouped to calculate the means and standard error of the means (SEM) from the original four groups (infant-child, juvenile, adolescent, and adult). **(a)** Legends: dotted red curve: smooth spline for females; dotted blue curve: smooth spline for males. **(b)** Mean age groups with their respective SEM.

What relationship has the cranial capacity measured from the bony endocranium with the brain volume?

The mean ECV measured for each year within a period from 0 to 31 years old are shown in Figure 6.12. The mean BV (GMV + WMV) calculated throughout the ontogenetic period analysed are depicted in Figure 6.13. As explained above, due to the scarce number of individuals ranging from 0 to 4 years old, they were not used to calculate the age mean ratio BV / ECV. Results regarding this ratio from 5 to 31 years old are depicted in Figure 6.14. The ANCOVA analysis showed no significant differences between sexes ($P > 0.05$) (Table B.16). However, a clear tendency can be observed in Figure 6.14 towards higher BV/ECV ratios for females. When analysing this ratio versus ECV (instead of age) the differences between sexes become more conspicuous and sexual dimorphism is statistically significant ($P < 0.01$) (Figure 6.15, Table B.17).

What degree of covariation exists between endocranial and brain shape?

As it was described above, to evaluate the degree of covariation between endocranial vault and brain, the age will be used as a proxy. This is due to the fact that endocranial and brain information come from different data sets; hence, no endocranium and brain information from the same individual was available. Therefore, covariation between these two structures can be assessed exploring the shape changes associated to age that occur in the endocranial vault and comparing them to those in the brain.

Endocranial vault results will be presented first. The morphometric vectors that explained more than 5% of the total variance and yielded strong significant correlations with age ($P < 0.001$) (Table 6.1) are described below. The infant-child to juvenile group

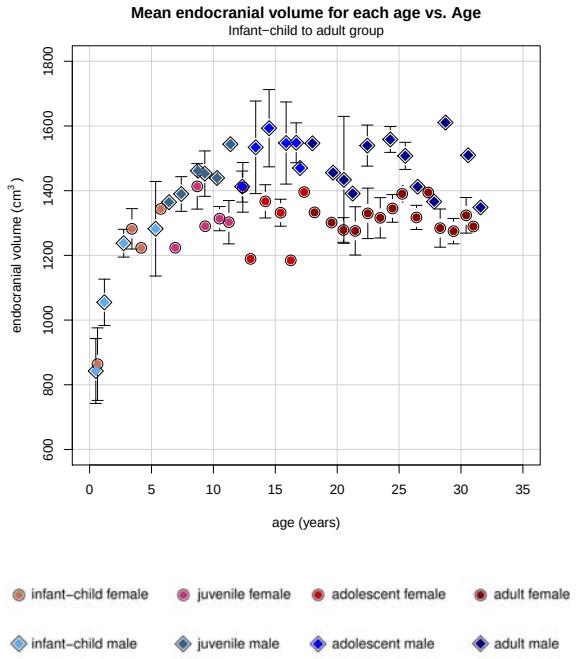

Figure 6.12: **Endocranial mean volumes per age.** For each age, from 0 to 31 years, and each sex a mean endocranial volume was measured with its corresponding standard error of the mean (SEM) schematized by the error bars.

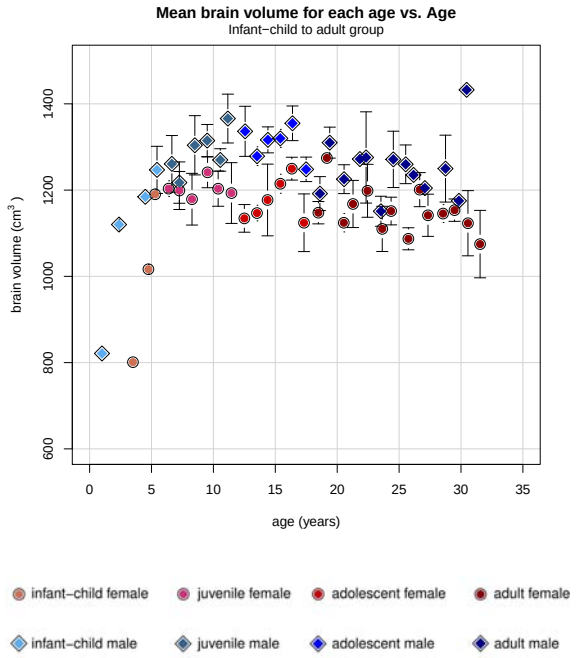

Figure 6.13: **Brain mean volumes per age.** For each age, from 0 to 31 years, and each sex a mean brain volume (calculated by the sum of gray and white matter volumes) was measured with its corresponding standard error of the mean (SEM) schematized by the error bars.

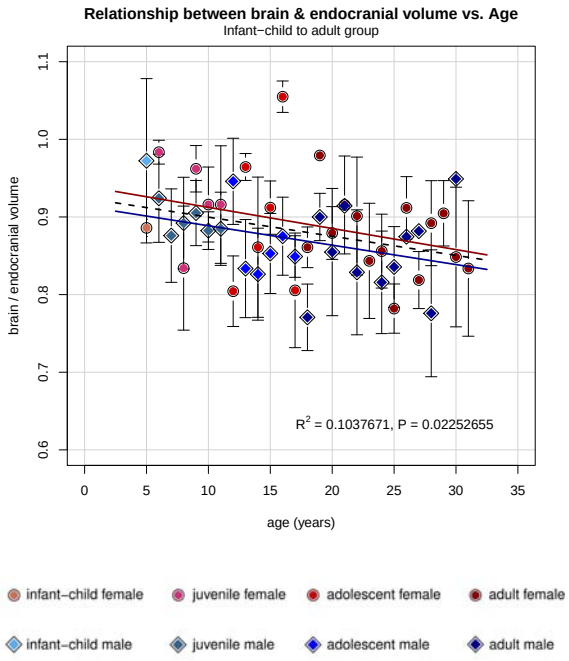

Figure 6.14: **Relationship between brain & endocranial mean volumes versus age.** From 5 to 31 years old, a relationship between brain and endocranial mean volumes for each age and each sex was calculated. This relation was quantified by a simple ratio between brain and endocranial means depicted in Figure 6.12 and 6.13 correspondingly. Means from 0 to 4 years old were excluded because not all means were represented at this period due to scarce data, rendering impossible to calculate the ratio. No dimorphism was found between sexes ($P > 0.05$) (see Table B.16 for details about ANCOVA results).

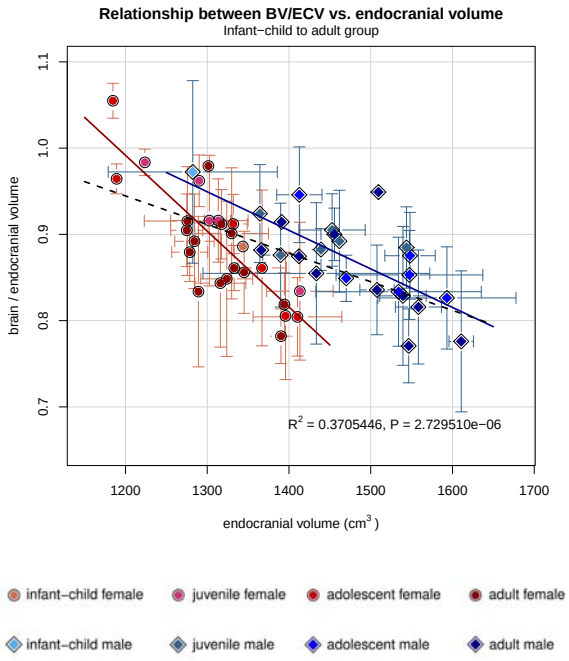

Figure 6.15: **Relationship between brain & endocranial mean volumes versus endocranial volume.** From 5 to 31 years old, a relationship between brain and endocranial mean volumes for each age and each sex was calculated. This relation was quantified by a simple ratio between brain and endocranial means depicted in Figure 6.12 and 6.13. Dimorphism was found between sexes ($P < 0.001$) (see Table B.17 for details about ANCOVA results).

Table 6.1: **Endocranial CCSVs.** Regression results of each group's CCSV vs. age.

CCSV	% of explained variance	R-Square	p-value
Infant-child and juveniles group	20.450	0.601	9.64E-011
Juveniles and adolescents group	11.510	0.284	1.42E-005
Adolescents and adults group	6.717	0.068	0.0070

showed a strong CCSV ($P \ll 0.0001$) (Figure 6.16), which summarizes the following shape changes: left-right proportional elongation and superior-inferior compression of the endocranial vault; proportional shortening of the vertex-bregma distance; a proportional expansion of the temporal poles in a posterior-anterior direction with an anteromedial rotation; and finally, the forwards localized expansion of the frontal poles (Figure 6.17). Sexual dimorphism was found ($P < 0.05$) for this regression axis (Table B.18). The juvenile to adolescent group presented a significant CCSV ($P < 0.0001$) (Figure 6.18) that summarizes the following shape modifications: proportional compression of the parietal superior area; strong forwards elongation of the frontal poles; and forwards protrusion of the temporal poles (Figure 6.19). No sexual dimorphism was found ($P > 0.05$) (Table B.19). Finally, the adolescent to adult group presented a CCSV that did not statistically correlate with age ($P > 0.005$).

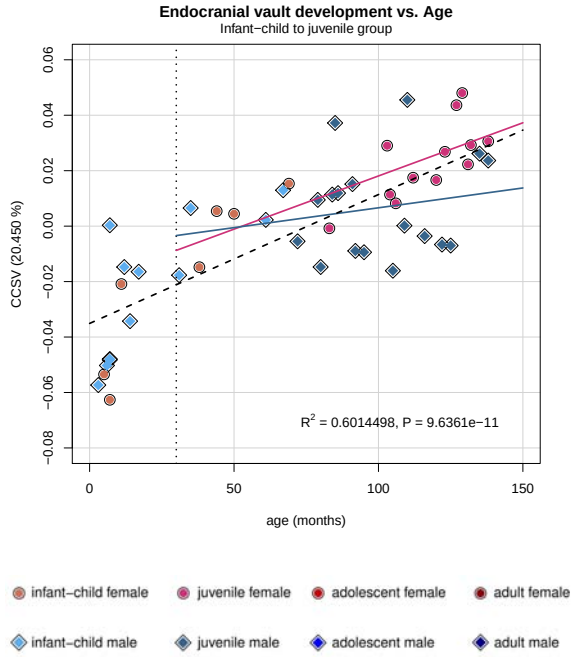

Figure 6.16: **Endocranial CCSV vs. age - infant-child to juvenile group.** Endocranial CCSV scores of infant-child to juvenile group. Legends: dashed black line represents the significant regression line between all individual CCSV scores and age; solid red line: lineal regression for females from 30 to 143 months; solid blue line: lineal regression for males from 30 to 143 months. Dimorphism was found between sexes from 30 to 143 motnhs ($P < 0.05$) (see Table B.18 for details about ANCOVA results).

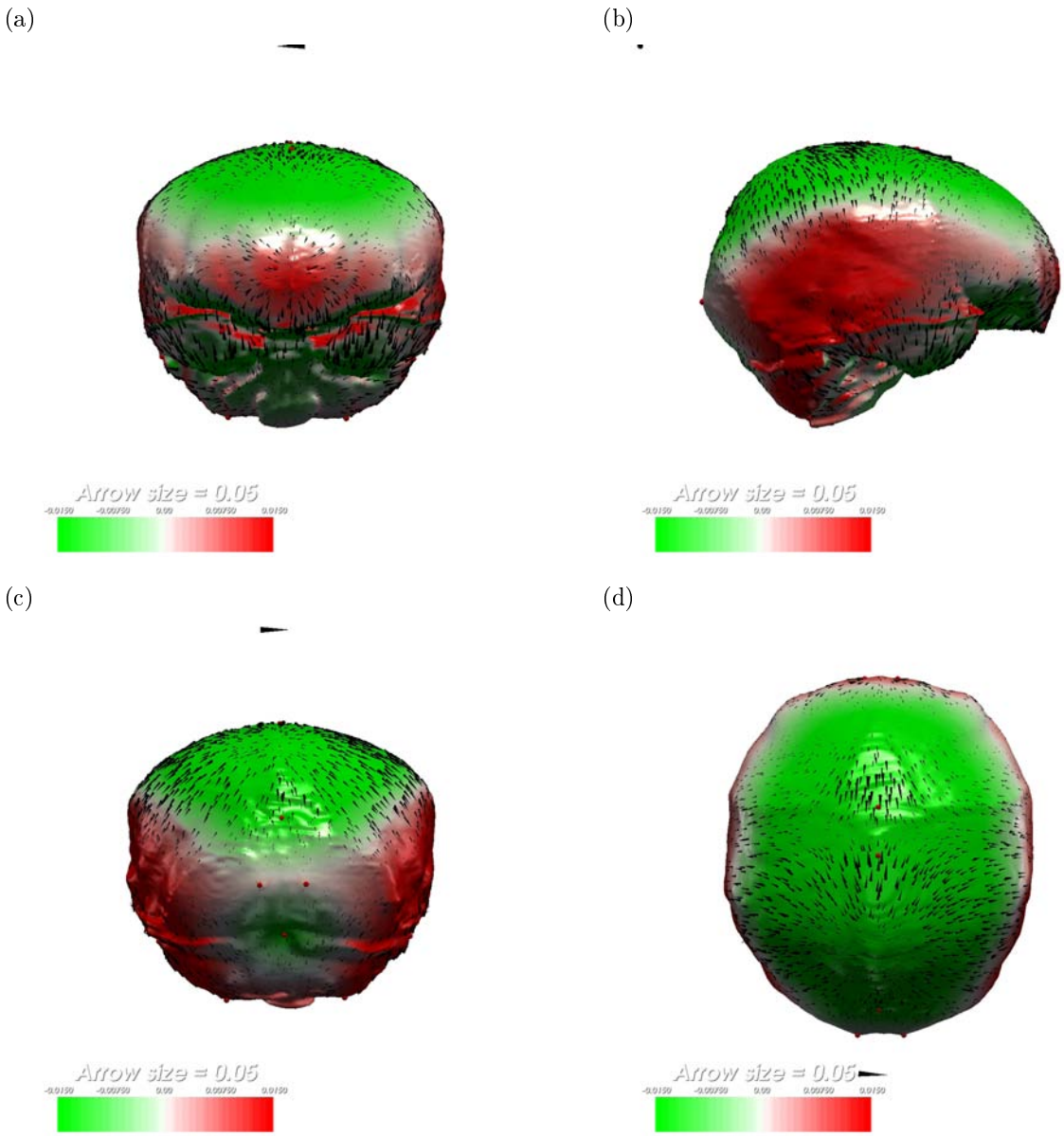

Figure 6.17: **Endocranial CCSV visualization - infant-child to juvenile group.** Endocranial vault CCSV visual representations of shape changes associated with age augmentation in infant-child to juvenile group. Green/red indicate the direction (inward/outward) and magnitude of shape transformation perpendicular to the surface; arrows indicate shape change parallel to the surface. **(a)** Coronal anterior view. **(b)** Sagital right view. **(c)** Coronal posterior view. **(d)** Horizontal superior view.

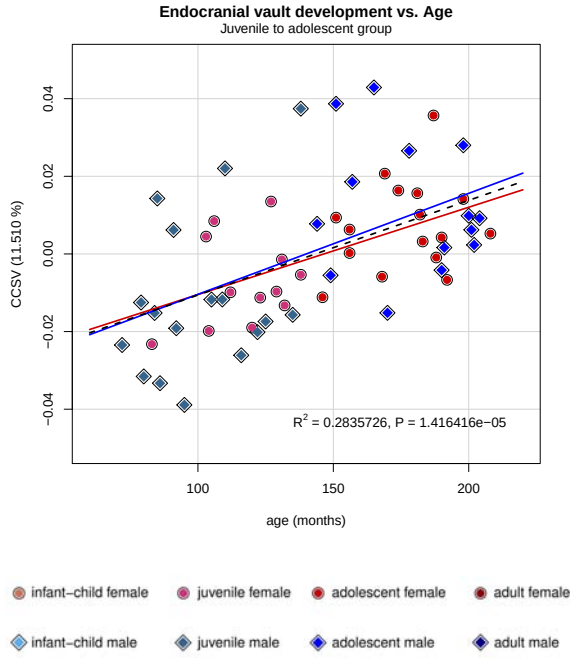

Figure 6.18: **Endocranial CCSV vs. age - juvenile to adolescent group.** Endocranial CCSV scores of juvenile to adolescent group. Legends: dashed black line represents the significant regression line between all individual CCSV scores and age; solid red line: lineal regression for females; solid blue line: lineal regression for males. No dimorphism was found between sexes ($P > 0.05$) (see Table B.19 for details about ANCOVA results).

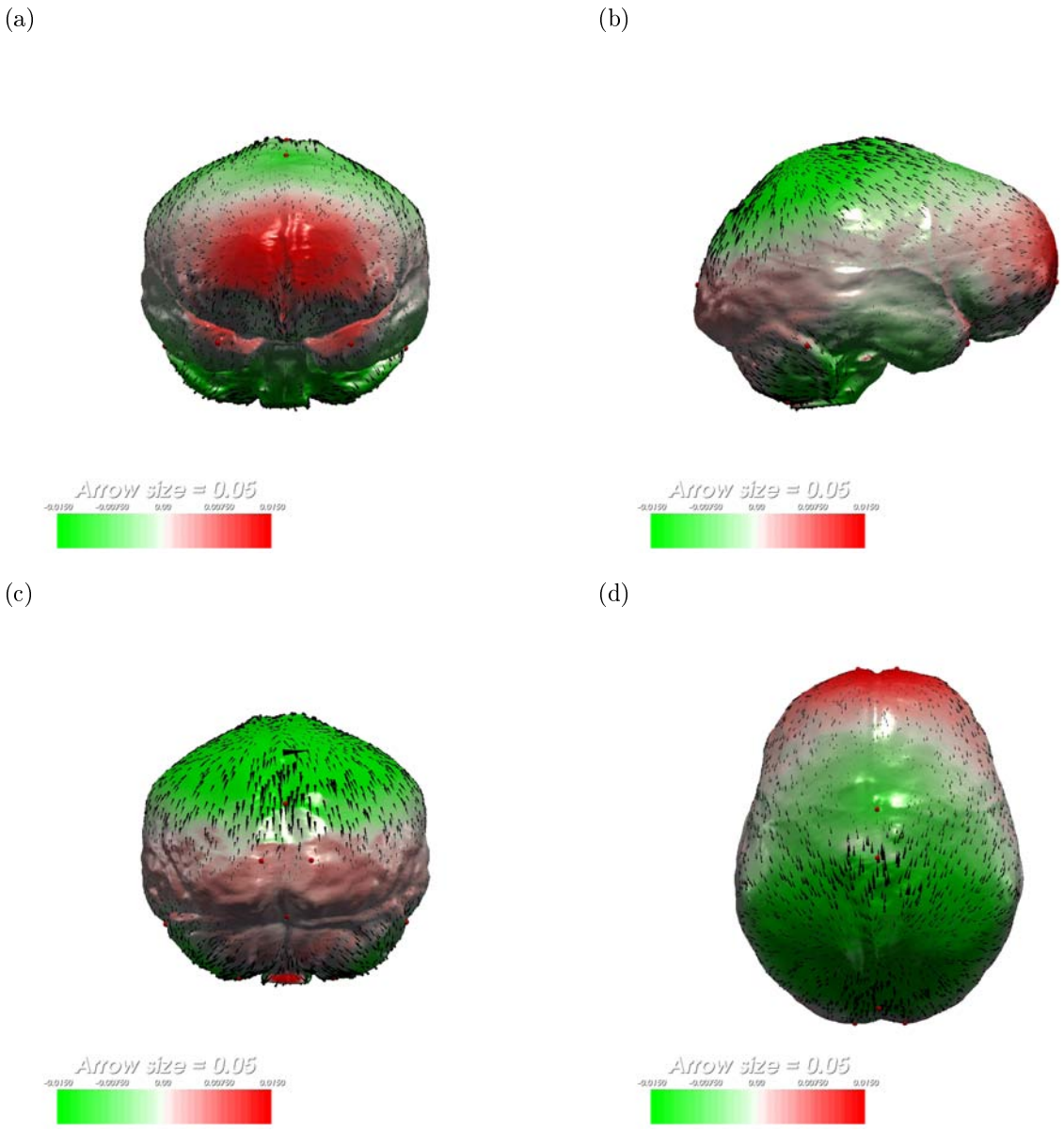

Figure 6.19: **Endocranial CCSV visualization - juvenile to adolescent group.** Endocranial vault CCSV visual representations of shape changes associated with age augmentation in juvenile to adolescent group. Green/red indicate the direction (inward/outward) and magnitude of shape transformation perpendicular to the surface; arrows indicate shape change parallel to the surface. **(a)** Coronal anterior view. **(b)** Sagital right view. **(c)** Coronal posterior view. **(d)** Horizontal superior view.

Next, cortical brain results will be presented. To describe better brain shape modifications, Brodmann's brain areas were used (Brodmann, 1909; Garey, 1994); a brief definition of each area and its cortical localization can be found in the Appendix A (Figure A.1). The GM analysis performed to distinguish brain shape changes associated with ageing resulted in one vector (CCSV) for each ontogenetic group, which summarizes all the changes associated with ageing. The morphometric vectors that explained more than 5% of the total variance and yielded significant correlations with age ($P < 0.001$) (Table 6.2) are described below. The infant-child to juvenile group presented a CCSV ($P \ll 0.0001$) (Figure 6.20) that summarizes the following shape modifications: a proportional left-right elongation and superior-inferior compression of the cortical brain shape; a proportional expansion of the brain superior margin, from the postcentral sulcus to the frontal poles; a forwards protrusion of the frontal and the temporal poles; and finally, a left-right expansion of the angular area and its boundaries (Figure 6.21). No sexual dimorphism was found ($P > 0.05$) (Table B.20). The juvenile to adolescent group showed a strong CCSV ($P \ll 0.0001$) (Figure 6.22), whose shape changes are described as follows: a strong proportional forwards protrusion of prefrontal, frontopolar, granular frontal regions and temporal poles; elongation of superior parietal lobule towards the midline; and the occipital lobe contraction (Figure 6.23). The CCSV axis corresponding to this group presented no sexual dimorphism ($P > 0.05$) (Table B.21). The adolescent to adult group also showed a strong CCSV ($P \ll 0.0001$) (Figure 6.24), whose shape changes can be described as: proportional backwards protrusion of the occipital pole; compression of the preoccipital notch towards the inferior and middle temporal areas; and forwards elongation of the temporal poles (Figure 6.25). Sexual dimorphism was found in this ontogenetic

Table 6.2: **Brain CCSVs.** Regression results of each group's CCSV vs. age.

CCSV	**% of explained variance**	**R-Square**	**p-value**
Infant-child and juveniles group	8.61	0.362	1.39E-008
Juveniles and adolescents group	10.26	0.513	8.51E-024
Adolescents and adults group	8.76	0.616	1.82E-038

period ($P < 0.05$) (Table B.22).

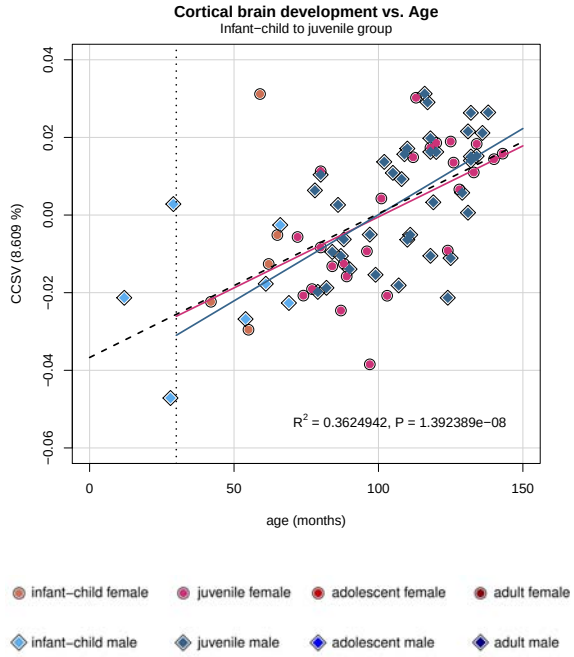

Figure 6.20: **Brain CCSV vs. age - infant-child to juvenile group.** Brain CCSV scores of infant-child to juvenile group. Legends: dashed black line represents the significant regression line between all individual CCSV scores and age; solid red line: lineal regression for females from 30 to 143 months; solid blue line: lineal regression for males from 30 to 143 months. No dimorphism was found between sexes from 30 to 143 motnhs ($P > 0.05$) (see Table B.20 for details about ANCOVA results).

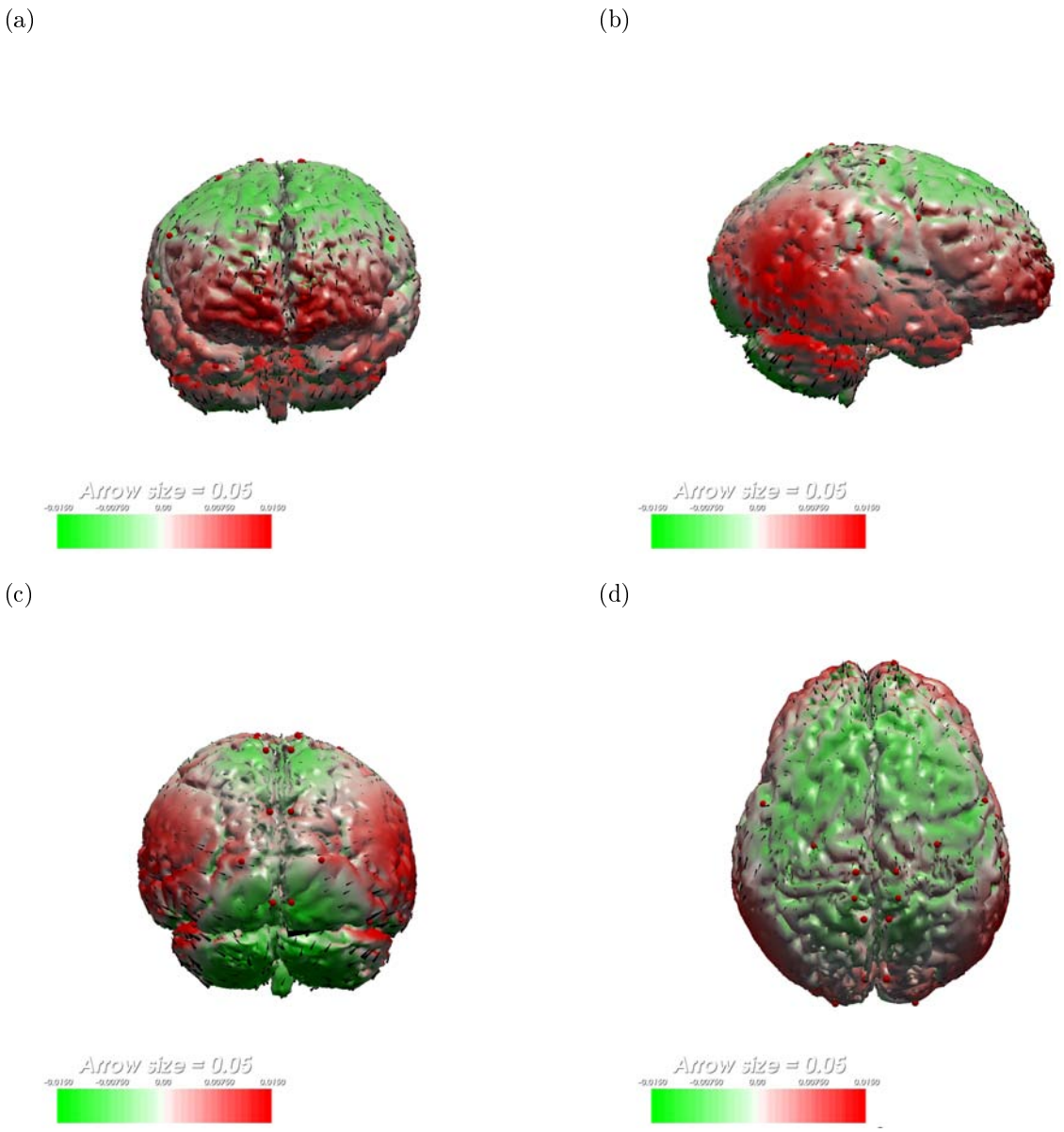

Figure 6.21: **Brain CCSV visualization - infant-child to juvenile group.** Brain CCSV visual representations of shape changes associated with age augmentation in infant-child to juvenile group. Green/red indicate the direction (inward/outward) and magnitude of shape transformation perpendicular to the surface; arrows indicate shape change parallel to the surface. **(a)** Coronal anterior view. **(b)** Sagital right view. **(c)** Coronal posterior view. **(d)** Horizontal superior view.

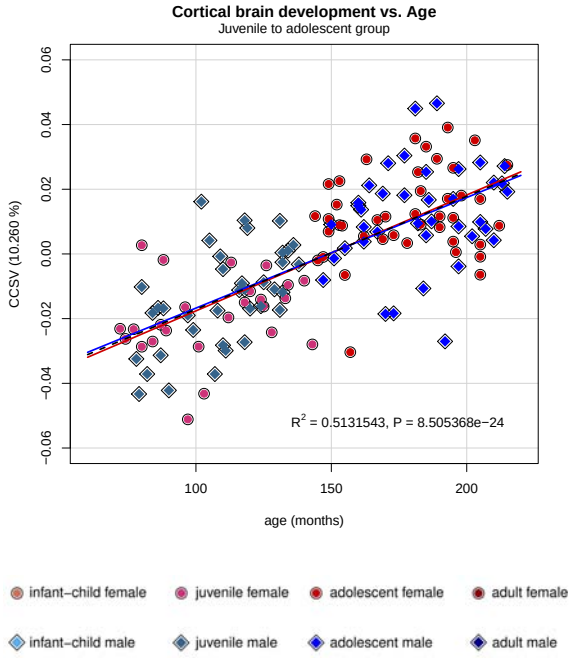

Figure 6.22: **Brain CCSV vs. age - juvenile to adolescent group.** Brain CCSV scores of juvenile to adolescent group. Legends: dashed black line represents the significant regression line between all individual CCSV scores and age; solid red line: lineal regression for females; solid blue line: lineal regression for males. No dimorphism was found between sexes ($P > 0.05$) (see Table B.21 for details about ANCOVA results).

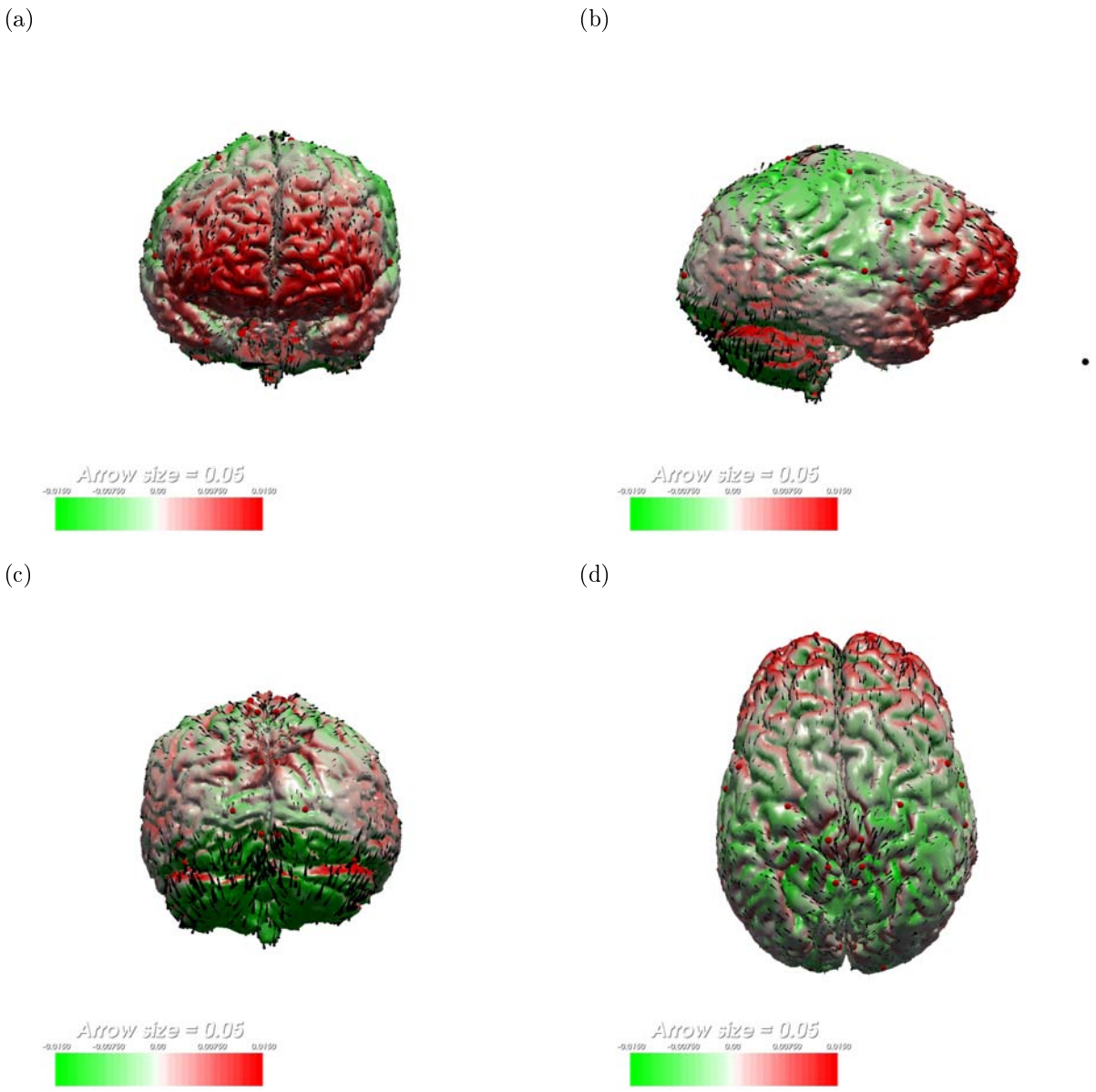

Figure 6.23: **Brain CCSV visualization - juvenile to adolescent group.** Brain CCSV visual representations of shape changes associated with age augmentation in juvenile to adolescent group. Green/red indicate the direction (inward/outward) and magnitude of shape transformation perpendicular to the surface; arrows indicate shape change parallel to the surface. **(a)** Coronal anterior view. **(b)** Sagital right view. **(c)** Coronal posterior view. **(d)** Horizontal superior view.

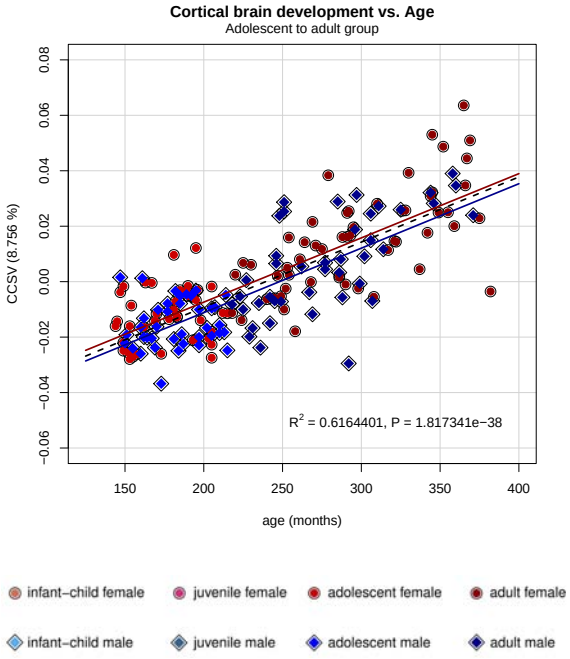

Figure 6.24: **Brain CCSV vs. age - adolescent to adult group.** Brain CCSV scores of adolescent to adult group. Legends: dashed black line represents the significant regression line between all individual CCSV scores and age; solid red line: lineal regression for females; solid blue line: lineal regression for males. Dimorphism was found between sexes ($P < 0.05$) (see Table B.22 for details about ANCOVA results).

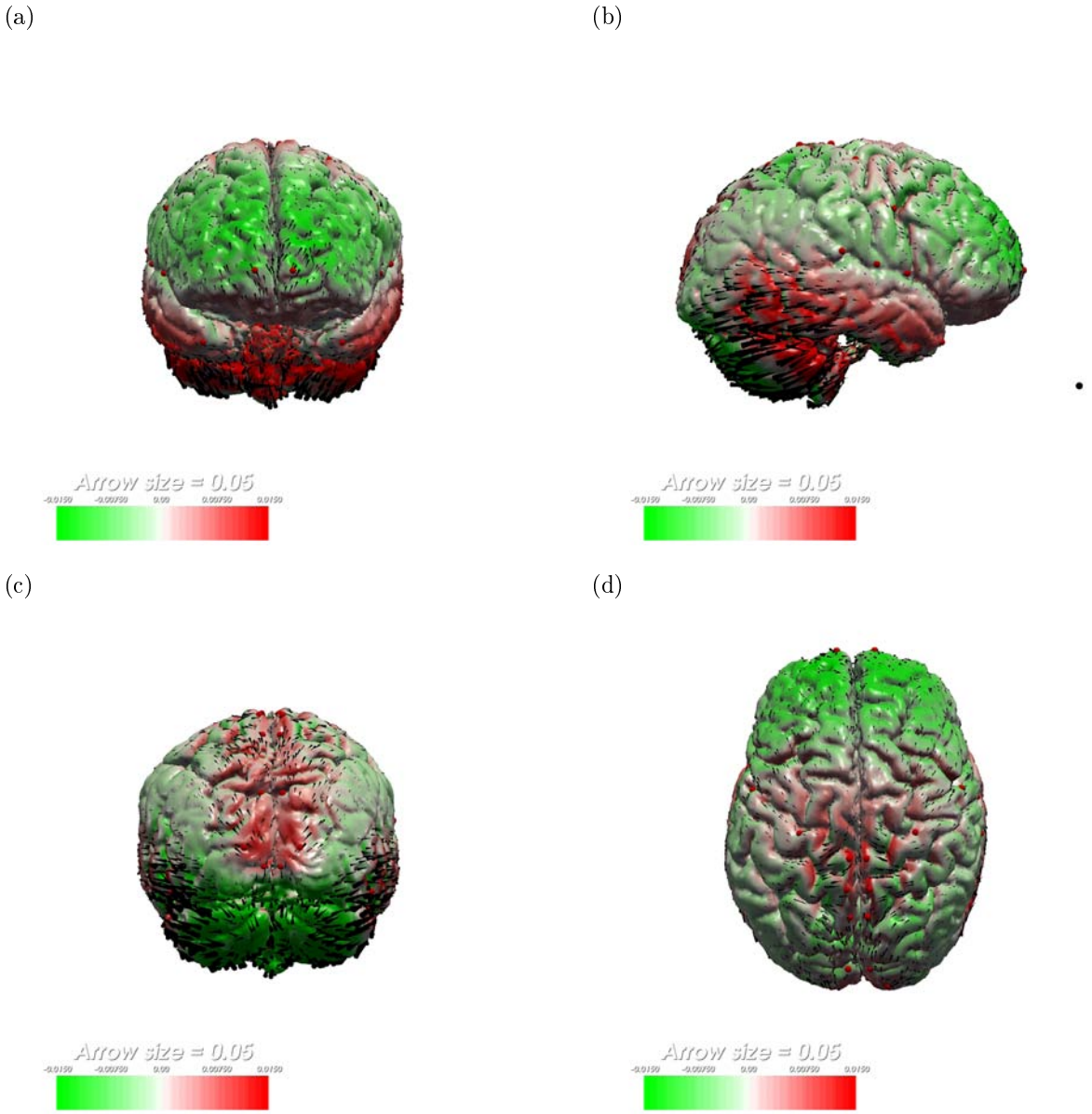

Figure 6.25: **Brain CCSV visualization - adolescent to adult group.** Brain CCSV visual representations of shape changes associated with age augmentation in adolescent to adult group. Green/red indicate the direction (inward/outward) and magnitude of shape transformation perpendicular to the surface; arrows indicate shape change parallel to the surface. **(a)** Coronal anterior view. **(b)** Sagital right view. **(c)** Coronal posterior view. **(d)** Horizontal superior view.

Similar shape modification trajectories of endocranial vault and brain may reflect certain degree of covariation throughout development. Therefore, the GM results corresponding to both structures were compared in order to detect possible similarities. To begin with, during the infant-child to juvenile ontogenetic period, endocranial vault shape changes (Figure 6.17) coincide with cortical brain shape modifications (Figure 6.21), which denotes an important degree of covariation during this period. Further, at the juvenile to adolescent period the endocranial vault shape changes (Figure 6.19) are very similar to those of the brain cortex (Figure 6.23). Finally, at the last period analysed, from adolescent to adulthood, no similarities between endocranial and brain shape modifications were found. In fact, the endocranium vault did not present any changes, while brain still showed important developmental modifications. Hence, no developmental covariation exists between both structures at this ontogenetic period. In summary, the brain and the endocranial vault seem to covary in shape changes until adolescence; from then to young adulthood the shape modifications observed in the brain are not followed by shape changes in the endocranial vault, which seems to end its growth and development during the adolescent period.

When do endocranial petal patterns and brain macroscopic asymmetries grow and develop?

In order to evaluate the development of endocranial and cortical macroscopic asymmetries, two different methodologies were used. A general quantification of asymmetry was obtained from the first analysis, which used the Procrustes distance between each individual and its mirror image as an asymmetry estimator, with no specification of the location of the asymmetries. For the endocranial vault, this analysis provided an approximately

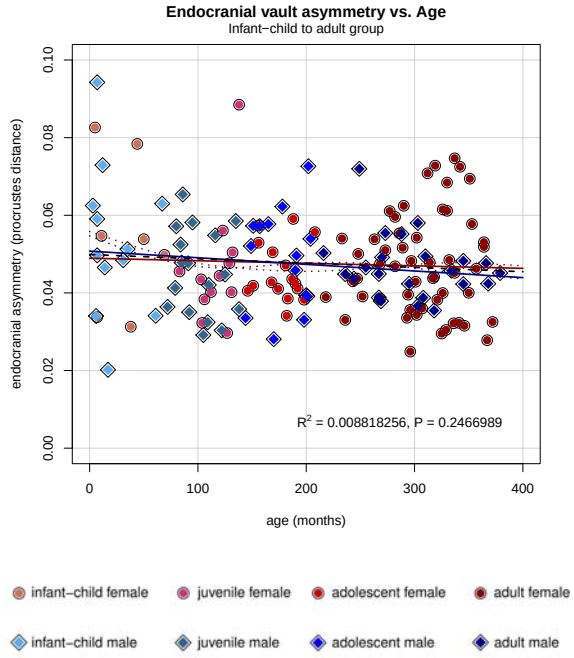

Figure 6.26: **Endocranial asymmetry through development - Procrustes distance.** Asymmetry through endocranial vault development was quantified by the morphometric distance between each individual and its mirror image, using the Procrustes distance, the conventional measure of a morphometric distance in geometric morphometrics. Legends: dashed black curve: linear regression for all individuals; solid red line: linear regression for females; solid blue line: linear regression for males; dotted red curve: smooth spline for females; dotted blue curve: smooth spline for males. No dimorphism was found between sexes ($P > 0.05$) (see Table B.23 for details about ANCOVA results).

constant value throughout the ontogenetic period analysed, with a slightly negative but non significant rate ($P > 0.05$) (Figure 6.26); no differences between sexes were found ($P > 0.05$) (Table B.23). The brain asymmetry analysis presented also a similar result, with a non significant positive rate ($P > 0.05$) (Figure 6.27), and no sexual dimorphism ($P > 0.05$) (Table B.24).

The second GM analysis performed to distinguish asymmetric shape changes of endocranial vault associated with ageing provided one vector (CCASV) for each ontogenetic group, which summarizes all the changes associated with ageing. The morphometric vectors that explained more than 5% of the total variance and yielded significant correlations

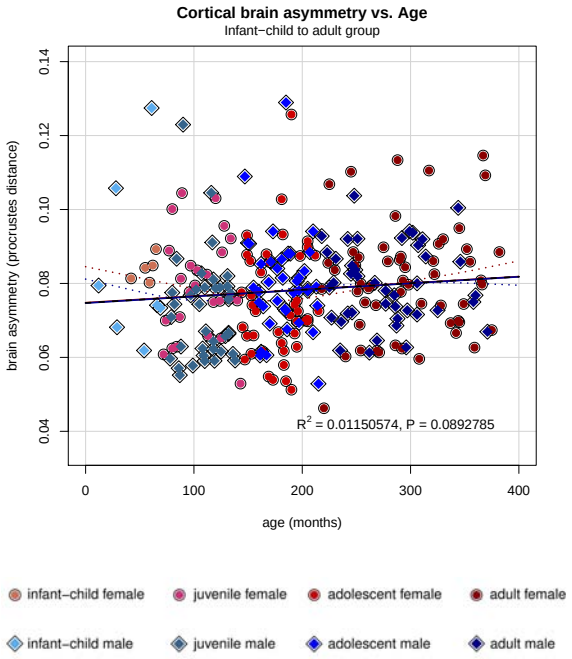

Figure 6.27: **Brain asymmetry through development - Procrustes distance.** Asymmetry through cortical brain development was quantified by the morphometric distance between each individual and its mirror image, using the Procrustes distance, the conventional measure of a morphometric distance in geometric morphometrics. Legends: dashed black curve: linear regression for all individuals; solid red line: linear regression for females; solid blue line: linear regression for males; dotted red curve: smooth spline for females; dotted blue curve: smooth spline for males. No dimorphism was found between sexes ($P > 0.05$) (see Table B.24 for details about ANCOVA results).

Table 6.3: **Endocranial CCASVs.** Regression results of each group's CCASV vs. age.

CCASV	% of explained variance	R-Square	p-value
Infant-child and juveniles group	11.33	0.342	1.29E-005
Juveniles and adolescents group	14.31	0.171	0.001
Adolescents and adults group	17.00	0.080	0.003

with age ($P < 0.001$) (Table 6.3) are described below. No significant differences were found between the CCASV calculated with and without the application of DAO, both vectors describing the same shape trajectories, but with stronger asymmetric signals in the first one, as it was expected. Hence, CCASV with DAO were chosen for graphical representation. The infant-child to juvenile group presented a CCASV ($P < 0.0001$) (Figure 6.28) that summarizes the following shape modifications: the right parieto-temporal region proportionately displaces upwards and towards the left one, while the opposite occurs in the occipital region; the left temporal pole protrudes anteriorly and the right one displaces backwards; the left and the right frontal poles displace downwards and upwards, respectively (Figure 6.29). No sexual dimorphism was found ($P > 0.05$) (Table B.25). The next two ontogenetic periods (juvenile to adolescent and adolescent to adult group) showed no significant CCASV ($P > 0.001$).

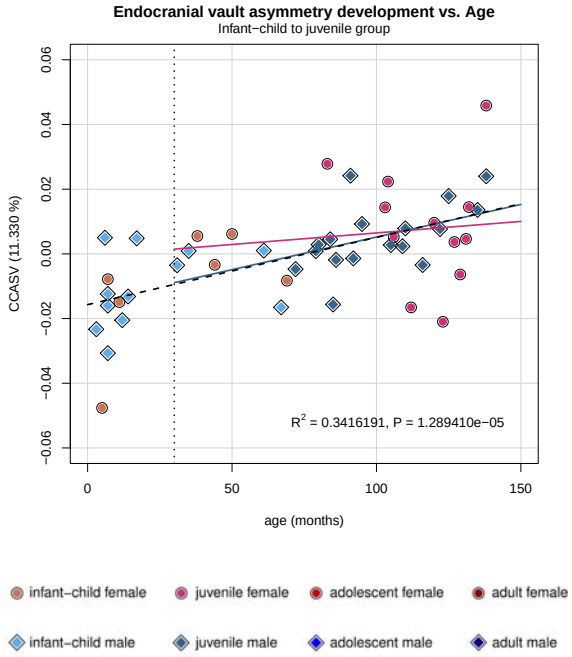

Figure 6.28: **Endocranial CCASV vs. age - infant-child to juvenile group.** Endocranial vault CCASV scores of infant-child to juvenile group. Legends: dashed black line represents the significant regression line between all individual CCASV scores and age; solid red line: lineal regression for females from 30 to 143 months; solid blue line: lineal regression for males from 30 to 143 months. No dimorphism was found between sexes from 30 to 143 motnhs ($P > 0.05$) (see Table B.25 for details about ANCOVA results).

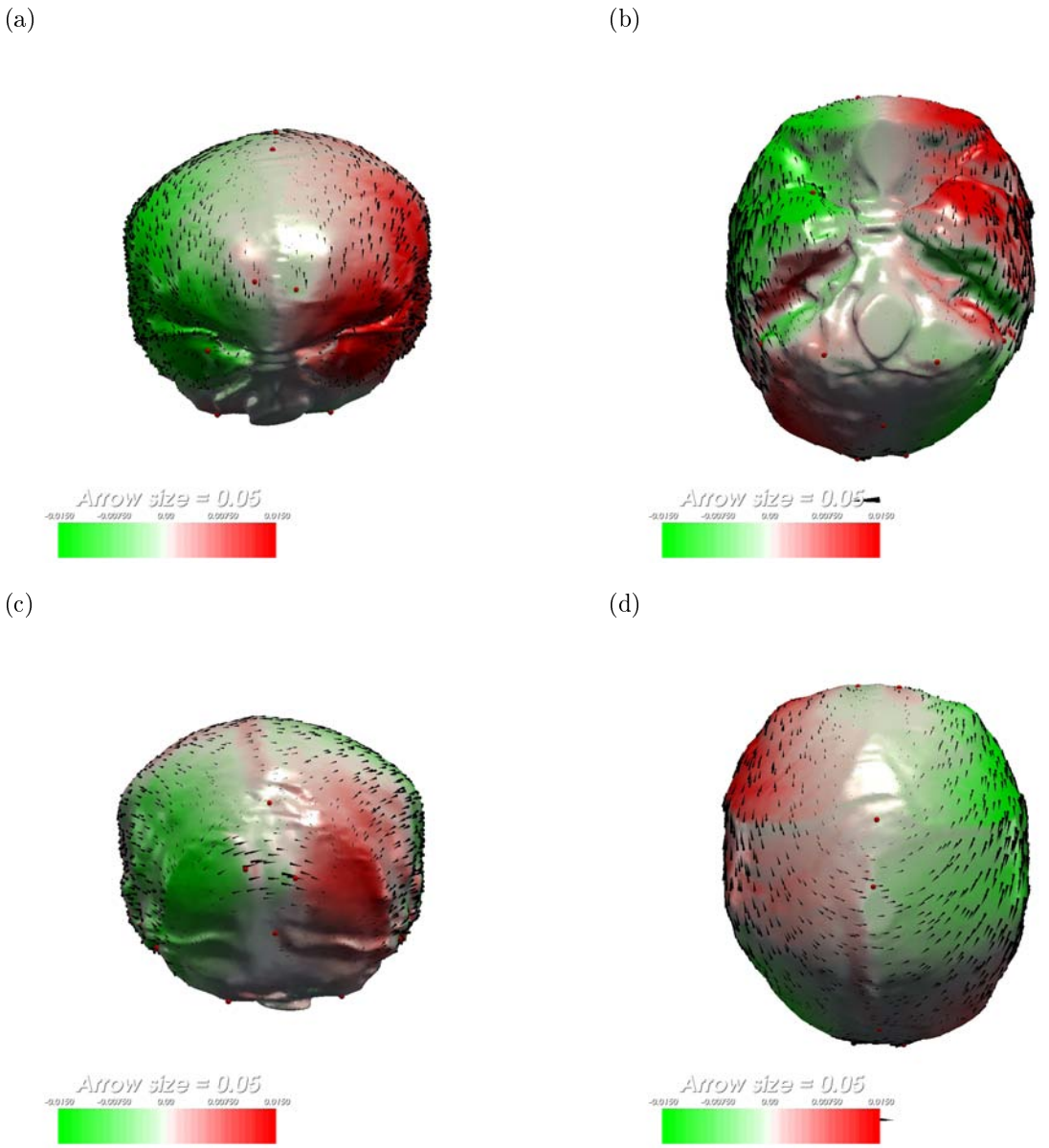

Figure 6.29: **Endocranial CCASV visualization - infant-child to juvenile group.** Endocranial vault CCASV visual representations of shape changes associated with age augmentation in infant-child to juvenile group. Green/red indicate the direction (inward/outward) and magnitude of shape transformation perpendicular to the surface; arrows indicate shape change parallel to the surface. **(a)** Coronal anterior view. **(b)** Horizontal inferior view. **(c)** Coronal posterior view. **(d)** Horizontal superior view.

With respect to asymmetric shape changes of cortical brain associated with ageing, the GM analysis provided one vector (CCASV) for each ontogenetic group, which summarizes all the changes associated with ageing. The morphometric vectors that explained more than 5% of the total variance and yielded significant correlations with age ($P < 0.001$) (Table 6.4) are described below. The infant-child to juvenile group CCASV ($P < 0.0001$) (Figure 6.30) summarized the following shape changes: a slight displacement of temporal and frontal poles towards the left; a small contraction of the left angular and supramarginal areas and the elongation of the contralateral ones (Figure 6.31). No sexual dimorphism was found ($P > 0.05$) (Table B.26). The juvenile to adolescent group presented a strong correlation between CCASV and age ($P \ll 0.0001$) (Figure 6.32). Such CCASV described the following shape modifications: the elongation and contraction of the right and the left occipital lobes, respectively, in a superior-inferior direction; the forwards protrusion of the right temporopolar area and the backwards depression of the left one (Figure 6.33). No sexual dimorphism was found ($P > 0.05$) (Table B.27). Finally, the adolescent to adult group showed a highly correlated CCASV ($P \ll 0.0001$) (Figure 6.34), which is associated with the following shape changes: the rotation of the occipital lobe towards the right; the forwards displacement of the right preoccipital notch and backwards elongation of the left one; the displacement of the frontal lobe towards the right; the forwards protrusion of the left temporopolar area and the backwards depression of the right one (Figure 6.35). No sexual dimorphism was found ($P > 0.05$) (Table B.28).

Table 6.4: **Brain CCASVs.** Regression results of each group's CCASV vs. age.

CCASV	% of explained variance	R-Square	p-value
Infant-child and juveniles group	7.14	0.231	1.47E-005
Juveniles and adolescents group	5.75	0.214	5.96E-009
Adolescents and adults group	6.04	0.245	2.25E-012

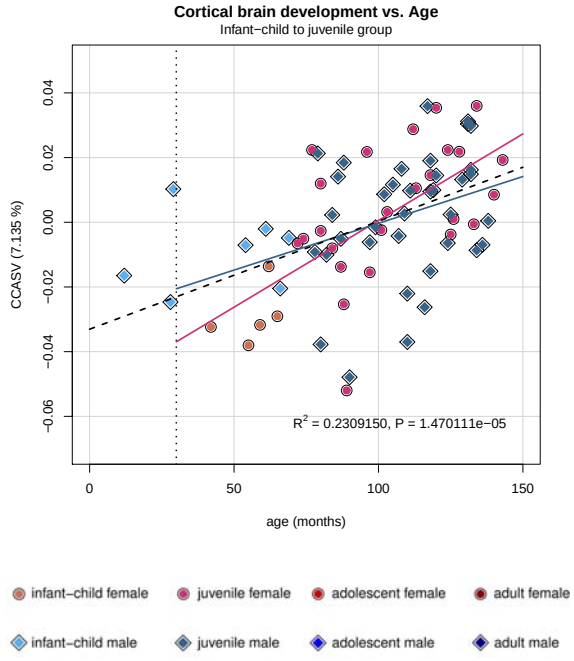

Figure 6.30: **Brain CCASV vs. age - infant-child to juvenile group.** Brain CCASV scores of infant-child to juvenile group. Legends: dashed black line represents the significant regression line between all individual CCASV scores and age; solid red line: lineal regression for females; solid blue line: lineal regression for males. No dimorphism was found between sexes ($P > 0.05$) (see Table B.26 for details about ANCOVA results).

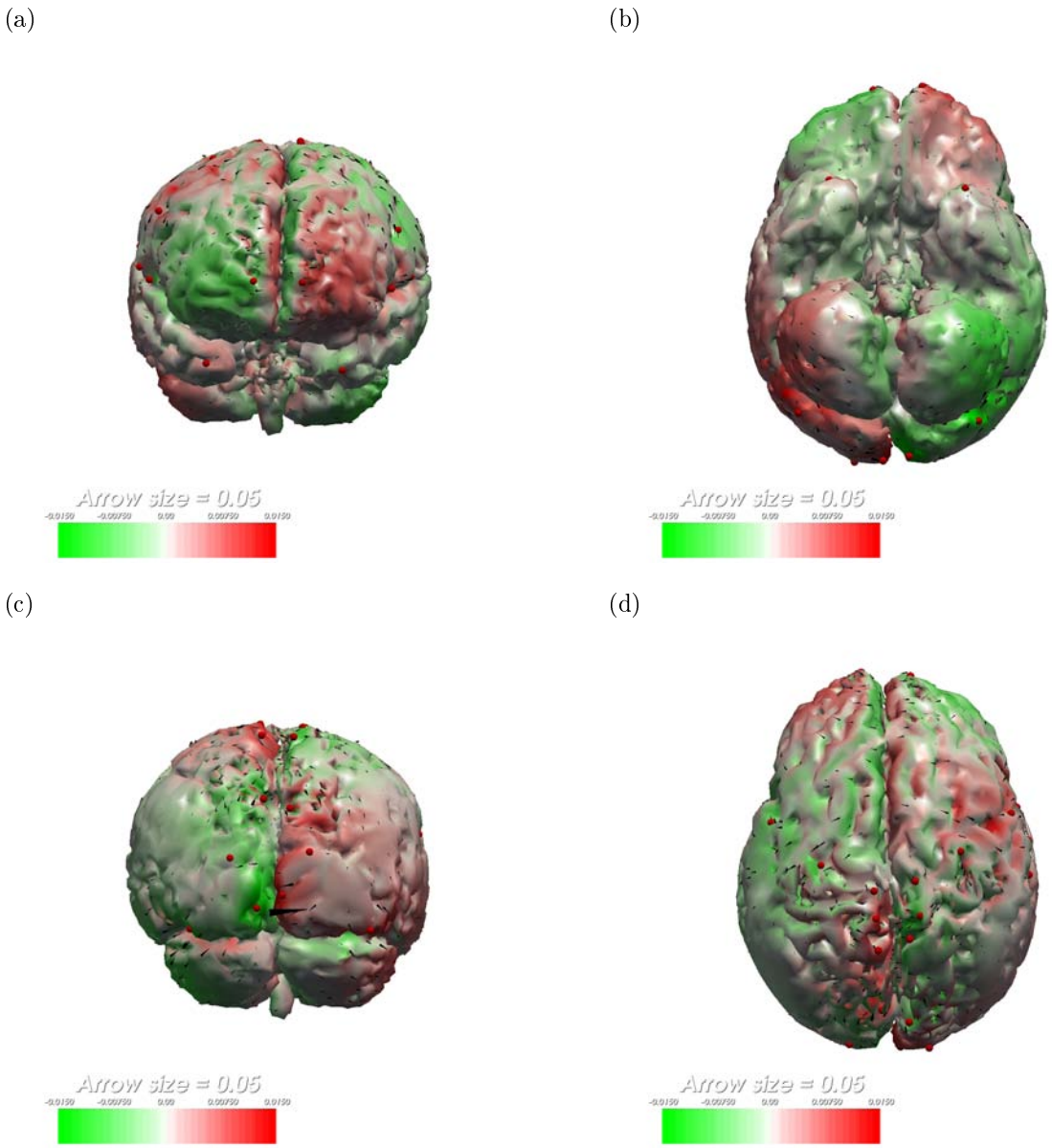

Figure 6.31: **Brain CCASV visualization - infant-child to juvenile group.** Brain CCASV visual representations of shape changes associated with age augmentation in infant-child to juvenile group. Green/red indicate the direction (inward/outward) and magnitude of shape transformation perpendicular to the surface; arrows indicate shape change parallel to the surface. **(a)** Coronal anterior view. **(b)** Sagital right view. **(c)** Coronal posterior view. **(d)** Horizontal superior view.

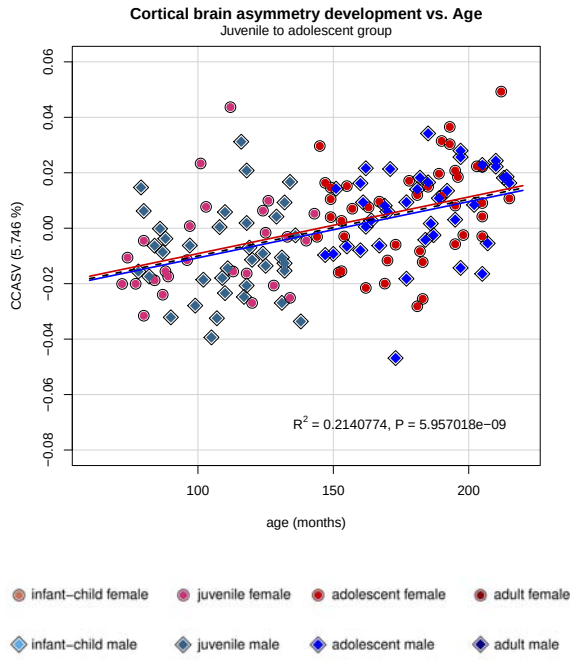

Figure 6.32: **Brain CCASV vs. age - juvenile to adolescent group.** Brain CCASV scores of juvenile to adolescent group. Legends: dashed black line represents the significant regression line between all individual CCASV scores and age; solid red line: lineal regression for females; solid blue line: lineal regression for males. No dimorphism was found between sexes ($P > 0.05$) (see Table B.27 for details about ANCOVA results).

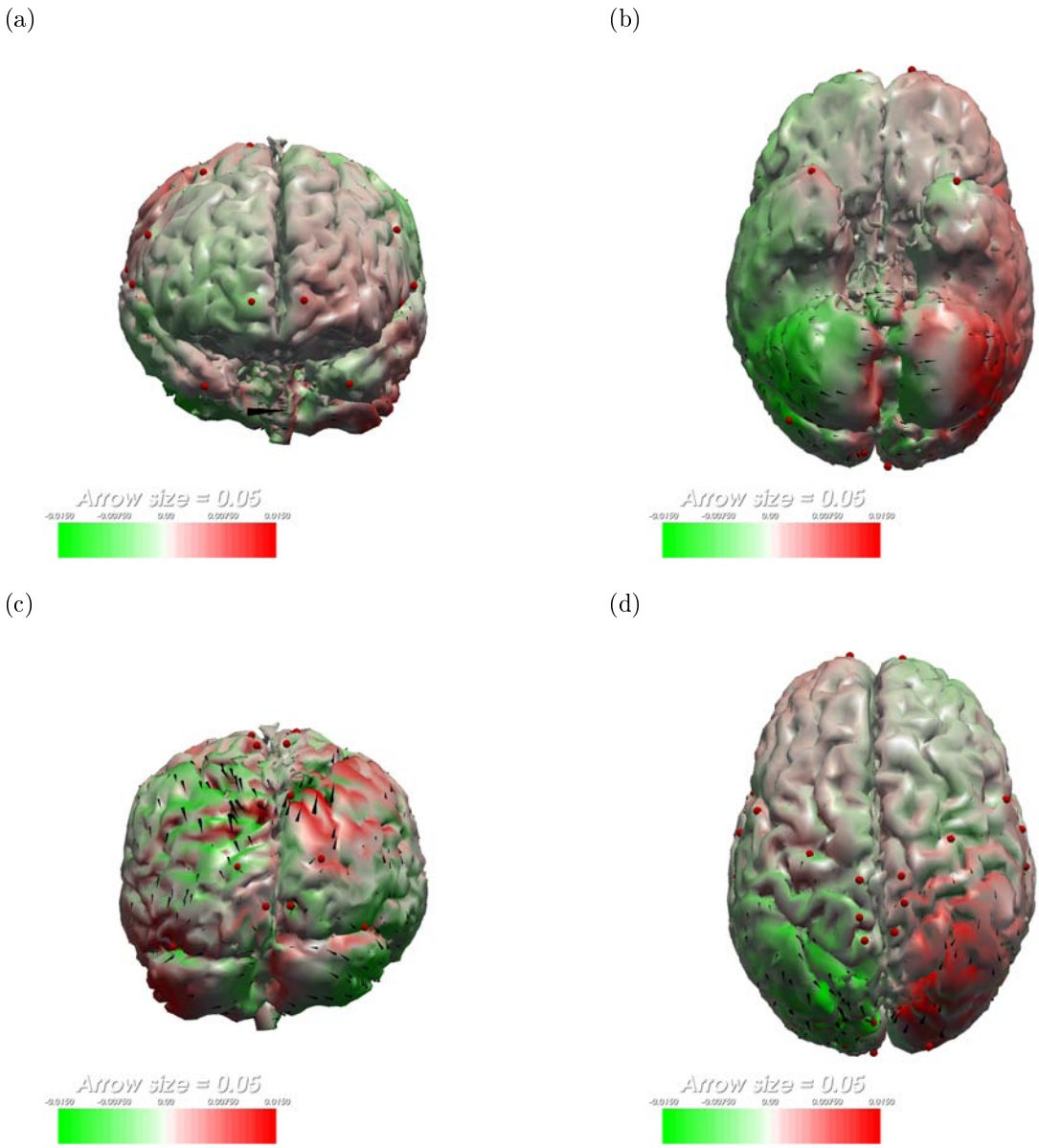

Figure 6.33: **Brain CCASV visualization - juvenile to adolescent group.** Brain CCASV visual representations of shape changes associated with age augmentation in juvenile to adolescent group. Green/red indicate the direction (inward/outward) and magnitude of shape transformation perpendicular to the surface; arrows indicate shape change parallel to the surface. **(a)** Coronal anterior view. **(b)** Sagital right view. **(c)** Coronal posterior view. **(d)** Horizontal superior view.

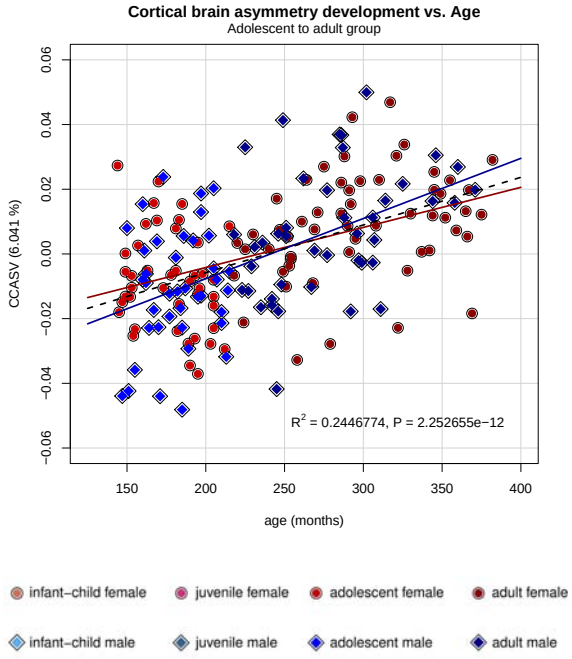

Figure 6.34: **Brain CCASV vs. age - adolescent to adult group.** Brain CCASV scores of adolescent to adult group. Legends: dashed black line represents the significant regression line between all individual CCASV scores and age; solid red line: lineal regression for females; solid blue line: lineal regression for males. No dimorphism was found between sexes ($P > 0.05$) (see Table B.28 for details about ANCOVA results).

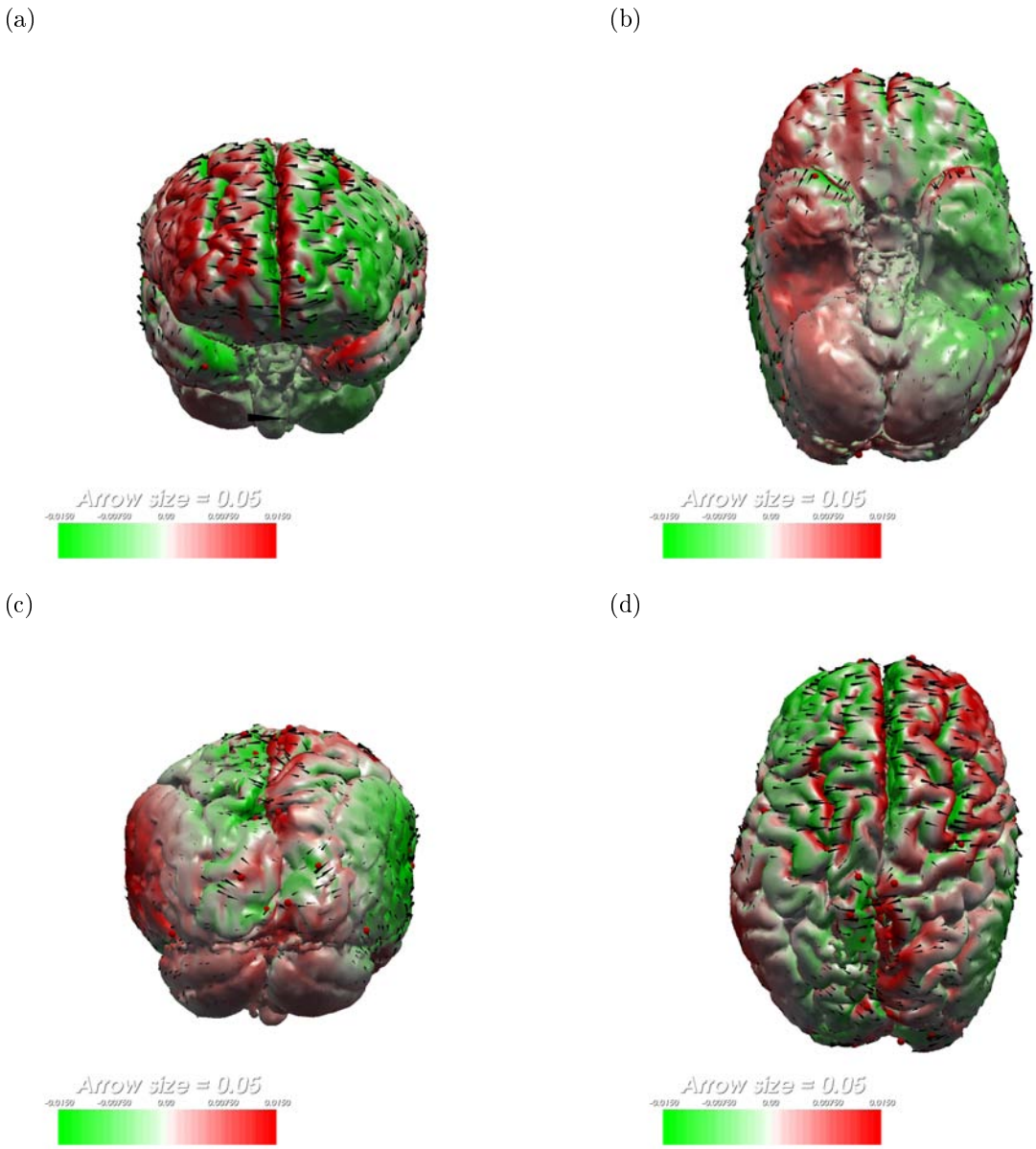

Figure 6.35: **Brain CCASV visualization - adolescent to adult group.** Brain CCASV visual representations of shape changes associated with age augmentation in adolescent to adult group. Green/red indicate the direction (inward/outward) and magnitude of shape transformation perpendicular to the surface; arrows indicate shape change parallel to the surface. **(a)** Coronal anterior view. **(b)** Sagital right view. **(c)** Coronal posterior view. **(d)** Horizontal superior view.

Both geometric morphometric analyses were compared in order to integrate the results obtained. There was no covariation between endocranial vault and brain asymmetric shape changes related to ageing; while most of the endocranial vault asymmetries were found in the infant-child to juvenile group, the most important brain asymmetries related to ageing were found in the adolescent to adult group.

Is there sexual dimorphism throughout endocranium and brain growth and development?

This question was assessed while answering each of the above questions. In summary, sexual differences in ECV, GMV, WMV, and BV growth were found throughout all the ontogenetic period analysed; with males presenting always larger volumes than females (Figure 6.1, 6.2, 6.3, and 6.5). In the case of the GMV/WMV relation, sexual dimorphism was only found in the last period analysed (Figure 6.4.d). With respect to endocranial vault development, dimorphism was detected in the infant-child to juvenile group; during this period females presented higher values of vault development than males (Figures 6.16 and 6.17). Also, dimorphism was found in cortical brain development of the adolescent to adult group; during this period, females seemed to present a more developed cortical brain when compared with males for the shape changes described (Figures 6.24 and 6.25). It is interesting to note that, although there was no significant difference between brain and endocranium relationship of females and males, the former seems to present a tighter relationship between brain and endocranial volumes, and therefore a larger ratio brain / endocranial volume (Figure 6.14). This tendency is confirmed and statistically significant ($P < 0.001$, Table B.17) when graphing BV/ECV ratio versus ECV (Figure 6.15).

Chapter 7

Discussion

The discussion will be organized in the following way: each of the five questions investigated in this thesis will be addressed in a separate subsection. In each subsection, endocranial and brain results will be discussed separately, comparing our results with current bibliography. When the question being answered requires it, the distinction between *growth* and *development* will be done, in accordance with the theoretical framework chosen (see Chapter 3: Theoretical / methodological framework).

What kind of growth and development curve has the endocranium and the brain?

For this question, null hypothesis 1 (H_1) was evaluated: *"The brain and the endocranium maturation curves are linear and constant."* This hypothesis was rejected, as growth (size) and development (shape) of the endocranium and the brain presented non-linear curves.

What kind of growth curve has the endocranium? Human ECV grows inside the uterus a 29 % of the final magnitude in the adult (DeSilva and Lesnik, 2006). Sgouros et al. (1999) published ECV measures from 24 children during the first 3 years of life obtained

from MR imaging data, and showed that in the first few months of life ECV averages 900 cm^3 for males and 600 cm^3 for females, increasing to 1300 and 1500 cm^3, respectively, by the age of 15. In the first 2 years, 77 % of growth was achieved. This kind of growth curve is consistent with the results obtained by Guihard-Costa and Ramirez-Rozzi (2004), who studied a sample of 199 children and teenagers from 2 months old to 21 years old, and showed that skull growth (quantified by glabella-opisthocranion and basion- vertex distance) slows down between the ages of 2 and 3, this phenomenon happening earlier in males. Neubauer et al. (2009) studied dried crania of a cross-sectional ontogenetic series (48 specimens) and 60 adult specimens. Age groups were established according to dental eruption stages of the maxillary dentition. They found that endocranial CS increases dramatically in the first 2 postnatal years. Thereafter, growth rates decelerate with increasing age, with endocranial size increasing slightly after deciduous dentition is completed (on average at 3.5 years old / 42 months old). They also reported that 90-95% of adult ECV is achieved at an approximate age of 7-8. Another recent contribution to this matter was Kamdar et al. (2009) work, which included 123 healthy children, from 8 days to 6 years old, that underwent CT imaging for head trauma evaluation. They reported a growth curve that shows a doubling of the ECV from birth to 9 months of age and a tripling of the ECV by 6 years of age. Growth is most rapid from birth to 12 months of age, with continued but slower growth during the following 5 years. In this thesis, ECV growth curves coincide with those observed in the studies mentioned above (Figure 6.1), and provide more detailed information about the ECV ontogenetic changes. At 2.5-3 years (30-36 months) of age, male and female ECV reaches 1200 cm^3 (in accordance with Kamdar et al. (2009) Figure 2), which represents 80.07% of an adult male ECV (mean

adult male ECV: 1498.75 cm^3) and 90.49% of an adult female ECV (mean adult female ECV: 1326.13 cm^3). From this age onwards, there is a clear difference in ECV growth curves between sexes (Figure 6.1.b). Although the growth rate decrease conspicuously in both sexes (in agreement with Guihard-Costa and Ramirez-Rozzi (2004)), such decreasing is much sharper in females than in males; this is mainly due to the fact that by the age of 3 females have almost already reached their final ECV. Females reach adult ECV size at 10 years (120 months) of age and males at 15 years (180 months) of age (Figure 6.1.c and 6.1.d).

What kind of growth curve has the brain? Giedd et al. (1999) accomplished a longitudinal study of 145 healthy individuals (89 males and 56 females), in which at least 1 scan was obtained from each individual (47 had 1 scan, 65 had 2 scans, 30 had 3 scans, 2 had 4 scans and 1 had 5 scans, acquired at approximately two-year intervals). The age range was from 4.2 to 21.6 years old. They observed linear increases in WMV and nonlinear changes in GMV, with a preadolescent increase followed by a postadolescent decrease. GMV tends to follow an "inverted U" growth curve with volumes peaking at different times in different lobes. In females, GMV of frontal, temporal and parietal lobes peak at the age of 11.0, 16.7 and 10.2, respectively. In the case of males, GMV of frontal, temporal and parietal lobes peak at the age of 12.1, 16.2 and 11.8, respectively. On the other hand, in the occipital lobe GMV does not follow an "inverted U" growth curve; it continues to increase at least until an age of 20 for both sexes. In general, BV reaches its maximum value at 14.5 years of age in males and 11.5 years of age in females, and by 6 years old the brain has approximately reached 95% of this peak. Courchesne et al. (2000) analysed 116 healthy volunteers (79 male, 37 female) from 1.6 to 80 years

old. They found that GMV reached its maximum value at 6-9 years of age and thereafter declined linearly. WMV increased rapidly until 12-15 years of age, and from then onwards it continued increasing at a slower rate, reaching a plateau by the 4th decade of life. Bellis et al. (2001) studied MR images from a cross-sectional sample of 118 healthy children and adolescents (61 males and 57 females), from 6 to 17 years old. They reported significant age-related reductions in GMV and increases in WMV and corpus callosal areas, while BV showed no significant changes. Significant sex by age interactions were detected for GMV and WMV and corpus callosal areas. Particularly, males had more pronounced age-related GMV decreases and WMV and corpus callosal area increases than females. Following Giedd et al. (1999) work, Lenroot and Giedd (2006) analysed more deeply sexual dimorphism. They found that throughout ontogeny male brains are on average 9% larger than those of females. This difference is statistically significant, even when controlling for height and weight. Also, the authors suggested that GMV growth trajectory follows a specific regional pattern, with areas subserving primary functions, such as motor and sensory systems, maturing earlier, and higher order association areas, which integrate those primary functions, maturing later. Finally, Wilke et al. (2007) studied MR images from 200 healthy children (102 females and 98 males) from 5 to 18 years old. For both sexes, the correlation of GMV with age was best described by a third order polynomial function, with a maximum GMV of 900 cm^3 at 91 months (7.6 years) of age and a minimum of 800 cm^3 at 183 months (15.25 years) of age for males, and a maximum GMV of 800 cm^3 at 102 months (8.5 years) of age and a minimum of 670 cm^3 at 202 months (16.8 years) of age for females. The results obtained in this thesis are similar to those described above, but certain differences arise after their analysis. In general, the pattern is conserved: GMV,

as well as BV, present an "inverted U" growth curve, with males showing significantly larger volumes than females throughout the whole ontogenetic period analysed. WMV presents an approximate linear growth curve with an initial high rate until an age of 12-13, and then a lower rate in accordance with Courchesne et al. (2000) work; significant differences between sexes are evident in all the periods analised. The maximum peaks for GMV and BV coincide with those obtained by Giedd et al. (1999): the GMV peak is reached at 131±27 months (8.7-13.2 years) of age in males (896.17±14.71 cm^3) and at 103±27 months (6.3-10.8 years) of age in females (833.13±13.48 cm^3). For BV, males show a maximum peak (1361.31±37.47 cm^3) at 147±15 months (11-13.5 years) of age, while the maximum peak for females (1204.64±26.20 cm^3) is reached at 113±18 months (7.9-10.9 years) of age. These results are in disagreement with those reported by Wilke et al. (2007), which show that males present their GMV peak before females; the contrary was observed in this thesis, in accordance with Giedd et al. (1999); Lenroot and Giedd (2006) study.

What kind of development curve has the endocranium? The only study found in the literature that presents an ontogenetic shape curve of the human endocranium is Neubauer et al. (2009) work. The authors studied shape changes of the entire endocranium and then divided and studied separately the vault and cranial base. The shape trajectory for the vault alone is more linear than the one for the entire endocranium or the endocranial base alone; this means that the curvilinearity originates mainly from the cranial base development. After the first postnatal year, the vault shape trajectory is rather linear, the amount of shape changes (the length of the trajectory) is very small and the age groups largely overlap. In this thesis, the ontogenetic vault shape trajectory

schematized by PC1, PC2, and PC3 (Figure 6.6) is also approximately linear from the juvenile group onwards, in accordance with Neubauer et al. (2009), with an overlap of the adolescent and adult groups at late ontogeny. There are almost no shape differences between male adolescents and male adults and between female adolescents and female adults. This means that from adolescence onwards, there is no much shape change at the endocranial vault, a fact also shown in Figure 6.10, in which the development curve of the vault is delineated by the Procrustes distance between groups. It is evident in this curve that the largest distance between groups arises between the infant-child and juvenile group, which implies that most of the vault shape changes occur in that period.

What kind of development curve has the brain? The brain development can be quantified by plenty of variables (Thompson et al., 2004; Toga et al., 2006): cortical surface sulcal displacement (Sowell et al., 2002), gray matter density variations (Sowell et al., 2003; Gogtay et al., 2004), proportional changes (Sowell et al., 1999, 2001), and cortical thickness variations (Sowell et al., 2004); moreover, these variables can be measured in several delimited brain areas. In contrast, there is only one way of quantifying the endocranium development: by its own shape. Hence, in order to make more adequate comparisons between the vault and the brain development, brain development was quantified in this thesis with a methodological approach different from the ones cited above: by measuring its shape modifications. The brain development curve defined by PC1, PC2, and PC3 (Figure 6.8) shows a curvilinear trajectory, which presents a certain degree of overlap between infant-child and juvenile groups. This clearly shows that the brain changes its shape throughout all the ontogenetic period analysed, and also that there is more variability at early ages. The other methodology used to quantify the brain shape curve

(through Procrustes distances between groups) showed a similar pattern (Figure 6.11), with the most near groups being juveniles and adolescents and the most distant ones being the infant-child and the adult groups. Therefore, we conclude that brain shape changes occur mainly while it is growing; then the brain arrives to a shape stasis while reaching its size peak, and afterwards, while loosing mainly GMV, it reorganizes its shape again. During this last period, when the brain begins to lose gray matter, sexual dimorphism emerges in young adults, as discussed below.

What relationship has the cranial capacity measured from the bony endocranium with the brain volume?

To answer this question, hypothesis 2 (H_2) was proposed considering previous concepts (Connolly 1950): *"The larger the endocranium, the lower will be the percentage of volume occupied by the brain within the cranial vault."* This hypothesis was not rejected; hence, we accept that there is an inverse relationship between the endocranium size and the volume percentage occupied by the brain within the cranial vault.

The relationship between ECV and BV has been systematically reviewed and studied (Zuckerman, 1928; Holloway, 1973; Jerison, 1973); however, at present no consistent ratio between these two values is available. Tobias (1965) asserts that it has long been customary to accept the ECV as an approximation of BV. On the other hand, Leigh (2006) states that BV and ECV are different variables, as ECV includes the brain and the associated soft tissues (*i.e.*, cranial nerves, meninges, meningeal blood vessels, blood, and cerebrospinal fluid). In spite of this, it is frequent to find in the literature both variables as interchangeable, even in one of Leigh's own works: "One can estimate brain mass from cranial capacity by multiplying the cranial capacity by the specific gravity of the nervous

system (1.036 g/cm^3)" (Leigh, 2004). The basis of this formula lies on the idea that there is a one-to-one relationship between BV and ECV, which has certain support for non-human primates (Isler et al., 2008). In this study, the authors quantified the relationship between ECV and brain mass using ECV data from 62 species and brain mass data from the compilations of Stephan et al. (1981). They found an isometric relationship between ECV and brain mass, and concluded from this result that the multiplication of ECV (in cm^3) by the density of fresh brain tissue (1.036 g/cm^3) is appropriate for brain mass estimation (in g). Although they expressed that they expected ECV to be greater than brain mass due to the added volume of the meningeal membranes, blood vessels, and the subarachnoid space, their analysis demonstrated that brain mass (in g) is approximately 4% larger than ECV (in cm^3). Therefore, they concluded that the formula for brain mass was BV = ECV x 1.036 g/cm^3 (the density of fresh brain tissue (Stephan, 1960)), and that this formula would be sufficient for comparative analyses. We agree that this formula may be useful to compare data from different species; however, when studying development of one species, or when attempting to extract information from just one fossilized endocast, we consider that a precise BV/ECV ratio should be used.

Three different studies specifically assess the BV/ECV ratio question. The first one (Hofman, 1983) mathematically relates BV with ECV as follows: BV = 0.95 x ECV, which means that the ratio BV/ECV equals 0.95. The second study (Ruff et al., 1997) quantified BV from ECV by using a least-squares regression of 27 primate species, with data available for both parameters. After correcting for logarithmic transformations bias, they found the following mathematical relation: BV = 1.147 x ECV$^{0.976}$; hence, BV/ECV would be 0.9642. The last study (Peters et al., 1998) states that the cerebrospinal fluid

surrounding the brain represents about 12% of the ECV; this is expressed in the following formula: BV = 0.88 x ECV. Therefore, in this case the BV/ECV ratio equals 0.88.

Although these values of BV/ECV ratio (0.95 - Hofman (1983), 0.9642 - Ruff et al. (1997), and 0.88 - Peters et al. (1998)) are contained in the variability found in this thesis, it is interesting to determine how this ratio changes throughout the ontogenetic period analysed (Figure 6.14) and when sexual dimorphism arises (Figure 6.15). In this sense, the extreme mean values of BV/ECV found for females were 0.926 and 0.858 at the age of 5 and 30, respectively. For males, the BV/ECV ratio values corresponding to those ages were 0.901 and 0.839, respectively. From these results, it is clear that 0.95 (Hofman, 1983) or 0.9642 (Ruff et al., 1997) are not good estimators of the BV/ECV ratio for young adults (30 years old). Although Peters et al. (1998) presents a closer estimator for this age group, it is important to highlight that BV/ECV ratio is closely and negatively related to age and ECV; hence, one single estimator would not be adequate for different age groups and different ECVs. For this purpose, we propose four different new equations to calculate BV/ECV ratio for males and females from a known age group and presenting a known ECV:

Females (from 5 to 30 years): BV/ECV = age x (-0.002723) + 0.939660

Females (from 1150 to 1650 cm^3): BV/ECV = ECV x (-0.0008794) + 2.0469751

Males (from 5 to 30 years): BV/ECV = age x (-0.0025) + 0.9137

Males (from 1150 to 1650 cm^3): BV/ECV = ECV x (-0.0004468) + 1.5302292

The female and male BV/ECV curves described in this thesis, although not significantly different, present a dimorphic pattern that will be discussed later. For future research, a new segmentation technique could be used (Keihaninejad et al., 2010) to esti-

mate the ECV from the MR images, in order to obtain both values (BV and ECV) from the same individual and be able to calculate a more precise and accurate BV/ECV ratio.

What degree of covariation exists between endocranial and brain shape?

The third null hypothesis (H_3) stated that: *"There is no covariation between the endocranium and the brain."* This hypothesis was evaluated separately for each ontogenetic period studied. H_3 was rejected for the first and second ontogenetic periods analysed (infant-child to juvenile group and juvenile to adolescent group), as the results showed a certain degree of shape covariation between endocranium and brain on those periods. On the other hand, H_3 was not rejected for the adolescent to adult group, as no covariation was found between brain and endocranium shape changes associated with ageing during this last period analysed.

What are the specific shape modifications that suffers the endocranium throughout the studied ontogenetic period? Sardi et al. (2007) analysed late prenatal and early postnatal ontogeny in 54 dry human skulls from 32 to 47 weeks of gestational age. The authors found that brain growth is the major influence on craniofacial shape change, which produces a relative elongation of the vault. Zollikofer and de Leon (2002) studied 12 immature and 8 adult cranio-mandibular skeletal specimens of *H. sapiens* from the age of 3 to adulthood. They performed a GPA followed by a PCA and found that the PC1, which positively correlates with ageing and size augmentation, describes shape changes occurring in the neurocranium: it flattens and undergoes a relative contraction, from broad, short and more paedomorphic skulls to narrow, elongated and more peramorphic skulls. The authors proposed that cranio-mandibular ontogeny follows a nearly linear tra-

jectory through shape space, implying that the spatial patterns of shape change remain constant between the age of 3 and adulthood. On the other hand, Neubauer et al. (2009) distinguished the vault shape changes in four different ontogenetic periods: from 0.13 to 1.19 years old, the neurocranial vault develops parietal bossing and consequently becomes more globular; there is also a relative enlargement of the parietals. From 1.19 to 3.55 years old, the occipital poles develop, and the temporal region become broader. From 3.55 to 9 years old, the temporal poles rotate anteromedially and there is a relative expansion of medial parts of the frontal areas. And finally, from 9 years old to adulthood, a posterior projection of the occipital area develops and the temporal poles rotate laterally; generally, in this last period, the endocast gets flatter and wider. It is important to mention that the sample did not include adolescent individuals, and for this reason, the last period mentioned (that covers a broad interval from 9 to adulthood) may contain vault shape changes that occur actually earlier in that ontogenetic period (*i.e.* from 9 years old to adolescence) and remain unchanged until adulthood. The vault shape changes described in this thesis from infant-child (mean age: 2.15 years old) to juvenile groups (mean age: 9.00 years old) (Figure 6.17) are in accordance with Neubauer et al. (2009) vault shape changes from 0.13 to 9 years old. The following ontogenetic period analysed in this thesis, from juveniles (mean age: 9.00 years old) to adolescents (mean age: 14.80 years old), coincide with the last ontogenetic group analysed by Neubauer et al. (2009) (from the age of 9 to adulthood) (Figure 6.19). The most important vault shape change in this period is the strong and marked elongation and protrusion of the frontal region. Then, from adolescent (mean age: 14.80 years old) to adult groups (mean age: 25.29 years old) there are no shape vault changes. The discrepancy observed between this thesis and Neubauer's

study may be due to the already noted fact that the latter did not include adolescents in the data sets.

What are the specific shape changes that suffers the brain during the studied period of time? Sowell et al. (1999) found differences in statistical parametric maps of gray matter between a group of nine children and nine adolescents. Certain differences were also observed in dorso-frontal and parietal regions and relatively few differences were detected in cortices of the temporal and occipital lobes. Such effects are expected given that myelin deposition occurs throughout this age range (from childhood to adolescence), and the association cortices of frontal and parietal regions are known to myelinate later than cortices of more ventral brain regions (Yakovlev and Lecours, 1967). In another study, Sowell et al. (2001) analysed 35 normally developed children, adolescents, and young adults, and constructed statistical maps of regional and temporal patterns of gray matter density reduction and gray matter distance from center, to quantify local brain growth. Overall brain growth was not significant from childhood to adolescence, but they found close spatial relationships between gray matter density reduction and brain growth in the dorso-parietal and frontal cortex. These results suggest that progressive cellular maturation events, such as increased myelinization, together with regressive events, such as synaptic pruning, may play an important role during the postadolescent years in determining the definitive density of mature cortical gray matter of the frontal lobe. Sowell et al. (2003) constructed statistical maps of nonlinear age effects on gray matter density for 176 individuals from 7 to 67 years old. The authors found a nonlinear decline in gray matter density with age; the sharpest decline was observed from the age of 7 to 60, approximately, in dorsal frontal and parietal association cortices of both the lateral and

interhemispheric surfaces, and it was more prominent in the left than in the right hemisphere. Age effects were inverted in the left posterior temporal region, where the increase of gray matter density continued up to the age of 30, and then declined rapidly. In a more recent study, Sowell et al. (2004) applied computer-matching algorithms and new techniques to measure cortical thickness (in millimeters) from the structural MR images of 45 children scanned twice (every 2 years) between the ages of 5 and 11. Statistical maps of brain size changes revealed the most important growth occurring in prefrontal cortex, as well as in temporal and occipital regions, in a bilateral way. Gray matter thickness increase was restricted to the classical language regions of the frontal (*i.e.*, Broca's area) and temporo-parietal cortex (Wernicke's area in the left). Gogtay et al. (2004) studied human cortical gray matter development between the age of 4 and 21, by means of quantitative four-dimensional maps and time-lapse sequences of 13 healthy children, whose anatomic brain MR scans were obtained every 2 years. Overall, the total GMV was found to increase at earlier ages, followed by its sustained decrease around puberty. However, the process of GMV loss (maturation) begins in dorsal parietal cortices, particularly in the primary sensorimotor areas near the interhemispheric margin; then, it spreads rostrally over the frontal cortex, and caudally and laterally over the parietal, occipital, and finally the temporal cortex.

Based on the studies mentioned above a general picture of brain development arises: it seems that a close relationship exists between GMV loss and gray matter density reductions, synaptic pruning and white matter myelinization, which at the same time cause brain size augmentation. The general pattern of this process begins in the dorsal parietal cortices, and then it expands rostrally towards the frontal regions and caudally towards

the parietal areas; it finally continues in the temporal cortex. This development pattern agrees with the fact that temporal regions have a late maturation. Thereafter, when a brain region receives and / or reinforces synaptic connections, it loses gray matter (in volume and density) and experiments a local size augmentation. This phenomenon can be quantified from developmental graphs presented in red in the present thesis (Figures 6.21, 6.23, and 6.25), as that color expresses outwards development, which corresponds to a local size increment.

Even though the approach used in this thesis to quantify brain development was different from those of the previously discussed studies, our results coincide with the general brain development pattern. Brain shape changes from infant-child (mean age: 4.18 years old) to juvenile (mean age: 9.09 years old) are principally localized at superior parietal and prefrontal areas (Figure 6.21). Afterward, during the juvenile (mean age: 9.09 years old) to adolescent period (mean age: 15.00 years old), the main shape changes occur in the frontopolar area, which protrudes anteriorly (Figure 6.23). And finally, from adolescence (mean age: 15.00 years old) to young adults (mean age: 24.06 years old), the main changes occur in the inferior, middle, and superior areas of the temporal lobes (including Wernicke's area) (Figure 6.25).

What information do we have about endocranial and brain shape covariation?

One of the first approaches to understand the complex relationship between brain and endocranium was that of Moss and Young (1960). They state that the expansion of the enclosed neural mass provides the magnitude of the neural growth vectors, and that the direction of these same vectors is determined primarily by preferentially oriented fiber tracts of the dura mater. From its inception the cerebral capsule is "tied down" to the

originally cartilagenous cranial base at five points: the crista galli, the smaller wings of the sphenoid, and the petrous crests of the temporal bone. Oriented fiber systems emerge very early within the capsule in association with the sites of basal attachment. Therefore, the characteristic form (*i.e.* size + shape) of the normal neurocranium is the result of the preferential direction of the growth vectors of the expanding neural mass by these dural fiber systems. Enlow and Hans (1996) also investigated this association from an ontogenetic point of view: as the brain expands, the separate bones of the calvaria are correspondingly displaced in outwards directions. This is a passive movement of the bones themselves in conjunction with the brain expansion. Brain enlargement does not "push" the bones outwards in a direct manner; instead, they are displaced by a connective tissue stroma attached to them. This stroma is continuous at the same time with the meninges endocranially and the integument outside. As these enclosing connective tissue membranes anchored to the bones enlarge with the growing brain, the bones are carried outwards by them, being "separated" at their sutural articulations. The primary displacement causes tension in the sutural membranes, which, according to present theory, respond immediately by depositing new bone on the sutural edges. Sperber (2001), continuing with Moss and Young's theory, explains that the dura mater and its septa (the falces cerebri and cerebelli, and the tentorium cerebelli) present distinctly organized fiber bundles closely related and strongly attached to the sutural systems that later develop in the vault. The adult form of the neurocranium is the final result of the preferential direction of the forces established by the brain growth, which is constrained by these dural fiber systems. Without the dural bands, the brain would expand as a perfect sphere. Because the dura mater serves as the endocranial periosteum, it also determines

the shape of the calvarial bones. The definitive shape and size of the cranial vault depend primarily on the internal pressures exerted on the inner table of the neurocranial bones. The expanding brain exerts separating tensional forces upon the bone sutures, stimulating in consequence compensatory sutural bone growth. The brain acts in this context as a "functional matrix" in determining the extent of neurocranial bone growth. Therefore, it is clear that during brain growth, the endocranium shape has a direct relationship with brain shape. Studies about cranial synostosis reinforce this statement, showing a close association between brain and endocranium shape development during the first couple of years after birth. Aldridge et al. (2005) studied 32 isolated sagittal synostosis patients from 10 to 116 weeks (0.21 to 2.42 years) of age, before and after neurocranial surgery, and compared them with 11 age-matched unaffected individuals. Their results show that the isolated sagital synostosis brain is altered following neurocranial surgery, but it does not resemble that of unaffected individuals. This suggests that even though the brain is affected by the skull manipulation, it retains a growth pattern that is, at least in part, independent of the skull. Additionally, Richtsmeier et al. (2006) studied the interaction between brain and endocranium using brain MR images and head CT images of 18 human infants from 8 to 86 weeks (0.17 to 1.79 years) of age, who were diagnosed with isolated sagital synostosis or isolated right unilateral coronal synostosis. They found on the whole strong and positive associations between brain and endocranium, which suggest that the brain, meninges, and skull are interacting in a coordinate and integrated way with the changing patterns of suture closure during early ontogeny. Hence, the process is rather clear in these first years of brain and cranium maturation, but what happens once the brain stops growing? In our thesis, we found an important covariation

between brain and endocranial shape changes during infant-child to juvenile, and during the juvenile to adolescence period. The location of the brain shape changes during these periods corresponds perfectly with those of the endocranium. However, during the last ontogenetic period analysed (from adolescents to young adults) there was no covariation at all; in fact, endocranium vault did not change during this period. Hence, the shape variations quantified for the brain in this period do not have its counterpart in the bony endocranium.

When do endocranial petal patterns and brain macroscopic asymmetries grow and develop?

With regard to this question, null hypothesis 4 (H_4) was evaluated: *"Endocranial petal patterns and macroscopic brain asymmetries are already present at birth."* H_4 was not rejected, as both in the brain and in the endocranium asymmetric patterns were detected in the first ontogenetic period analysed in this thesis.

Which are the known brain asymmetric patterns? The first study that investigated brain asymmetries using a significant sample of 100 postmortem adult human brains free of pathologies was that of Geschwind and Levitsky (1968). The authors found marked anatomical asymmetries between the upper surface of the right and left temporal lobes. The *planum temporale* was larger on the left or right lobe in 65 % and 11 % of the brains, respectively. The left *planum* was on average one-third longer than the right one. Wada (1969) was the first person to show that this *planum* asymmetry is also present in the fetus and the newborn. Chi et al. (1977) showed later that it can be observed as early as in week 31 of gestation. In a more recent study Hering-Hanit et al. (2001) analysed

51 male and 51 female fetuses of 20-22 weeks of gestation, using diagnostic ultrasound scanning. They found a greater diameter of the left hemisphere compared to the right one, with no significant differences between sexes. Moreover, Gilmore et al. (2007) studied a sample of 74 neonates in the first few weeks after birth, and found that, in contrast to what happens in adults and older children, the left hemisphere was larger than the right one; also, the normal pattern of fronto-occipital asymmetry described in older children and adults was not present in the neonates. On the other hand, Giedd et al. (1996) analysed brain MR images of 104 healthy children and adolescents, from 4 to 18 years old, and quantified volumes of several brain regions. Right cerebral hemisphere and caudate volumes were larger than the contralateral ones, whereas left lateral ventricles and putamen were larger than the right ones. There were no significant differences between sexes for these asymmetries. The cerebellar hemispheres did not present any kind of asymmetry. In general, the anteriormost subdivision of the cerebrum showed a right-greater-than-left asymmetry. In another study, Watkins et al. (2001) analysed gray matter brain asymmetries in 142 young adults, by means of voxel-based statistical techniques, and found similar results. The voxel-wise analysis detected the well-known frontal (right $>$ left) and occipital (left $>$ right) brain asymmetries. Their analysis also confirmed the presence of left-greater-than-right asymmetries in several posterior language areas, including the *planum temporale* and the angular *gyrus*; no significant asymmetry was detected in the anterior language regions. Finally, the same pattern of asymmetries was observed in males and females. Sowell et al. (2002) mapped age differences in structural cortical surface asymmetries, through the application of surface-based mesh modeling image analytic methods in the study of normal developing children (7-11 years old), adolescents

(12-16 years old) and young adults (23-30 years old). Their results reveal that perisylvian sulcal asymmetries (characterized by longer and less sloped left Sylvian fissure, compared to the right one) are much more prominent in the adults that in the children. They also found a positive relationship between asymmetry and local gray matter proportion. All this evidence demonstrates that the asymmetric patterns operating during the first years of life are different from those operating during adolescence and young adulthood. This was further investigated in this thesis through the analysis of brain asymmetries associated with increasing age in three different periods (infant-child to juveniles, juveniles to adolescents, and adolescents to young adults), revealing that asymmetries do not develop following the same pattern throughout maturation (Table 7.1). For example, in the first period the left frontal region protrudes more anteriorly than the right one (Figure 6.31), in accordance with Gilmore et al. (2007). After adolescence, this pattern is inverted and the right frontal area protrudes more forwardly than the left one (Figure 6.35). Consequently, the adult fronto-occipital asymmetric pattern (Toga and Thompson, 2003) is developed after adolescence, and not before. This is an important fact to keep in mind when describing petal patterns on adult endocraniums (see below).

Which endocranial petalias are recognized in the literature? The brain protuberances and the way they often result in local imprints on the endocranial vault were investigated and described in the 50th decade. Connolly (1950) studied endocasts of individuals from adolescence to the age of 51 and noted that the fissural detail is maximal from 12 to 17 years old. In his book he draws attention to the fact that the evidence found on endocasts can provide some clues on the sulcal pattern, but the author clearly agrees with the generally accepted conclusion that this evidence is usually very meagre

Table 7.1: Summary of described brain asymmetries per period: infant-child to juvenile (Figure 6.31), juvenile to adolescent (Figure 6.33), and adolescent to adult (Figure 6.35).

	Frontal				Occipital			
	Width of hemispheres		Protrudes anteriorly		Width of hemispheres		Protrudes posteriorly	
	left	right	left	right	left	right	left	right
Infant-child to juvenile	++	−−	++	−−	≅	≅	−−	++
Juvenile to adolescent	≅	≅	+	−	−	+	−−	++
Adolescent to adult	−−	++	−−	++	++	−−	+	−

(le Gros Clark, 1951). In general terms, Connolly found that the impressions are often less marked in older individuals. This was in accordance with the results obtained by Boulay (1956), who studied human radiographies and found that the impression formation on the endocranial vault was most marked during adolescence. On the other hand, Hadziselimovic and Ruzdic (1966); Hadziselimovic and Cus (1966) studied 250 skulls and noted that 44% presented symmetrical occipital poles, 36.8% and 19.2% presented left and right occipito-petalias, respectively. These works showed that there is a certain relationship between the position of intracerebral structures and the shape of the internal vault.

LeMay (1976) measured widths and relative positions of the frontal and occipital portions of the brain hemispheres from CT images of 340 individuals. He found that 63% of the persons had wider right hemisphere and 63% presented relatively the same anterior positions of the hemispheres in the frontal area. With respect to the occipital area, 54% of the individuals presented wider left hemispheres, while the 66% had posteriorly protruding left hemispheres. However, to obtain these results, measurements were performed on the brain limits and not on the internal vault. In this thesis, on the contrary, landmarks were

placed on the endocranium so that the asymmetric signals correspond directly to the bony endocranium and not to the soft tissue. The question posed in the present thesis is rather different from the studies reviewed above, as their objective is to find static asymmetries present in adults, while in this thesis the question is when this asymmetric pattern develops. Our results show that those asymmetries that develop associated to ageing are only present on the infant-child to juvenile group. This pattern coincides with the one described for the brain on that same period (Table 7.2), and constitutes another evidence that the brain is in close relationship with the endocranium from birth to 9 years old; subsequently, this relationship becomes weaker. In general, the asymmetric pattern described for endocranial petalias at adulthood (right-frontal and left-occipital) does not coincide with the described pattern in the infant-child to juvenile period. This discrepancy may be due to the fact that there are other asymmetric processes occurring in the endocranium not related to ageing, for example, size augmentation. Another reason that could explain the observed discrepancy is the fact that asymmetries are much more variable from 9 years old onwards, so that correlation with ageing may be very low and could not be statistically discriminated, in the case it exists. Even though these two factors could act together, a pre-analysis performed with our data would reinforce the first one, as statistical correlations between asymmetries and size augmentation were found in the juvenile to adolescent period; this would also coincide with the results showing that adolescence is the period when fissural detail is maximal (Connolly, 1950; Boulay, 1956). However, the relatively small sample size of the present ontogenetic study (154 CT for endocranial data and 252 MR for brain from 0 to 31 years old) should be also taken into account to explain the discrepancy considered above, since asymmetry results presented

Table 7.2: Summary of described endocranial asymmetries during infant-child to juvenile period (Figure 6.29).

	Frontal				Occipital			
	Width of hemispheres		Protrudes anteriorly		Width of hemispheres		Protrudes posteriorly	
	left	right	left	right	left	right	left	right
Infant-child to juvenile	++	−−	++	−−	−−	++	−−	++

here show complex patterns (even reversals of local asymmetries). Therefore, the results of this thesis about asymmetric patterns should be understood as preliminary results that need to be corroborated by further research with larger data samples.

Is there sexual dimorphism throughout endocranium and brain growth and development?

The null hypothesis 5 (H_5) states that: *"There is no sexual dimorphism throughout endocranium and brain growth and development."* In order to evaluate H_5 correctly, endocranium and brain were analysed separately.

Which size and shape endocranial dimorphism patterns were quantified? In the case of endocranial growth (size) dimorphism, ECV was used to determine the significance of H_5. For all the ontogenetic periods analysed H_5 was rejected. In the case of endocranial development (shape) dimorphism, H_5 was rejected solely for the infant-child to juvenile group. In the remaining groups no differences were recognized between sexes for endocranial shape changes associated with ageing.

The main sexual dimorphism in body size arises at puberty; by then however, 95% of the cranium growth is already completed, as it was found in this thesis, with the adult endocranial size being achieved by females at an age of 10 and by males at an age of 15. As sexual dimorphism in the cranium is as important as for other parts of the body, this suggests that it must arise at an earlier age. Baughan and Demirjian (1978) analysed a longitudinal sample of children to investigate when cranial dimorphism takes place, and they showed that it indeed arises before puberty. This finding is reinforced by our results, which demonstrates that such dimorphism develops at an early developmental stage, from infant-child to juvenile period. During this period, females grow (in size) and develop (in shape) faster than males (Figure 7.1), but they also mature earlier than males, so they arrive to a final stage with smaller endocranial sizes but with the same shape (it is important to remember that shape was quantified from the endocranial vault and not from

the entire endocranium). Females obtain the same endocranial shape because the faster maturation is compensated by the earlier developmental halt; which is not the case for the endocranial size, where females grow a little faster than males, and the early growth halt makes females reach smaller endocranial sizes. The comparison of endocranial size and shape maturation between males and females (Figure 7.1) shows that during the infant-child to juvenile period females have an accelerated but shorter growth and developmental period in relation to males; or equally, males have a slower and extended growth and developmental period in relation to females. Hence, females present higher endocranial growth (size) and development (shape) rates than males. As shape trajectory is more divergent between sexes than size trajectories, females achieve (approximately at 10 years old) the same endocranial shape than males but with a smaller size. This pattern could be interpreted under the heterochronic framework aided by Gould's clock model (Gould, 1977) (Figure 7.2, see Appendix C). Although the clock model was defined to recognize heterochronic patterns when comparing two different species that have an ancestor-descendant relationship, it can be also applied to clarify developmental relationships between different groups of the same species (Ramirez-Rozzi et al., 2005; Sardi, 2010).

(a)

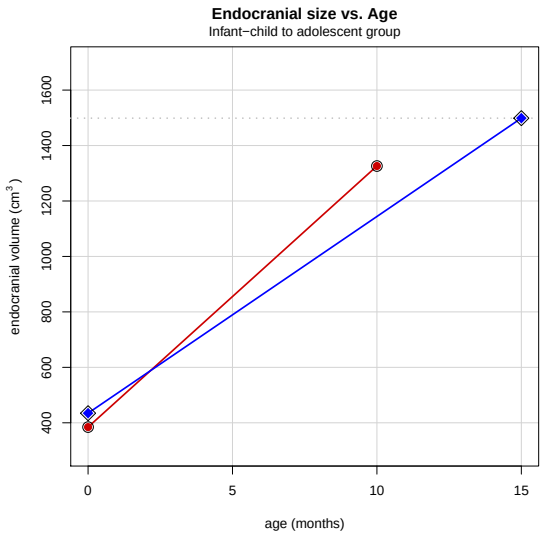

(b)

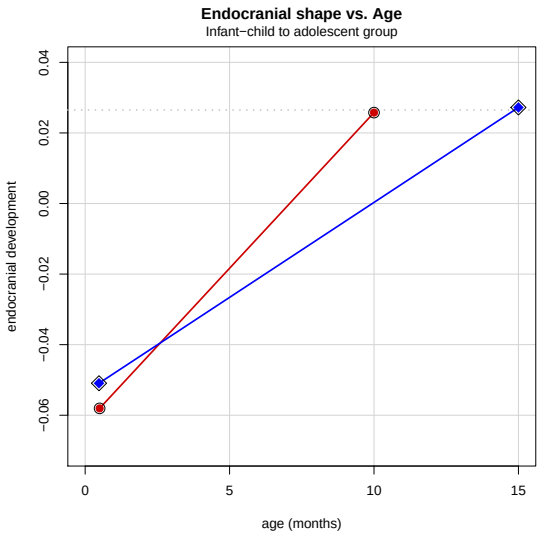

Figure 7.1: **Endocranial size & shape sexual dimorphism from infant-child to adolescent period. (a)** Endocranial size dimorphism. Birth values were calculated as 29% of adult endocranial volumes (DeSilva and Lesnik, 2006); adolescent values were calculated from mean adult ECVs (Figure 6.1.d). **(b)** Endocranial shape dimorphism. Initial values calculated from youngest individuals; adolescent values from regression curves of Figure 6.16.

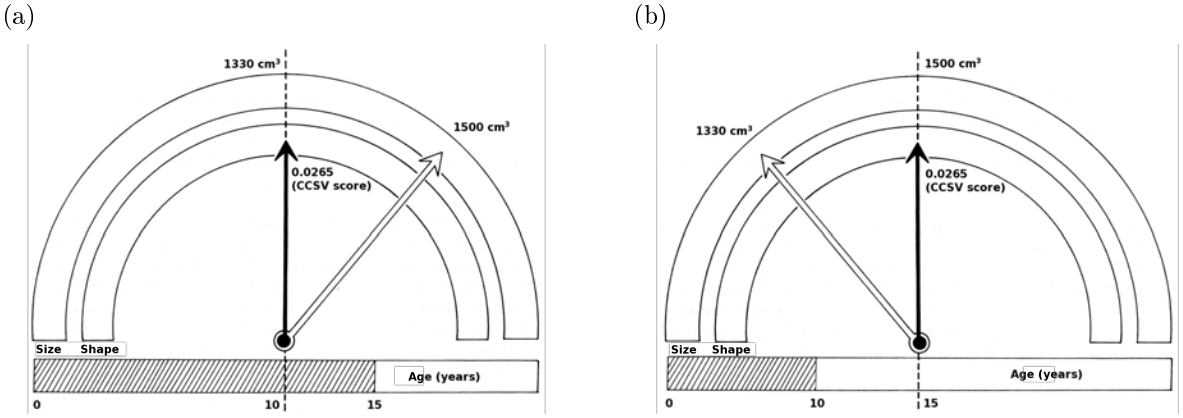

Figure 7.2: **Endocranial sexual dimorphism from infant-child to adolescent period explained as an heterochronic process.** **(a)** Clock model showing males in relation to females. **(b)** Clock model showing females in relation to males.

Which brain size differences were recognized? Null H_5 was rejected for GMV, WMV and BV throughout the ontogenetic periods studied.

In the 70th decade, Raisman and Field (1971) showed that neonatal exposure to testosterone organizes male-typical features of synaptic relationships in the rat hypothalamus. This was the first study that demonstrated that brain structure could be sexually dimorphic. From that time interest on sexually dimorphic structures raised considerably. Sexual dimorphism is evident in a wide variety of parameters, such as the volumes of certain brain regions, the size and number of specific cells, and the extent of dendritic and axonal branching and synapse formation (Vries et al., 1984). With respect to brain volume studies, is well known that brain mass is, on average, larger in males than in females (Jerison, 1982). Ankney (1992), after reanalysing a large data set of 1261 individuals from an age of 25 to 80, found that after correcting for body height or body surface area, male BV is still about 110 cm^3 larger than female BV. This volumetric difference is also reflected in the present thesis on GMV, WMV and BV, which are sexually dimorphic throughout the entirely ontogenetic period analysed. In fact, this volumetric sexual dimorphism was already recognized at birth, with males presenting larger GMV and WMV than females (Gilmore et al., 2007). These results agree with those obtained in the studies reviewed above about brain volume dimorphism (Giedd et al., 1999; Courchesne et al., 2000; Lenroot and Giedd, 2006; Wilke et al., 2007), as it was stated earlier on this discussion when comparing brain growth curves. It is interesting to highlight that the relationship between GMV and WMV changes similarly on both sexes throughout nearly the entire period analysed; a statistically significant slight difference ($P < 0.05$) between sexes was observed for GMV/WMV ratio when arriving young adulthood (Figure 6.4.d,

Table B.15). In this period, females present a more gradual slope, which is mainly due to the fact that females lose proportionally less GMV than males. This result is in accordance with most studies that report greater gray matter percentages and lower white matter percentages in females in relation to males (Filipek et al., 1994; Gur et al., 1999; Allen et al., 2003; Cosgrove et al., 2007). The GMV/WMV ratio difference observed is thought to be related to shape differences found at this same period (see discussion below).

Which dimorphic shape changes could be recognized in the brain? Null H_5 was rejected for the adolescent to adult group for brain shape changes associated with ageing; in the case of the other groups the null hypothesis 5 was not rejected.

Even though the whole adult human brain size is larger in males, several regions are proportionately larger in females, including the caudate nucleus, hippocampus, some prefrontal cortical areas, the superior temporal gyrus, and certain white matter structures such as the anterior commissure. Regions proportionately larger in the adult male brain include the hypothalamus, *stria terminalis*, cerebral ventricles, and the *splenium* and *genu* of the *corpus callosum* (Goldstein et al., 1999). Goldstein et al. (2001) compared relative sizes of different brain regions from 48 healthy adults, and found a greater sexual dimorphism among brain areas that are homologous with those identified in animal studies showing greater levels of sex steroid receptors during critical periods of brain development. Sexual differentiation of the nervous system is primarily attributable to the action of the testosterone and its metabolites early in development (Vries and Simerly, 2002). It has been presumed that once established perinatally, sexual dimorphisms in cell number are passively maintained throughout life. But a recent study in rats showed that pubertal

hormones contribute to the postnatal preservation of sexual dimorphisms, through sex-specific modulation of new cell addition to sexually dimorphic brain regions (Ahmed et al., 2008). Another evidence that supports this idea was provided by Witte et al. (2010), who demonstrated the existence of associations between certain cortical GMV regions and circulating level of sex hormones (17β-estradiol, testosterone, and progesterone). These studies point to a more dynamic preservation of sex dimorphism, a concept that is also reinforced in this thesis as developing sexual dimorphism was found in adolescence to young adulthood period associated with ageing. Females begins to lose GMV earlier than males (at an age of 9.4 in females and 12.3 in males) (Figure 7.3), and this phenomenon is associated with synaptic pruning and increased myelinization (Sowell et al., 2001, 2003, 2004), which is related at the same time to the emergence of the GMV/WMV ratio dimorphism mentioned before. Although brain development slope is the same for males and females (Figure 7.3.b), this earlier developmental start or onset confers young adult females a more developed brain shape when comparing with males from the same period. In this case, females present a slightly lower rate of brain volume loss (size) and the same rate of brain development (shape) in relation to males. The divergence between development trajectories arises at the onset of this process: females start loosing GMV before males and, therefore, they start rearranging their brain shapes before males. For this reason, females attain a much more developed brain at the age of 30 than males. To display a clearer picture for brain developmental differences between sexes, the clock model was used (Figure 7.4, see Appendix C).

(a) (b)

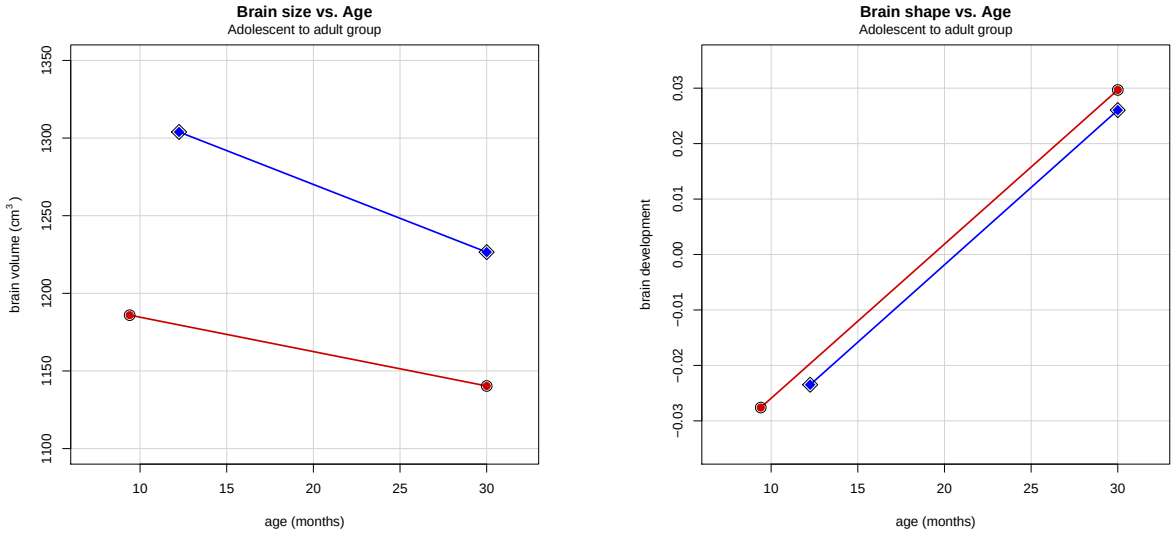

Figure 7.3: **Brain size & shape sexual dimorphism from adolescent to adult period. (a)** Brain size dimorphism. Adolescent and adult values were calculated from regression curves of Figure 6.5.d. **(b)** Brain shape dimorphism. Adolescent and adult values were calculated from regression curves of Figure 6.24.

(a)

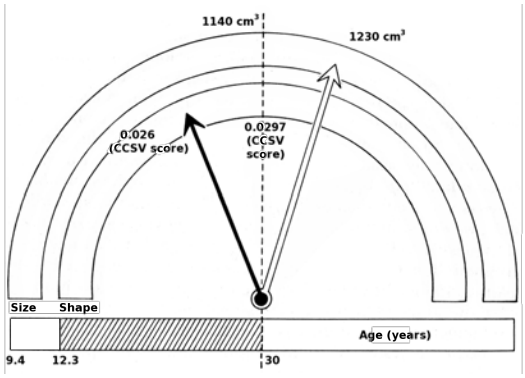

(b)

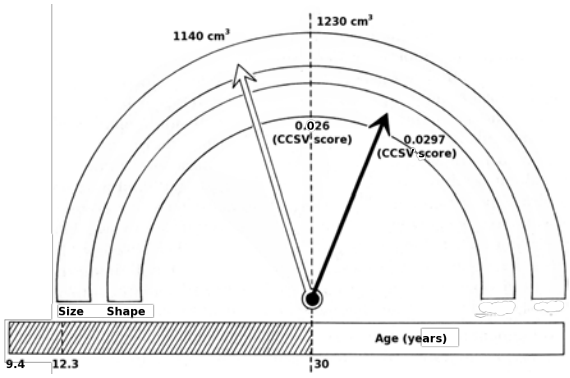

Figure 7.4: **Brain sexual dimorphism from adolescent to adult period explained as an heterochronic process. (a)** Clock model showing males in relation to females. **(b)** Clock model showing females in relation to males.

Does endocranium / brain relationship follows a dimorphic pattern? Another aspect that resulted sexually dimorphic was the ratio BV/ECV. The reason of this difference between sexes is principally due to the fact that males present bigger endocrania, and in accordance with Connolly's hypothesis (Connolly, 1950) ("The larger the endocranium, the lower will be the percentage of the volume occupied by the brain within the cranial vault"), they present in consequence lower BV/ECV ratios than females (Figure 6.14 and 6.15).

Chapter 8

Conclusions

How does this thesis work affect the current paleo-neuro-anthropological evidences of brain evolution?

"The endocranial vault has a close relation with the growing brain." In this thesis it was demostrated that this statement is not true, at least for the whole ontogenic period analyzed here (from birth to young adulthood). It was shown that brain and endocranial vault maintain a direct physical relation only until adolescence, specifically, until the endocranium stops growing (10 years for females and 15 for males), and when the brain starts loosing gray matter (9 years for females and 12 for males). The reported brain development (in shape) curves represent new data that demonstrates a more dynamically developing organ: that changes its shape while growing, then appears to arrive to an stasis point while reaching its maximum size, and then modifying again its shape while loosing mainly gray cortical matter. In comparison with the endocranium, that ceases to modify its form right after the growth period finishes, the brain suffers many shape changes throughout all the ontogenetic period analyzed. This characteristic is vital to understand what information an adult hominid fossil actually shows in its endocrast:

marks of an underdeveloped brain. Or, in other words, the internal grooves and marks that can be found and described in an adult human endocast vault actually correspond to soft tissue appertaining to the adolescent brain and not to its adult form.

Another contribution that directly affects human brain evolutionary studies is the revision and proposal of new equations for BV/ECV ratio measurements. The relationship between BV and ECV has been thoroughly reviewed (Zuckerman, 1928; Holloway, 1973; Jerison, 1973), and there was no consistent ratio between these two values; for that reason, it has long been customary to accept the ECV as an approximation to BV (Tobias, 1965). From this thesis onwards, this approximation cannot be accepted any more. Although this study contains only human data, this is the first work that reports BV/ECV changes through ontogeny and that also quantifies the presence of sexual dimorphism in this ratio. For comparative reasons, it would be very interesting to have these same parameters and equations for other non-human primates. New studies with CT and MR ontogenetic images will allow to clarify and expand our knowledge of how these two structures relate through growth and development in other primates, hence obtaining a more precise estimation for extinct hominids.

A third important point would be the clarification of the asymmetric pattern that follows the brain and the endocranium. It was shown that brain asymmetries, although already present from birth, do not follow the same asymmetric pattern throughout development. In fact, there are processes that develop in one direction during the infant-child to juvenile period, and then acquire the opposite direction during adolescent to adult period. This, summed to the fact that brain and endocranium do not preserve their close relation after adolescence, would have a direct impact on works that search brain asymmetric im-

pressions on the internal cranial bone (Holloway, 1981; Holloway and Costelareymondie, 1982).

Finally, current studies of endocranial development with hominid brain evolutionary perspectives should have in mind the fact that the brain and endocranium relationship is not that direct. For example, in a recent study Bruner and Holloway (2010) claim: "Because of the relationship between brain and braincase Richtsmeier et al. (2006); Bruner (2007), the morphology of the anterior cranial fossa is directly related to the shape of the frontal lobes, in particular the prefrontal areas. Because the thickness of the dura mater is negligible in terms of contribution to the general shape variability, changes in the morphology of the anterior fossa can be used as a proxy for changes in the spatial relationships (*e.g.*, volumes and geometry) of the frontal lobes." This is true just for the ontogenetic period specified in this thesis and should not be generalized to the whole ontogenetic period. As we have seen, during embryonal, fetal and first decade of postnatal life, the form of the cranium is molded specially by the surface of the expanding brain. In this way, the external brain cortex is printed in the internal cranial vault. In some areas, the brain gyri leave hollow impressiones gyrorum in the endocranial surface. Connolly (1950) showed that this impressions are maximal during youth and young adults and then decay with time, probably due to os reabsorption increases. This idea was tested and probed in this thesis. And we must keep in mind that this fact becomes an advantage for paleoneurologists, because of the high percentage in the fossil record of young individuals anatomically immature (Mann, 1968, 1975; Tobias, 1968, 1974). For this very reason it is highly relevant to study how the brain and endocranium relates in our own species during the first postnatal decade in order to improve our understanding of the hominid fossil

record endocranium.

How does this thesis work affect the current endocranial and brain sexual dimorphism knowledge?

In this thesis two heterochronic processes to describe sexual dimorphism during form maturation could be distinguished. One for the endocranial maturation and another one for brain maturation. Although heterochronic processes may not be directly measured physiologically; this is to say that, for example, if we measure an acceleration process between females and males it may not imply directly that there is a hormonal difference that causes this shape and size divergences. Of course there could be an example of such a simple case, but the norm is that heterochronic processes are actually just the expression in the form that there are complex and often difficult to elucidate sub processes that differ between groups (in this case sexes). Mainly, heterochronies settle a fertile ground to recognize group differences and easily catalog them into a theoretic framework (Gould, 1977; Alberch et al., 1979; Klingenberg, 1998; Gould, 2000) (see Appendix C) that allow us, in this specific case, to understand how dimorphism evolved in hominids. The fact that two different heterochronic processes can explain separately endocranial and brain dimorphism also shows the several times mentioned idea in this thesis that these two structures do not follow a close maturational relation throughout the entire ontogenetic period.

How does this thesis work affect the current brain development knowledge?

As Figures 6.21, 6.23, and 6.25 show, brain shape changes associated with ageing are in accordance with current knowledge of brain development, and could be the result of

myelinization and axonal pruning: "... the last vestiges of local brain growth and apparent concomitant cortical thinning during childhood primarily result from increases in myelinization, which confirm localized thickness increases in frontal and temporal perisylvian gray matter during childhood..." (Sowell et al., 2004). This thesis also contributes with new information about brain shape changes providing new details about maturational form changes in different ontogenetic periods by means of a new quantification methodology (CCSV measurements based on GM methods).

Table of Abbreviations

Abbreviation	Definition
3D	Three dimensional
ANCOVA	Analysis of covariance
BV	Brain volume (BV = GMV + WMV)
CCASV	Common chronological asymmetric shape vector
CCSV	Common chronological shape vector
CS	Centroid size
CT	Computed tomographic
DAO	directional asymmetric optimization
ECV	Endocranial volume
GM	Geometric morphometric
GMV	Gray matter volume
GPA	Generalized least squares Procrustes superimposition analysis
kVp	Kilovolts peak
mA	Mili Amperes
MR	Magnetic resonance
PC	Principal component
PCA	Principal component analysis
SEM	Standard error of the mean
TE	Echo time
TI	Inversion time
TR	Repetition time
WMV	White matter volume

Bibliography

Acharya, T. and A. K. Ray

2005. *Image Processing: Principles and Applications*. Wiley-Interscience.

Ahmed, E. I., J. L. Zehr, K. M. Schulz, B. H. Lorenz, L. L. DonCarlos, and C. L. Sisk

2008. Pubertal hormones modulate the addition of new cells to sexually dimorphic brain regions. *Nature neuroscience*, 11(9):995–997.

Aiello, L. and C. Dean

2002. *An Introduction to Human Evolutionary Anatomy*. Academic Press.

Alberch, P., S. Gould, G. Oster, and D. Wake

1979. Size and shape in ontogeny and phylogeny. *Paleobiology*, 5(3):296–317.

Aldridge, K., A. A. Kane, J. L. Marsh, P. Yan, D. Govier, and J. T. Richtsmeier

2005. Relationship of brain and skull in pre-and postoperative sagittal synostosis. *Journal of Anatomy*, 206(4):373–385.

Allen, J. S., H. Damasio, T. J. Grabowski, J. Bruss, and W. Zhang

2003. Sexual dimorphism and asymmetries in the gray-white composition of the human cerebrum. *NeuroImage*, 18(4):880–894.

Amunts, K., A. Schleicher, U. Bürgel, H. Mohlberg, H. Uylings, and K. Zilles

1999. Broca's region revisited: Cytoarchitecture and intersubject variability. *The Journal of Comparative Neurology*, 412:319–341.

Ankney, C. D.

1992. Sex differences in relative brain size: The mismeasure of woman, too? *Intelligence*, 16(3-4):329–336.

Annett, M.

2002. *Handedness and brain asymmetry: the right shift theory.* Psychology Press.

Anthony, R.

1913. L'encéphale de l'homme fossile de la quina. *Bulletins et Mémoires de la Société d'anthropologie de Paris*, 4(2):117–195.

Ashburner, J. and K. J. Friston

2000. Voxel-Based morphometry - the methods. *Neuroimage*, 11:805–821.

Balzeau, A., E. Gilissen, W. Wendelen, and W. Coudyzer

2009. Internal cranial anatomy of the type specimen of pan paniscus and available data for study. *Journal of Human Evolution*, 56(2):205–208.

Barkovich, A. J., B. O. Kjos, D. E. J. Jr, and D. Norman

1988. Normal maturation of the neonatal and infant brain: MR imaging at 1.5 t. *Radiology*, 166(1):173.

Bastir, M. and A. Rosas

2004. Comparative ontogeny in humans and chimpanzees: Similarities, differences and paradoxes in postnatal growth and development of the skull. *Annals of Anatomy*, 186(5-6):503–509.

Bastir, M., A. Rosas, and P. O'Higgins

2006. Craniofacial levels and the morphological maturation of the human skull. *Journal of Anatomy*, 209(5):637–654.

Baughan, B. and A. Demirjian

1978. Sexual dimorphism in the growth of the cranium. *American Journal of Physical Anthropology*, 49(3):383–390.

Bellis, M. D. D., M. S. Keshavan, S. R. Beers, J. Hall, K. Frustaci, A. Masalehdan, J. Noll, and A. M. Boring

2001. Sex differences in brain maturation during childhood and adolescence. *Cereb. Cortex*, 11(6):552–557.

Boulay, G. D.

1956. The significance of digital impressions in children's skulls. *Acta radiologica*, 46(1-2):112.

Boule, M. and R. Anthony

1911. L'encephale de l'homme fossile de la Chapelle-aux-Saints. *L'anthropologie*, 22:129–196.

Bradshaw, J. L.

1991. Animal asymmetry and human heredity: dextrality, tool use and language in evolution–10 years after walker (1980). *British Journal of Psychology (London, England: 1953)*, 82 (Pt 1):39–59. PMID: 2029604.

Broca, P.

1861. Remarques sur le siege de la faculte du langage articule; suivies d'une observation d'aphemie. *Bulletin de la Société Anatomique de Paris*, 6:330–357.

Brodmann, K.

1909. *Vergleichende Lokalisationslehre der Grosshirnrinde in ihren Prinzipien dargestellt auf Grund des Zellenbaues*. Leipzig: JA Barth.

Brown, M. A. and R. C. Semelka

2003. *MRI: Basic Principles and Applications*, 3 edition. Wiley-Liss.

Bruner, E.

2004. Geometric morphometrics and paleoneurology: brain shape evolution in the genus homo. *Journal of Human Evolution*, 47(5):279–303.

Bruner, E.

2007. Cranial shape and size variation in human evolution: structural and functional perspectives. *Child's Nervous System*, 23(12):1357–1365.

Bruner, E.

2008. Comparing endocranial form and shape differences in modern humans and neandertals: a geometric approach. *PaleoAnthropology*, 93:106.

Bruner, E.

2010. Morphological differences in the parietal lobes within the human genus: A neurofunctional perspective. *Current Anthropology*, 51(S1):S77–S88.

Bruner, E., M. Averini, and G. Manzi

2003. Endocranial traits. prevalence and distribution in a recent human population. *European Journal of Anatomy*, 7(1):23–34.

Bruner, E. and R. L. Holloway

2010. A bivariate approach to the widening of the frontal lobes in the genus homo. *Journal of Human Evolution*, 58:138–146.

Calvin, W. H.

1982. Did throwing stones shape hominid brain evolution? *Ethology and Sociobiology*, 3(3):115–124.

Cantalupo, C. and W. D. Hopkins

2001. Asymmetric broca's area in great apes: A region of the ape brain is uncannily similar to one linked with speech in humans. *Nature*, 414(6863):505.

Chi, J. G., E. C. Dooling, and F. H. Gilles

1977. Left-right asymmetries of the temporal speech areas of the human fetus. *Archives of Neurology*, 34(6):346.

Chiu, H. C. and A. R. Damasio

1980. Human cerebral asymmetries evaluated by computed tomography. *J Neurol Neurosurg Psychiatry*, 43(10):873–878.

Clark, A., N. MacLusky, and P. Goldman-Rakic

1988. Androgen binding and metabolism in the cerebral cortex of the developing rhesus monkey. *Endocrinology*, 123(2):932–940.

Clark, W., D. M. Cooper, and B. S. Z. Zuckerman

1936. *The Endocranial Cast of the Chimpanzee*. JSTOR.

Connolly, C. J.

1950. *External Morphology of the Primate Brain*. Springfield, Illinois: CC Thomas.

Corballis, M. C.

1989. Laterality and human evolution. *Psychological Review*, 96(3):492–505. PMID: 2667014.

Corner, B. D., S. Lele, and J. T. Richtsmeier

1992. Measuring precision of three-dimensional landmark data. *J Quant Anthropol*, 3(4):347–359.

Cosgrove, K. P., C. M. Mazure, and J. K. Staley

2007. Evolving knowledge of sex differences in brain structure, function, and chemistry. *Biological Psychiatry*, 62(8):847–855.

Courchesne, E., H. J. Chisum, J. Townsend, A. Cowles, J. Covington, B. Egaas, M. Harwood, S. Hinds, and G. A. Press

2000. Normal brain development and aging: Quantitative analysis at in vivo MR imaging in healthy volunteers 1. *Radiology*, 216(3):672–682.

Crawley, M. J.

2007. *The R Book*, 1 edition. Wiley.

Cunningham, D. J.

1892. *Contribution to the Surface Anatomy of the Cerebral Hemispheres*. Royal Irish Academy Dublin.

Dekaban, A. S. and D. Sadowsky

1978. Changes in brain weights during the span of human life: relation of brain weights to body heights and body weights. *Annals of Neurology*, 4(4):345–56. PMID: 727739.

DeLacoste-Utamsing, C. and R. L. Holloway

1982. Sexual dimorphism in the human corpus callosum. *Science*, 216(4553):1431–1432.

DeSilva, J. and J. Lesnik

2006. Chimpanzee neonatal brain size: Implications for brain growth in homo erectus. *Journal of Human Evolution*, 51:207–212.

Dryden, I. L. and K. V. Mardia

1998. *Statistical Shape Analysis*, 1 edition. Wiley.

Dubois, E.

1899. Abstract of remarks on the brain-cast of pithecanthropus erectus. *Journal of Anatomy and Physiology*, 33(Pt 2):273–276. undefinedPMCID: 1328010.

Eberstaller, O.

1884. Zur oberflachenanatomie der grosshirnhemispharen. *Wien Med Blaetter*, 7:479–482.

Elton, S., L. C. Bishop, and B. Wood

2001. Comparative context of Plio-Pleistocene hominin brain evolution. *Journal of Human Evolution*, 41(1):1–27.

Enlow, D. H.

1990. *Facial Growth*. Philadelphia: WB Saunders Company.

Enlow, D. H. and M. G. Hans

1996. *Essentials of Facial Growth*. W.B. Saunders Company.

Falk, D.

1980. A reanalysis of the south african australopithecine natural endocasts. *American Journal of Physical Anthropology*, 53(52):5–539.

Falk, D.

1987. Brain lateralization in primates and its evolution in hominids. *American Journal of Physical Anthropology*, 30.

Falk, D.

2006. Evolution of the primate brain. In *Handbook of palaeoanthropology*, volume 2, Pp. 1133–1162.

Falk, D., C. Hildebolt, J. Cheverud, M. Vannier, R. Helmkamp, and L. Konigsberg

1990. Cortical asymmetries in frontal lobes of rhesus monkeys (Macaca mulatta). *Brain research*, 512(1):40–45.

Falzi, G., P. Perrone, and L. A. Vignolo

1982. Right-left asymmetry in anterior speech region. *Archives of Neurology*, 39(4):239–240.

Filipek, P. A., C. Richelme, D. N. Kennedy, and V. S. Caviness

1994. The young adult human brain: An MRI-based morphometric analysis. *Cereb. Cortex*, 4(4):344–360.

Fleschig, P.

1908. Bemerkungen über die hörsphare des menschlichen gehirns. *Neurol. Zent. Bl.*, 27:2–7.

Free, S. L., P. O'Higgins, D. D. Maudgil, I. L. Dryden, L. Lemieux, D. R. Fish, and S. D. Shorvon

2001. Landmark-Based morphometrics of the normal adult brain using MRI. *Neuroimage*, 13(5):801–813.

Friston, K. J., J. T. Ashburner, S. J. Kiebel, T. E. Nichols, and W. D. Penny

2006. *Statistical Parametric Mapping: The Analysis of Functional Brain Images*, 1 edition. Academic Press.

Galaburda, A., M. LeMay, T. Kemper, and N. Geschwind

1978. Right-Left asymmetries in the brain structural differences between the hemispheres may underlie cerebral dominance. *Science*, 199:852–856.

Gannon, P., N. Kheck, and P. Hof

2001. Language areas of the hominoid brain: a dynamic communicative shift on the upper east side planum. In *Falk D., Gibson K.R. (eds) Evolutionary Anatomy of the Primate Cerebral Cortex*, Pp. 216–240. Cambridge: Cambridge University Press.

Gannon, P. J., R. L. Holloway, D. C. Broadfield, and A. R. Braun

1998. Asymmetry of chimpanzee planum temporale: Humanlike pattern of wernicke's brain language area homolog. *Science*, 279(5348):220.

Garey, L.

1994. *Brodmann's 'Localisation in the cerebral cortex'*, 3 edition. London: Smith-Gordon & Co.

Geschwind, N. and A. M. Galaburda

1985a. Cerebral lateralization: Biological mechanisms, associations, and pathology: I. a hypothesis and a program for research. *Arch Neurol.*, 42(5):428–459.

Geschwind, N. and A. M. Galaburda

1985b. Cerebral lateralization: Biological mechanisms, associations, and pathology: II. a hypothesis and a program for research. *Arch Neurol.*, 42(6):521–552.

Geschwind, N. and A. M. Galaburda

1985c. Cerebral lateralization: Biological mechanisms, associations, and pathology: III. a hypothesis and a program for research. *Arch Neurol.*, 42(7):634–654.

Geschwind, N. and W. Levitsky

1968. Human brain: Left-Right asymmetries in temporal speech region. *Science*, 161(3837):186–187.

Giedd, J. N., J. Blumenthal, N. O. Jeffries, F. X. Castellanos, H. Liu, A. Zijdenbos, T. Paus, A. C. Evans, and J. L. Rapoport

1999. Brain development during childhood and adolescence: a longitudinal MRI study. *Nature Neuroscience*, 2(10):861–3. PMID: 10491603.

Giedd, J. N., J. W. Snell, N. Lange, J. C. Rajapakse, B. J. Casey, P. L. Kozuch, A. C. Vaituzis, Y. C. Vauss, S. D. Hamburger, D. Kaysen, and J. L. Rapoport

1996. Quantitative magnetic resonance imaging of human brain development: Ages 4-18. *Cereb. Cortex*, 6(4):551–559.

Gilmore, J. H., W. Lin, M. W. Prastawa, C. B. Looney, Y. S. K. Vetsa, R. C. Knickmeyer, D. D. Evans, J. K. Smith, R. M. Hamer, J. A. Lieberman, and G. Gerig

2007. Regional gray matter growth, sexual dimorphism, and cerebral asymmetry in the neonatal brain. *J. Neurosci.*, 27(6):1255–1260.

Gogtay, N., J. N. Giedd, L. Lusk, K. Hayashi, D. Greenstein, A. Vaituzis, T. N. III, D. Herman, L. Clasen, A. Toga, J. Rapoport, and P. Thompson

2004. Dynamic mapping of human cortical development during childhood through early adulthood. *PNAS*, 101(21):8174–8179.

Goldstein, J. M., D. N. Kennedy, and V. S. Caviness

1999. Brain development, XI: sexual dimorphism. *Am J Psychiatry*, 156(3):352.

Goldstein, J. M., L. J. Seidman, N. J. Horton, N. Makris, D. N. Kennedy, V. S. Caviness, S. V. Faraone, and M. T. Tsuang

2001. Normal sexual dimorphism of the adult human brain assessed by in vivo magnetic resonance imaging. *Cerebral Cortex (New York, N.Y.: 1991)*, 11(6):490–7. PMID: 11375910.

Gonzalez, R. C. and R. E. Woods

2002. *Digital Image Processing*, 2nd edition. Prentice Hall.

Gould, S.

2000. Of coiled oysters and big brains: how to rescue the terminology of heterochrony, now gone astray. *Evolution & Development*, 2(5):241–248.

Gould, S. J.

1977. *Ontogeny and phylogeny*. Belknap press.

Guihard-Costa, A. and F. Ramirez-Rozzi

2004. Growth of the human brain and skull slows down at about 2.5 years old. *C R Palevol*.

Gur, R. C., B. I. Turetsky, M. Matsui, M. Yan, W. Bilker, P. Hughett, and R. E. Gur

1999. Sex differences in brain gray and white matter in healthy young adults: Correlations with cognitive performance. *J. Neurosci.*, 19(10):4065–4072.

Habib, M., F. Robichon, O. Levrier, R. Khalil, and G. Salamon

1995. Diverging asymmetries of temporo-parietal cortical areas: A reappraisal of Geschwind/Galaburda theory. *Brain and Language*, 48(2):238–258.

Hadziselimovic, H. and M. Cus

1966. The appearance of internal structures of the brain in relation to configuration of the human skull. *Cells Tissues Organs*, 63(3):289–299.

Hadziselimovic, H. and N. Ruzdic

1966. Appearance of the base of the brain in relation to the configuration of human skull. *Cells Tissues Organs*, 65(1-3):146–156.

Hering-Hanit, R., R. Achiron, S. Lipitz, and A. Achiron

2001. Asymmetry of fetal cerebral hemispheres: in utero ultrasound study. *Archives of Disease in Childhood - Fetal and Neonatal Edition*, 85(3):F194–F196.

Hofman, M. A.

1983. Evolution of brain size in neonatal and adult placental mammals: a theoretical approach. *J Theor Biol*, 105(2):317–32.

Hofman, M. A. and D. F. Swaab

1991. Sexual dimorphism of the human brain: myth and reality. *Experimental and Clinical Endocrinology*, 98(2):161–170. PMID: 1778230.

Holland, B. A.

1986. MRI of normal brain maturation. *American Journal of Neuroradiology*, 7(2):201–208.

Holloway, R.

1996. Evolution of the human brain. In *Handbook of human symbolic evolution*, Pp. 74–116.

Holloway, R. L.

1966. Cranial capacity and neuron number: a critique and proposal. *Am J Phys Anthropol*, 25(3):305–14.

Holloway, R. L.

1973. Endocranial volumes of early african hominids, and the role of the brain in human mosaic evolution. *Journal of Human Evolution*, 2(6):449–459.

Holloway, R. L.

1974. The casts of fossil hominid brains. *Sci Am*, 231(1):106–15.

Holloway, R. L.

1980. Indonesian "Solo" (Ngandong) endocranial reconstructions: Some preliminary observations and comparisons with neandertal and homo erectus groups. *American Journal of Physical Anthropology*, 53(2):285–295.

Holloway, R. L.

1981. Volumetric and asymmetry determinations on recent hominid endocasts: Spy i and II, djebel ihroud i, and the salê <I>Homo erectus</I> specimens, with some notes on neandertal brain size. *American Journal of Physical Anthropology*, 55(3):385–393.

Holloway, R. L., D. C. Broadfield, M. S. Yuan, J. H. Schwartz, and I. Tattersall

2004. *Human Fossil Record, Brain Endocasts: The Paleoneurological Evidence*. Wiley-Liss.

Holloway, R. L. and M. C. D. L. Costelareymondie

1982. Brain endocast asymmetry in pongids and hominids: Some preliminary findings on the paleontology of cerebral dominance. *American Journal of Physical Anthropology*, 58(1):101–110.

Howells, W. W.

1978. *Cranial Variation in Man: A Study by Multivariate Analysis of Patterns of Difference Among Recent Human Populations*. Harvard University Press.

Hsieh, J.

2009. *Computed Tomography: Principles, Design, Artifacts, and Recent Advances, Second Edition*, 2nd revised edition edition. SPIE Publications.

Inder, T. E. and P. S. Huppi

2000. In vivo studies of brain development by magnetic resonance techniques. *Mental Retardation and Developmental Disabilities Research Reviews*, 6(1):59–67. PMID: 10899798.

Isler, K., E. C. Kirk, J. M. Miller, G. A. Albrecht, B. R. Gelvin, and R. D. Martin

2008. Endocranial volumes of primate species: scaling analyses using a comprehensive and reliable data set. *Journal of Human Evolution*, 55(6):967–978.

Jerison, H.

1973. *Evolution of the Human Brain and Intelligence.* Academic Press, London.

Jerison, H. J.

1982. The evolution of biological intelligence. In *Handbook of human intelligence*, P. 723–791.

Jernigan, T. L. and P. Tallal

1990. Late childhood changes in brain morphology observable with MRI. *Developmental Medicine and Child Neurology*, 32(5):379–85. PMID: 2354751.

Johnson, M. A. and G. M. Bydder

1984. NMR imaging of the brain in children. *British Medical Bulletin*, 40(2):175–8. PMID: 6378316.

Jolliffe, I.

2002. *Principal Component Analysis*, 2nd edition. Springer.

Kamdar, M. R., R. A. Gomez, and J. A. Ascherman

2009. Intracranial volumes in a large series of healthy children. *Plastic and Reconstructive Surgery*, 124(6):2072–2075.

Kappelman, J.

1996. The evolution of body mass and relative brain size in fossil hominids. *Journal of Human Evolution*, 30(3):243–276.

Keihaninejad, S., R. A. Heckemann, G. Fagiolo, M. R. Symms, J. V. Hajnal, and A. Hammers

2010. A robust method to estimate the intracranial volume across MRI field strengths (1.5T and 3T). *NeuroImage*, 50(4):1427–1437. PMID: 20114082.

Keller, S. S., J. R. Highley, M. Garcia-Finana, V. Sluming, R. Rezaie, and N. Roberts

2007. Sulcal variability, stereological measurement and asymmetry of broca's area on MR images. *Journal of Anatomy*, 211(4):534.

Kendall, D. G.

1977. The diffusion of shape. *Advances in Applied Probability*, 9(3):428–430. ArticleType: primary_article / Full publication date: Sep., 1977 / Copyright © 1977 Applied Probability Trust.

Kent, J. T. and K. V. Mardia

2001. Shape, procrustes tangent projections and bilateral symmetry. *Biometrika*, 88(2):469–485.

Klingenberg, C.

1998. Heterochrony and allometry: the analysis of evolutionary change in ontogeny. *Biol Rev*, 73:79–123.

le Gros Clark, W. E.

1951. Review: External morphology of the primate brain (C. j. connolly). *Journal of Anatomy*, 85(Pt 2):213–213. undefinedPMCID: 1273599.

Leigh, S.

2004. Brain growth, life history, and cognition in primate and human evolution. *American Journal of Primatology*, 62:139–164.

Leigh, S. R.

2006. Brain ontogeny and life history in homo erectus. *J Hum Evol*, 50:104–108.

LeMay, M.

1976. Morphological cerebral asymmetries of modern man, fossil man, and nonhuman primate. *Annals of the New York Academy of Sciences*, 280:349–366. PMID: 827951.

Lenroot, R. K. and J. N. Giedd

2006. Brain development in children and adolescents: insights from anatomical magnetic resonance imaging. *Neuroscience and Biobehavioral Reviews*, 30(6):718–29. PMID: 16887188.

Levene, M. I., A. Whitelaw, V. Dubowitz, G. M. Bydder, R. E. Steiner, C. P. Randell,

and I. R. Young

1982. Nuclear magnetic resonance imaging of the brain in children. *British Medical Journal (Clinical Research Ed.)*, 285(6344):774–6. PMID: 6810994.

Lieberman, D., J. Carlo, M. P. de Leon, and C. P. E. Zollikofer

2007. A geometric morphometric analysis of heterochrony in the cranium of chimpanzees and bonobos. *J Hum Evol*.

Lynn, R.

1994. Sex differences in intelligence and brain size: A paradox resolved. *Personality and Individual Differences*, 17(2):257–271.

MacLusky, N. J., A. S. Clark, F. Naftolin, and P. S. Goldman-Rakic

1987. Estrogen formation in the mammalian brain: Possible role of aromatase in sexual differentiation of the hippocampus and neocortex. *Steroids*, 50:459–474.

Mann, A. E.

1968. *The paleodemography of Australopithecus*. PhD thesis, University of California, Berkeley.

Mann, A. E.

1975. *Some paleodemographic aspects of the South African australopithecines*. Dept. of Anthropology, University of Pennsylvania.

Marcus, L., M. Corti, A. Loy, G. J. P. Naylor, and D. E. Slice

1996. *Advances in Morphometrics, Part I: Theory and Methods; Section 1. Data Acquisition, Section 2. Landmark Methods*, volume A284.

Mardia, K., F. L. Bookstein, and I. J. Moreton

2000. Statistical assessment of bilateral symmetry of shapes. *Biometrika*, 87(2):285–300.

Maudgil, D. D., S. L. Free, S. M. Sisodiya, L. Lemieux, F. G. Woermann, D. R. Fish, and S. D. Shorvon

1998. Identifying homologous anatomical landmarks on reconstructed magnetic resonance images of the human cerebral cortical surface. *Journal of Anatomy*, 193(4):559–571.

McArdle, C. B., C. J. Richardson, D. A. Nicholas, M. Mirfakhraee, C. K. Hayden, and E. G. Amparo

1987. Developmental features of the neonatal brain: MR imaging. part i. gray-white matter differentiation and myelination. *Radiology*, 162(1 Pt 1):223–9. PMID: 3786767.

McAuliffe, M., F. Lalonde, D. McGarry, W. Gandler, K. Csaky, and B. Trus

2001. Medical image processing, analysis and visualization in clinical research. In *Proceedings 14th IEEE Symposium on Computer-Based Medical Systems. CBMS 2001*, Pp. 381–386, Bethesda, MD, USA.

McCarthy, R. C.

2001. Anthropoid cranial base architecture and scaling relationships. *Journal of Human Evolution*, 40(1):41–66.

McManus, I. C. and M. P. Bryden

1991. Geschwind's theory of cerebral lateralization: developing a formal, causal model. *Psychological Bulletin*, 110(2):237–253. PMID: 1946868.

Mechelli, A. ., C. J. Price, K. J. Friston, and J. . Ashburner

2005. Voxel-Based morphometry of the human brain: Methods and applications. *Current Medical Imaging Reviews*, 1:105–113.

Moss, M. L. and R. W. Young

1960. A functional approach to craniology. *American Journal of Physical Anthropology*, 18(4):281–292.

Neubauer, S., P. Gunz, and J. Hublin

2009. The pattern of endocranial ontogenetic shape changes in humans. *Journal of Anatomy*, 215(3):240–255. PMID: 19531085.

Neubauer, S., P. Gunz, and J. Hublin

2010. Endocranial shape changes during growth in chimpanzees and humans: A morphometric analysis of unique and shared aspects. *Journal of Human Evolution*, In Press, Corrected Proof.

Neuroscience Division, National Primate Research Center, U. o. W.

2007. BrainInfo. http://www.braininfo.org.

Ogle, R. C., S. S. Tholpady, K. A. McGlynn, and R. A. Ogle

2004. Regulation of cranial suture morphogenesis. *Cells Tissues Organs*, 176(1-3):54–66.

O'Higgins, P. and N. Jones

1998. Facial growth in cercocebus torquatus: an application of three-dimensional geometric morphometric techniques to the study of morphological variation. *Journal of Anatomy*, 193(02):251–272.

Paus, T., D. L. Collins, A. C. Evans, G. Leonard, B. Pike, and A. Zijdenbos

2001. Maturation of white matter in the human brain: a review of magnetic resonance studies. *Brain Research Bulletin*, 54(3):255–66. PMID: 11287130.

Peters, M., L. Jäncke, J. F. Staiger, G. Schlaug, Y. Huang, and H. Steinmetz

1998. Unsolved problems in comparing brain sizes in homo sapiens. *Brain and Cognition*, 37(2):254–285.

Pfaff, D. and M. Keiner

1973. Atlas of estradiol-concentrating cells in the central nervous system of the female rat. *The Journal of Comparative Neurology*, 151(2):121–157.

Pickering, S. P.

1930. Correlation of brain and head measurements, and relation of brain shape and size to shape and size of the head. *American Journal of Physical Anthropology*, 15(1):1–52.

Price, C. J.

2000. The anatomy of language: contributions from functional neuroimaging. *Journal of Anatomy*, 197(Pt 3):335–359. PMC1468137.

Raisman, G. and P. M. Field

1971. Sexual dimorphism in the preoptic area of the rat. *Science*, 173(3998):731–733.

Ramirez-Rozzi, F., R. Gonzalez-Jose, and H. Pucciarelli

2005. Cranial growth in normal and low-protein-fed saimiri. an environmental heterochrony. *J Hum Evol*, 49:515–535.

Reiss, A. L., M. T. Abrams, H. S. Singer, J. L. Ross, and M. B. Denckla

1996. Brain development, gender and IQ in children. a volumetric imaging study. *Brain: A Journal of Neurology*, 119 (Pt 5):1763–74. PMID: 8931596.

Richtsmeier, J. T., K. Aldridge, V. B. DeLeon, J. Panchal, A. A. Kane, J. L. Marsh, P. Yan, and T. M. C. 3rd

2006. Phenotypic integration of neurocranium and brain. *J Exp Zoolog B Mol Dev Evol*, 306(4):360–78.

Ricklan, D. E. and P. V. Tobias

1986. Unusually low sexual dimorphism of endocranial capacity in a zulu cranial series. *American Journal of Physical Anthropology*, 71(3):285–293. PMID: 3812650.

Rightmire, G. P.

2004. Brain size and encephalization in early to Mid-Pleistocene <I>Homo</I>. *American Journal of Physical Anthropology*, 124(2):109–123.

Rohlf, F. J.

1990. Morphometrics. *Annual Reviews in Ecology and Systematics*, 21(1):299–316.

Rohlf, F. J. and F. L. Bookstein

1990. *Proceedings of the Michigan Morphometrics Workshop*. Univ of Michigan Museum of Zoology.

Ruff, C. B., E. Trinkaus, and T. W. Holliday

1997. Body mass and encephalization in pleistocene homo. *Nature*, 387(6629):173–176.

Rushton, J. P.

1992. Cranial capacity related to sex, rank, and race in a stratified random sample of 6,325 U.S. military personnel. *Intelligence*, 16(3-4):401–413.

Rushton, J. P.

1993. Corrections to a paper on race and sex differences in brain size and intelligence. *Personality and Individual Differences*, 15(2):229–231.

Rushton, J. P.

1994. Sex and race differences in cranial capacity from international labour office data. *Intelligence*, 19(3):281–294.

Sardi, M.

2010. La evolución de la ontogenia craneofacial en las poblaciones humanas. In *Pensando a Darwin desde el Sur. Contribuciones de la primera Reunión de Biología Evolutiva del Cono Sur*. Buenos Aires, Argentina: Editorial Centro Cultural Ricardo Rojas.

Sardi, M., F. Ventrice, and F. Ramirez-Rozzi

2007. Allometries throughout the late prenatal and early postnatal human craniofacial ontogeny. *The Anatomical Record*, 290:1112–1120.

Sardi, M. L. and F. R. Rozzi

2007. Developmental connections between cranial components and the emergence of the first permanent molar in humans. *Journal of Anatomy*, 210(4):406–417. PMID: 17428202 PMCID: 2100294.

Schaefer, G. B., J. N. Thompson, J. B. Bodensteiner, M. Hamza, R. R. Tucker, W. Marks, C. Gay, and D. Wilson

1990. Quantitative morphometric analysis of brain growth using magnetic resonance imaging. *Journal of Child Neurology*, 5(2):127–30. PMID: 2345279.

Schoenemann, P. T.

2006. Evolution of the size and functional areas of the human brain. *Annual Review of Anthropology*, 35:379–406.

Semendeferi, K., H. Damasio, R. Frank, and G. W. V. Hoesen

1997. The evolution of the frontal lobes: a volumetric analysis based on three-dimensional reconstructions of magnetic resonance scans of human and ape brains. *Journal of Human Evolution*, 32(4):375–388.

Sgouros, S., J. H. Goldin, A. D. Hockley, M. J. C. Wake, and K. Natarajan

1999. Intracranial volume change in childhood. *Journal of Neurosurgery*, 91(4):610–616.

Shea, B.

1983. Allometry and heterochrony in the african apes. *Am J Phys Anthropol*, 62:275–289.

Shea, B.

1992. Developmental perspective on size change and allometry in evolution. *Evolutionary Anthropology*, Pp. 125–134.

Sibug, R. M., W. E. Stumpf, P. J. Shughrue, and R. B. Drews

1991. Distribution of estrogen target sites in the 2-day-old mouse forebrain and pituitary gland during the 'critical period' of sexual differentiation. *Developmental Brain Research*, 61(1):11–22.

Smith, B.

1994. Patterns of dental development in homo, australopithecus, pan, and gorilla. *Am J Phys Anthropol*, 94:307–325.

Smith, E.

1913. Preliminary report on the cranial cast; an appendix to a paper by dawson and woodward: "On the discovery of a palaeolithic human skull and mandible in a flint-bearing gravel overlying the wealden (Hastings beds) at piltdown, fletching (Sussex)" the quarterly journal of the geological society, vol. 69, pp. 117-123, 1913. *Quarterly Journal of the Geological Society*, 69(1-4):117–123.

Smith, S. M.

2002. Fast robust automated brain extraction. *Human Brain Mapping*, 17(3):143–155.

Smith, S. M., M. Jenkinson, M. W. Woolrich, C. F. Beckmann, T. E. J. Behrens, H. Johansen-Berg, P. R. Bannister, M. D. Luca, I. Drobnjak, and D. E. Flitney

2004. Advances in functional and structural MR image analysis and implementation as FSL. *Neuroimage*, 23:208–219.

Sowell, E. R., B. S. Peterson, P. M. Thompson, S. E. Welcome, A. L. Henkenius, and

A. W. Toga

2003. Mapping cortical change across the human life span. *nature neuroscience*, 6(3):309–315.

Sowell, E. R., P. M. Thompson, C. J. Holmes, R. Batth, T. L. Jernigan, and A. W. Toga

1999. Localizing Age-Related changes in brain structure between childhood and adolescence using statistical parametric mapping* 1. *Neuroimage*, 9(6):587–597.

Sowell, E. R., P. M. Thompson, C. M. Leonard, S. E. Welcome, E. Kan, and A. W. Toga

2004. Longitudinal mapping of cortical thickness and brain growth in normal children. *Journal of Neuroscience*, 24(38):8223.

Sowell, E. R., P. M. Thompson, D. Rex, D. Kornsand, K. D. Tessner, T. L. Jernigan, and A. W. Toga

2002. Mapping sulcal pattern asymmetry and local cortical surface gray matter distribution in vivo: Maturation in perisylvian cortices. *Cereb. Cortex*, 12(1):17–26.

Sowell, E. R., P. M. Thompson, K. D. Tessner, and A. W. Toga

2001. Mapping continued brain growth and gray matter density reduction in dorsal frontal cortex: Inverse relationships during postadolescent brain maturation. *J. Neurosci.*, 21(22):8819–8829.

Specht, M., R. Lebrun, and C. P. E. Zollikofer

2007. Visualizing shape transformation between chimpanzee and human braincases. *Visual Comput*, 23:743–751.

Sperber, G. H.

2001. *Craniofacial Development and Growth*, 1st edition. pmph usa.

Spocter, M. A. and P. R. Manger

2007. The use of cranial variables for the estimation of body mass in fossil hominins. *American Journal of Physical Anthropology*, 134(1):92–105.

Stephan, H.

1960. Methodische studien über den quantitativen vergleich architektonischer struktureinheiten des gehirns. *Z. Wiss. Zool.*, 164:143–172.

Stephan, H., H. Frahm, and G. Baron

1981. New and revised data on volumes of brain structures in insectivores and primates. *Folia Primatologica*, 35(1):1–29.

Stewart, T. D.

1934. Cranial capacity studies. *American Journal of Physical Anthropology*, 18(3):337–361.

Stringer, C.

2001. Modern human Origins—Distinguishing the models. *African Archaeological Review*, 18(2):67–75.

Swaab, D. F. and M. A. Hofman

1984. Sexual differentiation of the human brain: A historical perspective. In *Progress in Brain Research*, volume 61, Pp. 361–374. Amsterdam: Elsevier Science Publishers B.V.

Symington, J.

1916. Endocranial casts and brain form: A criticism of some recent speculations. *Journal of Anatomy and Physiology*, 50(Pt 2):111.

Team, R. D. C.

2010. R: A language and environment for statistical computing.

Thompson, P. M., K. M. Hayashi, E. R. Sowell, N. Gogtay, J. N. Giedd, J. L. Rapoport, G. I. D. Zubicaray, A. L. Janke, S. E. Rose, J. Semple, et al.

2004. Mapping cortical change in alzheimer's disease, brain development, and schizophrenia. *NeuroImage*, 23:S2–S18.

Tobias, P. V.

1965. Cranial capacity of zinjanthropus and other australopithecines. *Current Anthropology*, 6(4):414–417.

Tobias, P. V.

1968. The age of death among the australopithecines. *The Anthropologist (University of Delhi)*, Special Volume:23–28.

Tobias, P. V.

1974. Aspects of pathology and death among early hominids. *The Leech, Johannesburg*, 44:119–124.

Tobias, P. V.

1987. The brain of homo habilis: A new level of organization in cerebral evolution. *Journal of Human Evolution*, 16:741–61.

Toga, A. W. and P. M. Thompson

2003. Mapping brain asymmetry. *Nature Reviews. Neuroscience*, 4(1):37–48. PMID: 12511860.

Toga, A. W., P. M. Thompson, and E. R. Sowell

2006. Mapping brain maturation. *Trends in Neurosciences*, 29(3):148–159.

Tommasi, L.

2009. Mechanisms and functions of brain and behavioural asymmetries. *Philosophical Transactions of the Royal Society of London. Series B, Biological Sciences*, 364(1519):855–859. PMID: 19064348.

Toth, N.

1985. Archaeological evidence for preferential right-handedness in the lower and middle pleistocene, and its possible implications. *Journal of Human Evolution*, 14(6):607–614.

Vallortigara, G., L. J. Rogers, and A. Bisazza

1999. Possible evolutionary origins of cognitive brain lateralization. *Brain Research Reviews*, 30(2):164–175.

Ventrice, F.

2010. Tomographie assistée par ordinateur (CT) et imagerie par résonance magnétique (MR) pour mieux comprendre et caractériser la croissance et le développent du cerveau et du crâne. *L'anthropologie du vivant : objets et méthodes*, Pp. 109–112.

Virchow, R.

1856. *Uber den Cretinismus, etc.* Frankfurt: Gesammelte Abhandiungen.

von Cramon-Taubadel N., F. B. C. . L. M. M.

2007. The problem of assessing landmark error in geometric morphometrics: Theory, methods, and modifications. *Am J Phys Anthropol*, 134:24–35.

Vrba, E.

1996. Climate, heterochrony, and human evolution. *Journal of Anthropological Research*, 52(1):1–28.

Vries, G. D. and R. Simerly

2002. Anatomy, development, and function of sexually dimorphic neural circuits in the mammalian brain. In *Hormones, Brain and Behavior*, volume 4, Pp. 137–191. San Diego: Academic Press.

Vries, G. J. D., J. P. C. D. Bruin, H. B. M. Uylings, and M. A. Corner

1984. *Progress in Brain Research, Volume 61 Sex Differences in the Brain: The Relation Between Structure and Function*, volume 61 of *Progress in Brain Research*. Amsterdam: Elsevier Science.

Wada, J.

1969. Interhemispheric sharing and shift of cerebral speech function. *Excerpta Medica International Congress Series*, 193:296–297.

Watkins, K., T. Paus, J. Lerch, A. Zijdenbos, D. Collins, P. Neelin, J. Taylor, K. Worsley, and A. Evans

2001. Structural asymmetries in the human brain: a voxel-based statistical analysis of 142 MRI scans. *Cereb. Cortex*, 11(9):868–877.

Wernicke, C.

1874. *Der aphasische Symptomencomplex: Eine psychologische Studie auf anatomischer Basis*. Cohn & Weigert.

Wilke, M., S. K. Holland, and I. Krägeloh-Mann

2007. Global, regional, and local development of gray and white matter volume in normal children. *Experimental brain research. Experimentelle Hirnforschung. Experimentation cerebrale*, 178(3):296–307. PMID: 17051378 PMCID: 2265798.

Witte, A. V., M. Savli, A. Holik, S. Kasper, and R. Lanzenberger

2010. Regional sex differences in grey matter volume are associated with sex hormones in the young adult human brain. *NeuroImage*, 49(2):1205–1212.

Yakovlev, P. I. and A. R. Lecours

1967. The myelogenetic cycles of regional maturation of the brain. *Regional development of the brain in early life*, P. 3–70.

Zelditch, M., D. Swiderski, D. H. Sheets, and W. Fink

2004. *Geometric Morphometrics for Biologists*. Academic Press.

Zelditch, M. L., B. L. Lundrigan, H. D. Sheets, and T. Garland

2003. Do precocial mammals develop at a faster rate? a comparison of rates of skull development in sigmodon fulviventer and mus musculus domesticus. *Journal of Evolutionary Biology*, 16(4):708–720.

Zollikofer, C. and M. P. de Leon

2002. Visualizing patterns of craniofacial shape variation in homo sapiens. *The Royal Society*.

Zuckerman, S.

1928. Age-changes in the chimpanzee, with special reference to growth of brain, eruption of teeth, and estimation of age; with a note on the taungs ape. *Proceedings of the Zoological Society of London*, 98(1):1–42.

Index

Appendix A

Brodman's areas

Based on the cortical cytoarchitectonic organization of neurons in the brain cortex, Brodmann defined several areas (Brodmann, 1909; Garey, 1994). These areas became of great importance to define and delimitate the brain cortex in neuroscience studies. In this appendix a brief description of each of those areas is presented (Neuroscience Division, 2007).

(1) Intermediate postcentral (*area postcentralis intermedia*). Located in the postcentral gyrus. Bounded cytoarchitecturally by the rostral postcentral area 3 and the caudal postcentral area 2 and, at its ventral tip, by the subcentral area 43.

(2) Caudal postcentral (*area postcentralis caudalis*). Located primarily in the caudal portion of the postcentral gyrus and the rostral lip of the postcentral sulcus with a caudal extension along the intraparietal sulcus. Cytoarchitecturally bounded rostrally by the intermediate postcentral area 1 and caudally by the preparietal area 5, the superior parietal area 7 and the supramarginal area 40.

(3) Rostral postcentral (*area postcentralis oralis*). Located primarily in the rostral portion of the postcentral gyrus including the caudal bank of the central sulcus.

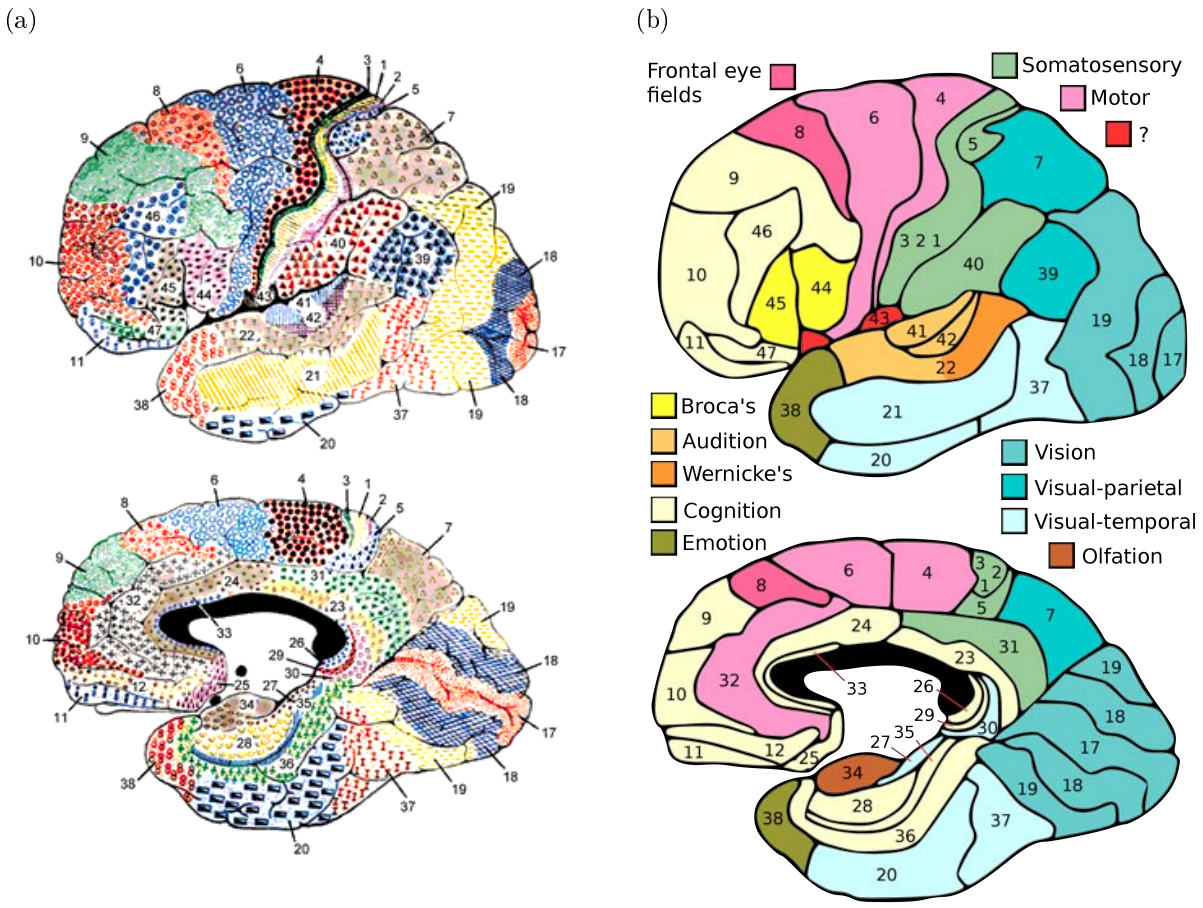

Figure A.1: **Brodmann areas.** **(a)** Original Brodmann colorized map. **(b)** Outlines from Brodmann areas with their respective functional attribution.

At either end of the sulcus it can extend beyond the depth of the sulcus into the precentral gyrus. Cytoarchitecturally bounded rostrally by the gigantopyramidal area 4 and caudally by the intermediate postcentral area 1.

(4) Gigantopyramidal (*area gigantopyramidalis*). Located in the precentral gyrus. Cytoarchitecturally the caudal boundary with the rostral postcentral area 3 does not coincide precisely with the floor of the central sulcus but lies variably in the banks of the postcentral gyrus and the precentral gyrus. The area also does not extend in all cases to the cingulate sulcus medially or to the end of the central sulcus ventro-laterally. Bounded rostrally by the frontal agranular area 6.

(5) Preparietal (*area praeparietalis*). Occupies the superior parietal lobule and a portion of the postcentral gyrus, particularly on the medial aspect of the hemisphere. Bounded approximately by the cingulate sulcus on the medial aspect of the hemisphere and by the superior postcentral sulcus on the lateral aspect. Cytoarchitecturally bounded by the caudal postcentral area 2, the superior parietal area 7 and on the medial bank of the hemisphere by the gigantopyramidal area 4 and the dorsal posterior cingulate area 31.

(6) Agranular frontal (*area frontalis agranularis*). Located primarily in the caudal portions of the superior frontal gyrus and the middle frontal gyrus and the rostral portions of the precentral gyrus not occupied by the gigantopyramidal area 4. It extends from the cingulate sulcus on the medial aspect of the hemisphere to the lateral sulcus on the lateral aspect. Cytoarchitecturally bounded rostrally by the frontal region and caudally by the gigantopyramidal area 4.

(7) Superior parietal (*area parietalis superior*). Occupies much of the supe-

rior parietal lobule and some of the precuneus. Bounded approximately by the superior postcentral sulcus rostrally, the intraparietal sulcus laterally, the parieto-occipital sulcus caudally and, on the medial bank of the hemisphere, the subparietal sulcus. Cytoarchitecturally bounded rostrally by the preparietal area 5 and the caudal postcentral area 2; caudally by the peristriate area 19; and medially by the dorsal posterior cingulate area 31.

(8) Intermediate frontal (*area frontalis intermedia*). Located primarily in the superior frontal gyrus extending from the cingulate sulcus on the medial surface over the margin of the hemisphere to the middle frontal gyrus. Cytoarchitecturally bounded caudally by the agranular frontal area 6 and ventrally by the granular frontal area 9.

(9) Granular frontal (*area frontalis granularis*). Occupies portions of the superior frontal gyrus and the middle frontal gyrus. Its approximate boundary on the medial aspect of the hemisphere is the cingulate sulcus and, on the lateral aspect, the inferior frontal sulcus. Cytoarchitecturally bounded dorsocaudally by the intermediate frontal area 8, caudally by the agranular frontal area 6, and ventrally by the frontopolar area 10, the middle frontal area 46 and the opercular area 44.

(10) Frontopolar (*area frontopolaris*). Occupies the most rostral portions of the superior frontal gyrus and the middle frontal gyrus. On the medial aspect of the hemisphere it is bounded ventrally by the superior rostral sulcus. It does not extend as far as the cingulate sulcus. Cytoarchitecturally bounded dorsally by the granular frontal area 9, caudally by the middle frontal area 46, and ventrally by the orbital area 47 and by the frontopolar area 12.

(11) Prefrontal (*area praefrontalis*). Constitutes most of the orbital gyri, gyrus

rectus and the most rostral portion of the superior frontal gyrus. Bounded medially by the inferior rostral sulcus and laterally approximately by the frontomarginal sulcus. Cytoarchitecturally bounded on the rostral and lateral aspects of the hemisphere by the frontopolar area 10, the orbital area 47, and the triangular area 45; on the medial surface it is bounded dorsally by the area 12 and caudally by the subgenual area 25.

(12) Prefrontal (*area praefrontalis*). Occupies the area between the superior rostral sulcus and the inferior rostral sulcus. Cytoarchitecturally bounded dorsally by the frontopolar area 10 and the dorsal anterior cingulate area 32; caudally, ventrally and rostrally it is bounded by the prefrontal area 11. (Originally described as part of prefrontal area 11 but not shown in the map, subsequently it was labeled as an independent area 12.)

(17) Striate (*area striata*). Part of the occipital lobe of the cerebral cortex that is defined on the basis of cyto- and myeloarchitecture, primarily by the band/stripe of Gennari.

(18) Parastriate (*area parastriata*). Located in parts of the cuneus, the lingual gyrus and the lateral occipital gyrus of the occipital lobe. Cytoarchitecturally bounded on one side by the striate area 17, from which it is distinguished by absence of a band/stripe of Gennari, and on the other by the peristriate area 19.

(19) Peristriate (*area peristriata*). Located in parts of the lingual gyrus, the cuneus, the lateral occipital gyrus and the superior occipital gyrus of the occipital lobe where it is bounded approximately by the parieto-occipital sulcus. Cytoarchitecturally bounded on one side by the parastriate area 18 which it surrounds. Rostrally it is bounded by the angular area 39 and the occipitotemporal area 37.

(20) Inferior temporal (*area temporalis inferior*). Corresponds approximately to the inferior temporal gyrus. Cytoarchitecturally bounded medially by the ectorhinal area 36, laterally by the middle temporal area 21, rostrally by the temporopolar area 38 and caudally by the occipitotemporal area 37.

(21) Middle temporal (*area temporalis media*). Corresponds approximately to the middle temporal gyrus. Bounded rostrally by the temporopolar area 38, ventrally by the inferior temporal area 20, caudally by the occipitotemporal area 37, and dorsally by the superior temporal area 22.

(22) Superior temporal (*area temporalis superior*). Corresponds approximately to the lateral and caudal two thirds of the superior temporal gyrus. Bounded rostrally by the temporopolar area 38, medially by the posterior transverse temporal area 42, ventrocaudally by the middle temporal area 21 and dorsocaudally by the supramarginal area 39.

(23) Ventral posterior cingulate (*area cingularis posterior ventralis*). Occupies most of the posterior cingulate gyrus adjacent to the corpus callosum. At the caudal extreme it is bounded approximately by the parieto-occipital sulcus. Cytoarchitecturally bounded dorsally by the dorsal posterior cingulate area 31, rostrally by the ventral anterior cingulate area 24, and ventrorostrally in its caudal half by the retrosplenial region.

(24) Ventral anterior cingulate (*area cingularis anterior ventralis*). Occupies most of the anterior cingulate gyrus in an arc around the genu of corpus callosum. Its outer border corresponds approximately to the cingulate sulcus. Cytoarchitecturally bounded internally by the pregenual area 33, externally by the dorsal anterior cingulate area 32, and caudally by the ventral posterior cingulate area 23 and the dorsal posterior cingulate

area 31.

(25) Subgenual (*area subgenualis*). A narrow band located in the caudal portion of the subcallosal area adjacent to the paraterminal gyrus from which it is separated by the posterior parolfactory sulcus. It is bounded by the prefrontal area 11rostrally and by the paraterminal gyrus caudally.

(26) Ectosplenial (*area ectosplenialis*). A narrow band located in the isthmus of cingulate gyrus adjacent to the fasciolar gyrus internally. It is bounded externally by the granular retrolimbic area 29.

(28) Entorhinal (*area entorhinalis*). Located in the entorhinal area on the medial aspect of the temporal lobe. It and the dorsal entorhinal area 34 together constitute approximately the entorhinal area.

(29) Granular retrolimbic (*area retrolimbica granularis*). A narrow band located in the isthmus of cingulate gyrus. Cytoarchitecturally bounded internally by the ectosplenial area 26 and externally by the agranular retrolimbic area 30.

(30) Agranular retrolimbic (*area retrolimbica agranularis*). Located in the isthmus of cingulate gyrus. Cytoarchitecturally bounded internally by the granular retrolimbic area 29, dorsally by the ventral posterior cingulate area 23 and ventrolaterally by the ectorhinal area 36.

(31) Dorsal posterior cingulate (*area cingularis posterior dorsalis*). Occupies portions of the posterior cingulate gyrus and medial aspect of the parietal lobe. Approximate boundaries are the cingulate sulcus dorsally and the parieto-occipital sulcus caudally. It partially surrounds the subparietal sulcus. Cytoarchitecturally bounded rostrally by the ventral anterior cingulate area 24, ventrally by the ventral posterior cingulate

area 23, dorsally by the gigantopyramidal area 4 and preparietal area 5 and caudally by the superior parietal area 7.

(32) Dorsal anterior cingulate (*area cingularis anterior dorsalis*). Forms an outer arc around the anterior cingulate gyrus. The cingulate sulcus defines approximately its inner boundary and the superior rostral sulcus its ventral boundary; rostrally it extends almost to the margin of the frontal lobe. Cytoarchitecturally bounded internally by the ventral anterior cingulate area 24, externally by medial margins of the agranular frontal area 6, intermediate frontal area 8, granular frontal area 9, frontopolar area 10, and prefrontal area 11.

(33) Pregenual (*area praegenualis*). A narrow band located in the anterior cingulate gyrus adjacent to the supracallosal gyrus in the depth of the callosal sulcus. Cytoarchitecturally bounded by the ventral anterior cingulate area 24 and the supracallosal gyrus.

(34) Dorsal entorhinal (*area entorhinalis dorsalis*). Located in the entorhinal area on the medial aspect of the temporal lobe. It and the entorhinal area 28 together constitute approximately the entorhinal area.

(35) Perirhinal (*area perirhinalis*). Located along the rhinal sulcus. Cytoarchitectually bounded medially by the entorhinal area 28 and laterally by the ectorhinal area 36.

(36) Ectorhinal (*area ectorhinalis*). Located primarily in the fusiform gyrus, with its medial boundary corresponding approximately to the rhinal sulcus. Cytoarchitecturally bounded laterally and caudally by the inferior temporal area 20, medially by the perirhinal area 35 and rostrally by the temporopolar area 38.

(37) Occipitotemporal (*area occipitotemporalis*). Located primarily in the caudal portions of the fusiform gyrus and inferior temporal gyrus on the mediobasal and lateral surfaces at the caudal extreme of the temporal lobe. Cytoarchitecturally bounded caudally by the peristriate area 19, rostrally by the inferior temporal area 20 and middle temporal area 21 and dorsally on the lateral aspect of the hemisphere by the angular area 39.

(38) Temporopolar (*area temporopolaris*). Located primarily in the most rostral portions of the superior temporal gyrus and the middle temporal gyrus. Cytoarchitecturally bounded caudally by the inferior temporal area 20, the middle temporal area 21, the superior temporal area 22 and the ectorhinal area 36.

(39) Angular (*area angularis*). Corresponds to the angular gyrus surrounding the caudal tip of the superior temporal sulcus. Dorsally it is bounded approximately by the intraparietal sulcus. Cytoarchitecturally bounded rostrally by the supramarginal area 40, dorsally and caudally by the peristriate area 19, and ventrally by the occipitotemporal area 37.

(40) Supramarginal (*area supramarginalis*). Located primarily in the supramarginal gyrus surrounding the posterior ascending limb of lateral sulcus. Bounded approximately by the intraparietal sulcus, the inferior postcentral sulcus the posterior subcentral sulcus and the lateral sulcus. Cytoarchitecturally bounded caudally by the angular area 39, rostrally and dorsally by the caudal postcentral area 2, and ventrally by the subcentral area 43 and the superior temporal area 22.

(41) Anterior transverse temporal (*area temporalis transversa anterior*). Occupies the anterior transverse temporal gyrus in the bank of the lateral sulcus on

the dorsal surface of the temporal lobe. Cytoarchitecturally bounded medially by the parainsular area 52 and laterally by the posterior transverse temporal area 42.

(42) Posterior transverse temporal (*area temporalis transversa posterior*). Located in the bank of the lateral sulcus on the dorsal surface of the temporal lobe. Cytoarchitecturally bounded medially by the anterior transverse temporal area 41 and laterally by the superior temporal area 22.

(43) Subcentral (*area subcentralis*). Occupies the postcentral gyrus and the precentral gyrus between the ventrolateral extreme of the central sulcus and the depth of the lateral sulcus at the insula. Its rostral and caudal borders are approximated by the anterior subcentral sulcus and the posterior subcentral sulcus respectively. Cytoarchitecturally bounded rostrally by the agranular frontal area 6 and caudally, for the most part, by the caudal postcentral area 2 and the supramarginal area 40.

(44) Opercular (*area opercularis*). Corresponds approximately to the opercular part of the inferior frontal gyrus. Bounded caudally by the inferior precentral sulcus and rostrally by the anterior ascending limb of lateral sulcus. It surrounds the diagonal sulcus. In the depth of the lateral sulcus it borders on the insula. Cytoarchitectonically bounded caudally and dorsally by the agranular frontal area 6, dorsally by the granular frontal area 9 and rostrally by the triangular area 45.

(45) Triangular (*area triangularis*). Occupies the triangular part of the inferior frontal gyrus and, surrounding the anterior horizontal limb of lateral sulcus, a portion of the orbital part of inferior frontal gyrus. Bounded caudally by the anterior ascending limb of lateral sulcus, it borders on the insula in the depth of the lateral sulcus . Cytoarchitectonically bounded caudally by the opercular area 44, rostrodorsally by the middle

frontal area 46 and ventrally by the orbital area 47.

(46) Middle frontal (*area frontalis media*). Occupies approximately the middle third of the middle frontal gyrus and the most rostral portion of the inferior frontal gyrus. Cytoarchitecturally bounded dorsally by the granular frontal area 9, rostroventrally by the frontopolar area 10 and caudally by the triangular area 45.

(47) Orbital (*area orbitalis*). Surrounds the caudal portion of the orbital sulcus from which it extends laterally into the orbital part of inferior frontal gyrus. Cytoarchitectonically bounded caudally by the triangular area 45, medially by the prefrontal area 11, and rostrally by the area frontopolaris 10.

(48) Retrosubicular (*area retrosubicularis*). Located on the medial surface of the temporal lobe. Cytoarchitectually bounded rostrally by the perirhinal area 35 and medially by the presubiculum. (While described by Brodmann, it was not included in his areal maps of human cortex.)

(52) Parainsular (*area parainsularis*). Located in the bank of the lateral sulcus on the dorsal surface of the temporal lobe. Its medial boundary corresponds approximately to the junction between the temporal lobe and the insula. Cytoarchitecturally bounded laterally by the anterior transverse temporal area 41.

(13), **(14)**, **(15)**, **(16)**, **(27)**, **(49)**, **(50)**, and **(51)** are only present in monkeys.

Appendix B

Analysis of Covariance - ANCOVA

Analysis of covariance (ANCOVA) is a general linear model that combines elements of regression and analysis of variance. The response variable is continuous, and there is at least one continuous explanatory variable and at least one categorical explanatory variable. Two null hypotheses are tested: the first one states that the slopes of the regression curves are all the same. If this hypothesis is not rejected, the second null hypothesis is tested, and it states that the Y-intercepts of the regression curves are all the same. If the slopes of the regression curves are different, such curves interweave each other at a certain point, and consequently each group present higher Y values in one part of the graph and lower Y values in another part of the graph, in relation to the other groups.

The interaction term (*age*sex*) tests whether the slopes of the regression curves for females and males are significantly different. If there is no interaction, the term *sex* tests whether the axis Y intercept (b) is significantly different between the regression curves. Finally, the term *age* tests the signification of the linear relationship between the response measured (*e.g.* endocranial volume) and age. All ANCOVAs were performed using R (Crawley, 2007; Team, 2010).

Table B.1: ANCOVA results measuring dimorphism between female and male endocranial volume corresponding to infant-child to juvenile group. See Figure 6.1.b.

Response: endoVol infant-child to juvenile group

	Df	**Sum Sq**	**Mean Sq**	**F value**	**Pr(>F)**	
age	1	77868	77868	9.245300	0.004600	**
sex	1	76903	76903	9.130700	0.004830	**
age:sex	1	49351	49351	5.859500	0.021160	*
Residuals	33	277940	8422			

Table B.2: ANCOVA results measuring dimorphism between female and male endocranial volume corresponding to juvenile to adolescent group. See Figure 6.1.c.

Response: endoVol juvenile to adolescent group

	Df	**Sum Sq**	**Mean Sq**	**F value**	**Pr(>F)**	
age	1	23372	23372	2.138700	0.149320	
sex	1	358739	358739	32.826900	4.38E-007	***
age:sex	1	62211	62211	5.692700	0.020510	*
Residuals	55	601051	10928			

Table B.3: ANCOVA results measuring dimorphism between female and male endocranial volume corresponding to adolescent to adult group. See Figure 6.1.d.

Response: endoVol adolescent to adult group

	Df	**Sum Sq**	**Mean Sq**	**F value**	**Pr(>F)**	
age	1	20703	20703	1.820100	0.180300	
sex	1	778872	778872	68.475900	5.16E-013	***
age:sex	1	1815	1815	0.159600	0.690400	
Residuals	102	1160188	11374			

Table B.4: ANCOVA results measuring dimorphism between female and male gray matter volume corresponding to infant-child to juvenile group. See Figure 6.2.b.

Response: gmVol infant-child to juvenile group

	Df	**Sum Sq**	**Mean Sq**	**F value**	**Pr(>F)**	
age	1	40214	40214	6.769500	0.011403	*
sex	1	70962	70962	11.945700	0.000956	***
age:sex	1	1634	1634	0.275000	0.601723	
Residuals	67	398007	5940			

Table B.5: ANCOVA results measuring dimorphism between female and male gray matter volume corresponding to juvenile to adolescent group. See Figure 6.2.c.

Response: gmVol juvenile to adolescent group

	Df	**Sum Sq**	**Mean Sq**	**F value**	**Pr(>F)**	
age	1	33550	33550	6.273900	0.013410	*
sex	1	219570	219570	41.060000	2.13E-009	***
age:sex	1	2790	2790	0.521800	0.471280	
Residuals	139	743309	5348			

Table B.6: ANCOVA results measuring dimorphism between female and male gray matter volume corresponding to adolescent to adult group. See Figure 6.2.d.

Response: gmVol adolescent to adult group

	Df	**Sum Sq**	**Mean Sq**	**F value**	**Pr(>F)**	
age	1	185720	185720	41.138000	1.29E-009	***
sex	1	201500	201500	44.633500	3.09E-010	***
age:sex	1	14172	14172	3.139100	0.078190	.
Residuals	174	785532	4515			

Table B.7: ANCOVA results measuring dimorphism between female and male white matter volume corresponding to infant-child to juvenile group. See Figure 6.3.b.

Response: wmVol infant-child to juvenile group

	Df	**Sum Sq**	**Mean Sq**	**F value**	**Pr(>F)**	
age	1	58220	58220	34.109700	1.68E-007	***
sex	1	20208	20208	11.839300	0.001003	**
age:sex	1	1103	1103	0.646300	0.424283	
Residuals	67	114359	1707			

Table B.8: ANCOVA results measuring dimorphism between female and male white matter volume corresponding to juvenile to adolescent group. See Figure 6.3.c.

Response: wmVol juvenile to adolescent group

	Df	**Sum Sq**	**Mean Sq**	**F value**	**Pr(>F)**	
age	1	39049	39049	25.922000	1.14E-006	***
sex	1	44068	44068	29.253800	2.70E-007	***
age:sex	1	45	45	0.029600	0.863700	
Residuals	139	209388	1506			

Table B.9: ANCOVA results measuring dimorphism between female and male white matter volume corresponding to adolescent to adult group. See Figure 6.3.d.

Response: wmVol adolescent to adult group

	Df	**Sum Sq**	**Mean Sq**	**F value**	**Pr(>F)**	
age	1	19932	19932	10.201000	0.001666	**
sex	1	70891	70891	36.281000	9.90E-009	***
age:sex	1	2020	2020	1.034000	0.310626	
Residuals	174	339987	1954			

Table B.10: ANCOVA results measuring dimorphism between female and male brain volume corresponding to infant-child to juvenile group. See Figure 6.5.b.

Response: brainVol infant-child to juvenile group

	Df	**Sum Sq**	**Mean Sq**	**F value**	**Pr(>F)**	
age	1	195206	195206	15.896200	0.000168	***
sex	1	166907	166907	13.591700	0.000457	***
age:sex	1	52	52	0.004200	0.948353	
Residuals	67	822765	12280			

Table B.11: ANCOVA results measuring dimorphism between female and male brain volume corresponding to juvenile to adolescent group. See Figure 6.5.c.

Response: brainVol juvenile to adolescent group

	Df	**Sum Sq**	**Mean Sq**	**F value**	**Pr(>F)**	
age	1	209	209	0.019600	0.889000	
sex	1	460371	460371	43.170300	9.32E-010	***
age:sex	1	3540	3540	0.332000	0.565400	
Residuals	139	1482306	10664			

Table B.12: ANCOVA results measuring dimorphism between female and male brain volume corresponding to adolescent to adult group. See Figure 6.5.d.

Response: brainVol adolescent to adult group

	Df	**Sum Sq**	**Mean Sq**	**F value**	**Pr(>F)**	
age	1	83967	83967	8.562100	0.003890	**
sex	1	511427	511427	52.150700	1.54E-011	***
age:sex	1	5490	5490	0.559800	0.455335	
Residuals	174	1706369	9807			

Table B.13: ANCOVA results measuring dimorphism between female and male gray / white matter volume corresponding to infant-child to juvenile group. See Figure 6.4.b.

Response: gmVol/wmVol infant-child to juvenile group

	Df	**Sum Sq**	**Mean Sq**	**F value**	**Pr(>F)**	
age	1	0.886290	0.886290	28.937200	0.000001	***
sex	1	0.016640	0.016640	0.543400	0.463600	
age:sex	1	0.029810	0.029810	0.973400	0.327400	
Residuals	67	2.052080	0.030630			

Table B.14: ANCOVA results measuring dimorphism between female and male gray / white matter volume corresponding to juvenile to adolescent group. See Figure 6.4.c.

Response: gmVol/wmVol juvenile to adolescent group

	Df	**Sum Sq**	**Mean Sq**	**F value**	**Pr(>F)**	
age	1	2.159300	2.159280	88.684200	< 2.00E-016	***
sex	1	0.011000	0.011030	0.453100	0.502000	
age:sex	1	0.021100	0.021140	0.868400	0.353000	
Residuals	139	3.384400	0.024350			

Table B.15: ANCOVA results measuring dimorphism between female and male gray / white matter volume corresponding to adolescent to adult group. See Figure 6.4.d.

Response: gmVol/wmVol adolescent to adult group

	Df	**Sum Sq**	**Mean Sq**	**F value**	**Pr(>F)**	
age	1	2.351300	2.351320	88.456700	< 2.00E-016	***
sex	1	0.002300	0.002290	0.086000	0.769650	
age:sex	1	0.122100	0.122070	4.592100	0.033510	*
Residuals	174	4.625200	0.026580			

Table B.16: ANCOVA results measuring dimorphism between female and male brain / endocranial volume relationship versus age. See Figure 6.14.

Response: brain/endo relationship vs. age

	Df	**Sum Sq**	**Mean Sq**	**F value**	**Pr(>F)**	
age	1	0.017176	0.017176	5.551700	0.022780	*
sex	1	0.005999	0.005999	1.938900	0.170480	
age:sex	1	0.000035	0.000035	0.011200	0.916270	
Residuals	46	0.142314	0.003094			

Table B.17: ANCOVA results measuring dimorphism between female and male brain / endocranial volume relationship versus ECV. See Figure 6.15.

Response: brain/endo relationship vs. ECV

	Df	**Sum Sq**	**Mean Sq**	**F value**	**Pr(>F)**	
endoVol	1	0.061334	0.061334	47.002500	1.50E-008	***
sex	1	0.033399	0.033399	25.595100	7.21E-006	***
endoVol:sex	1	0.010765	0.010765	8.249400	0.006147	**
Residuals	46	0.060025	0.001305			

Table B.18: ANCOVA results measuring dimorphism between female and male CCSV scores from endocranial GM analysis corresponding to infant-child to juvenile group. See Figure 6.16.

Response: CCSV endocranial vault infant-child to juvenile group

	Df	**Sum Sq**	**Mean Sq**	**F value**	**Pr(>F)**	
age	1	0.002879	0.002879	13.287500	0.000910	***
sex	1	0.000980	0.000979	4.521200	0.041045	*
age:sex	1	0.000486	0.000486	2.241800	0.143829	
Residuals	33	0.007149	0.000217			

Table B.19: ANCOVA results measuring dimorphism between female and male CCSV scores from endocranial GM analysis corresponding to juvenile to adolescent group. See Figure 6.18.

Response: CCSV endocranial vault juvenile to adolescent group

	Df	**Sum Sq**	**Mean Sq**	**F value**	**Pr(>F)**	
age	1	0.005585	0.005585	21.871800	1.94E-005	***
sex	1	0.000040	0.000040	0.157700	0.692900	
age:sex	1	0.000026	0.000026	0.099900	0.753200	
Residuals	55	0.014044	0.000255			

Table B.20: ANCOVA results measuring dimorphism between female and male CCSV scores from brain GM analysis corresponding to infant-child to juvenile group. See Figure 6.20.

Response: RegrAxis pcs cortex infant-child to juvenile group

	Df	**Sum Sq**	**Mean Sq**	**F value**	**Pr(>F)**	
age	1	0.007290	0.007290	35.910400	9.14E-008	***
sex	1	0.000008	0.000008	0.040800	0.840600	
age:sex	1	0.000066	0.000066	0.323400	0.571400	
Residuals	67	0.013601	0.000203			

Table B.21: ANCOVA results measuring dimorphism between female and male CCSV scores from brain GM analysis corresponding to juvenile to adolescent group. See Figure 6.22.

Response: RegrAxis pcs cortex juvenile to adolescent group

	Df	**Sum Sq**	**Mean Sq**	**F value**	**Pr(>F)**	
age	1	0.029154	0.029154	146.598300	$<$ 2.00E-016	***
sex	1	0.000000	0.000000	0.000600	0.980200	
age:sex	1	0.000016	0.000016	0.081800	0.775300	
Residuals	139	0.027643	0.000199			

Table B.22: ANCOVA results measuring dimorphism between female and male CCSV scores from brain GM analysis corresponding to adolescent to adult group. See Figure 6.24.

Response: RegrAxis pcs cortex adolescent to adult group

	Df	**Sum Sq**	**Mean Sq**	**F value**	**Pr(>F)**	
age	1	0.041397	0.041397	286.487200	< 2.00E-016	***
sex	1	0.000615	0.000615	4.256800	0.040580	*
age:sex	1	0.000000	0.000000	0.000600	0.979820	
Residuals	174	0.025143	0.000144			

Table B.23: ANCOVA results measuring dimorphism between female and male Procrustes distance between each asymmetric vault configuration and its mirror image. See Figure 6.26.

Response: endoAsymProcrustDist

	Df	**Sum Sq**	**Mean Sq**	**F value**	**Pr(>F)**
age	1	0.000221	0.000221	1.337100	0.249400
sex	1	0.000003	0.000003	0.018200	0.892800
age:sex	1	0.000045	0.000045	0.272400	0.602500
Residuals	150	0.024804	0.000165		

Table B.24: ANCOVA results measuring dimorphism between female and male Procrustes distance between each asymmetric cortex configuration and its mirror image. See Figure 6.27.

Response: brainAsymProcrustDist

	Df	**Sum Sq**	**Mean Sq**	**F value**	**Pr(>F)**	
age	1	0.000582	0.000582	2.886700	0.090570	.
sex	1	0.000000	0.000000	0.001900	0.965090	
age:sex	1	0.000000	0.000000	0.000039	0.994990	
Residuals	248	0.049964	0.000201			

Table B.25: ANCOVA results measuring dimorphism between female and male CCASV scores from endocranial corresponding to infant-child to juvenile group. See Figure 6.28.

Response: CCASV endocranial vault infant-child to juvenile group

	Df	**Sum Sq**	**Mean Sq**	**F value**	**Pr(>F)**	
age	1	0.000679	0.000679	3.973300	0.054550	.
sex	1	0.000029	0.000029	0.167500	0.685000	
age:sex	1	0.000143	0.000143	0.834000	0.367750	
Residuals	33	0.005641	0.000171			

Table B.26: ANCOVA results measuring dimorphism between female and male CCASV scores from brain corresponding to infant-child to juvenile group. See Figure 6.30.

Response: Brain CCASV infant-child to juvenile group

	Df	**Sum Sq**	**Mean Sq**	**F value**	**Pr(>F)**	
age	1	0.007575	0.007575	24.225400	5.87E-006	***
sex	1	0.000029	0.000029	0.091100	0.763700	
age:sex	1	0.000655	0.000655	2.095000	0.152400	
Residuals	67	0.020949	0.000313			

Table B.27: ANCOVA results measuring dimorphism between female and male CCASV scores from brain corresponding to juvenile to adolescent group. See Figure 6.32.

Response: Brain CCASV juvenile to adolescent group

	Df	**Sum Sq**	**Mean Sq**	**F value**	**Pr(>F)**	
age	1	0.009956	0.009956	37.957000	7.35E-009	***
sex	1	0.000091	0.000091	0.347700	0.556400	
age:sex	1	0.000000	0.000000	0.000500	0.982000	
Residuals	139	0.036460	0.000262			

Table B.28: ANCOVA results measuring dimorphism between female and male CCASV scores from brain corresponding to adolescent to adult group. See Figure 6.34.

Response: Brain CCASV adolescent to adult group

	Df	**Sum Sq**	**Mean Sq**	**F value**	**Pr(>F)**	
age	1	0.016295	0.016295	57.186000	2.19E-012	***
sex	1	0.000060	0.000060	0.210700	0.646800	
age:sex	1	0.000662	0.000662	2.323500	0.129300	
Residuals	174	0.049582	0.000285			

Appendix C

Heterochronic processes

Heterochronies are defined as changes in the rate, time of onset and offset, and duration of developmental processes. They provide a fertile theoretic framework to study differences in ontogeny between closely related species, and also between groups of the same species (Gould, 1977; Alberch et al., 1979; Klingenberg, 1998; Gould, 2000; Ramirez-Rozzi et al., 2005; Sardi, 2010). In this thesis two models were used to quantify and define these processes: Gould's clock model (Gould, 1977), and Alberch's formalism (Alberch et al., 1979). The two models will be presented first in their original version, and then, the fusion of both will be explained. Through this fusion they acquire a broader explanatory capacity, further defining the heterochronic processes included originally in both models.

Gould's clock model

Gould's clock model (Gould, 1977) is based on the comparison of three variables (age, size and shape) on a determined period of time during ontogeny between two related species (and, as mentioned earlier, it could also be used to compare two defined groups of the same species). These variables are plotted on a semicircular clock with two hands, which represent size and shape, and a bar that represents age (Figure C.1). Also, they

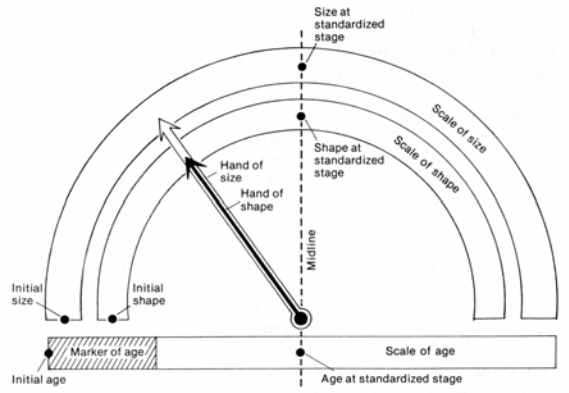

Figure C.1: **Clock model.** Framework for clock model of heterochrony, showing scales of size, shape, and age.

are standardized so that the clock middle is scaled to the ancestor variables and the clock hands quantify descendant size and shape obtained at the final developmental stage analysed; the bar show the age at which the descendant arrives to this stage in relation to the ancestor (which is represented in the middle of the bar).

Using this clock Gould defined different heterochronic processes in their "pure" form depending on the relationships between the three variables (shape, size and age). Four basic types of heterochrony emerge on the clock model (Gould, 1977):

(i) Paedomorphosis by progenesis (also called "temporal hipomorphosis" by Shea (1983)): Descendant ontogeny is simply truncated by the early attainment of sexual maturity (Figure C.2). In somatic development, the descendant is both smaller and paedomorphic, in other words, it is a sexually mature juvenile. The correlation of size and shape is unchanged.

(ii) Paedomorphosis by neoteny: In this case, the vector of shape is retarded while size and developmental stage remain unchanged from the ancestral condition (Figure C.3).

(iii) Peramorphosis by hypermorphosis (also called "temporal hypermorphosis" by Shea (1983)): The correlation between size and shape is unchanged from the ancestral

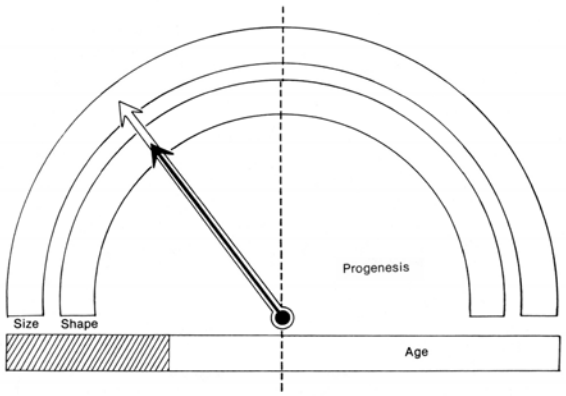

Figure C.2: **Clock model - Progenesis.** Progenesis by truncation of ontogeny with early sexual maturation.

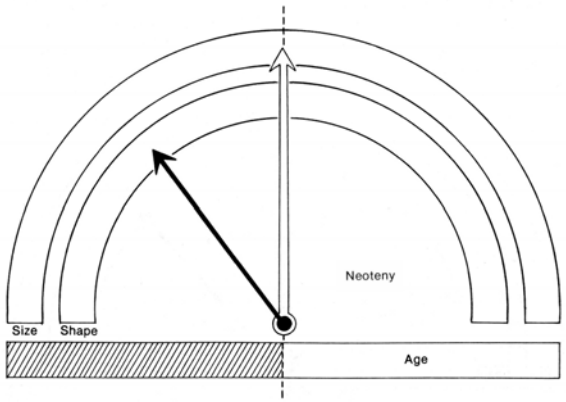

Figure C.3: **Clock model - Neoteny.** Neoteny by retardation in somatic development.

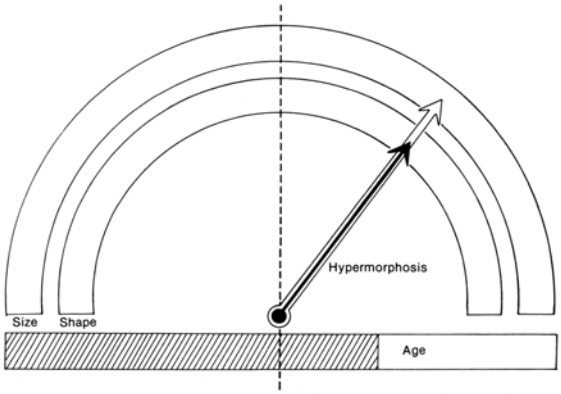

Figure C.4: **Clock model - Hypermorphosis.** Hypermorphosis by delay in maturation and simple extension of growth.

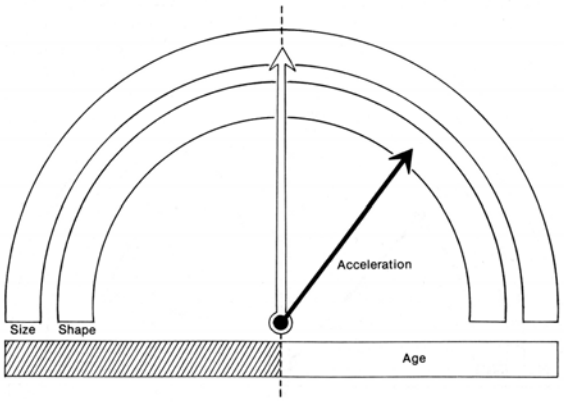

Figure C.5: **Clock model - Acceleration.** Acceleration by speeding up of somatic development.

condition (Figure C.4). Ontogeny is simply prolonged because maturation is delayed. The age marker shows that the selected developmental stage occurs at a later age in descendants.

(iv) Peramorphosis by acceleration: At the selected developmental stage, the descendant presents the same age and size than its ancestor. But the vector of shape has been dissociated and "accelerated//speeded up" (Figure C.5).

Although not considered as heterochronic processes, a "pure" alteration of size would produce the following two processes:

(v) Isomorphosis by proportioned dwarfism: A retardation in the rate of size increase

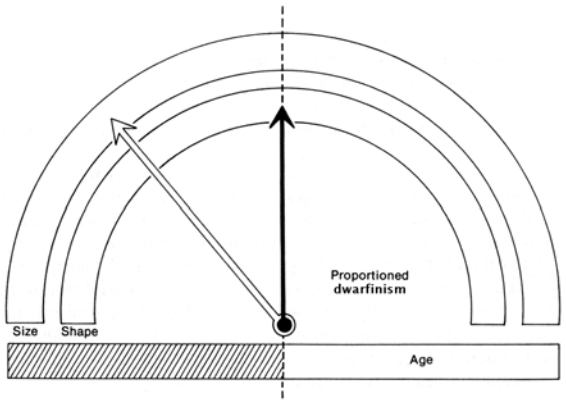

Figure C.6: **Clock model - Proportioned dwarfism.** Pproportioned dwarfism by slower growth with constant rate of development.

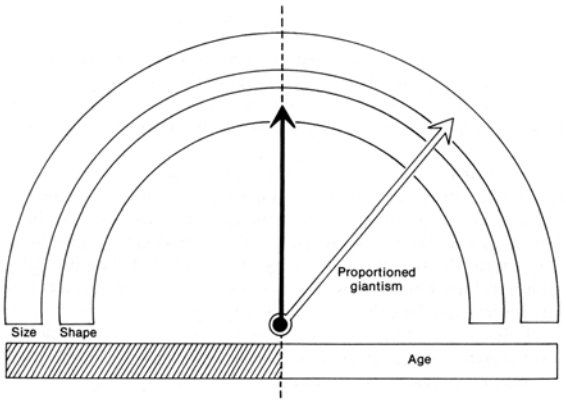

Figure C.7: **Clock model - Proportioned giantism.** Proportioned giantism by more rapid growth.

produces a dwarfed form geometrically similar to its ancestor (Figure C.6).

(vi) Isomorphosis by proportioned giantism: If the rate of size increase is accelerated, a proportioned giant evolves (Figure C.7).

Alberch's formalism

Alberch et al. (1979) proposed another framework to quantify and catalog heterochronies. This new approach used two variables (shape and age) from the ancestor and descendant, which were measured at the onset (alpha) and the offset (beta) of the developmental stage or ontogenetic period that was being compared. In this way, the developmental rate

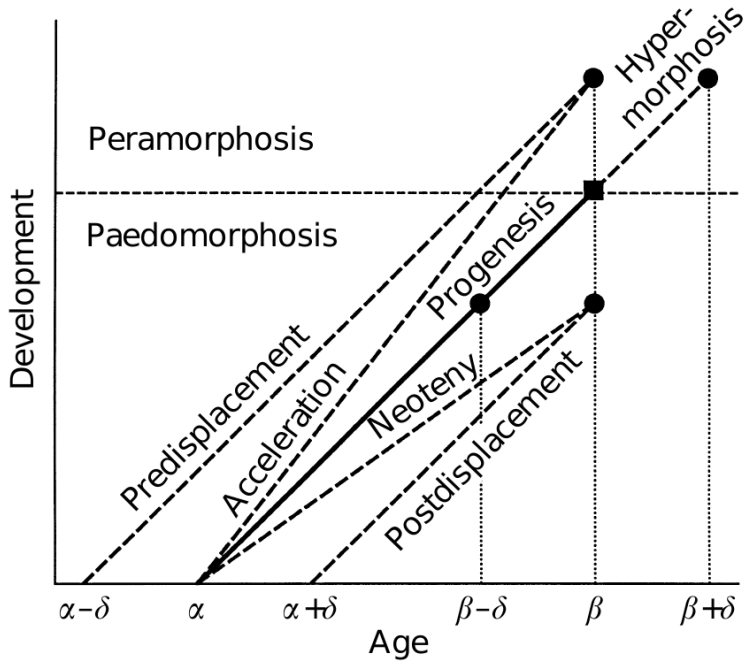

Figure C.8: **Formalism - Heterocrhonic processes.** Alberch's formalism (Alberch et al., 1979). A variable that measures shape (development) is plotted on the vertical axis. The solid line represents the growth trajectory of the ancestor, and the square its morphology when growth has ended. Dashed lines and circles correspond to descendants. α, time of onset; β, time of offset; δ, time displacement of onset or offset. Figure 4 from Klingenberg (1998).

(k) during the ontogenetic period analysed could be quantified. Therefore, the temporal shifts that can occur during ontogeny were recognized, and two new "pure" heterochronic processes were defined (Figure C.8):

(vii) Peramorphosis by predisplacement: This process occurs when the developmental process starts in the descendant on a previous stage (or age) in relation to the ancestor, conserving the same rate and offset time. Therefore, the descendant reaches a more developed shape at the offset time.

(viii) Paedomorphosis by postdisplacement: This process is defined by the late onset of the developmental signal in the descendant in relation to the ancestor. This results in a less developed shape at the offset time.

Merging complementary heterochronic models

Although both models are complementary, the distinction between shape and size was not clearly made when the formalism framework was established. Hence, heterochronic processes were defined from a not very clear developmental variable (Figure C.8) and it was not explained what exactly happen with size during these processes. Although it was mentioned that the formalism could be used for development and growth changes, only developmental graphs were presented in the original article. For this reason, it is important to improve these definitions by unambiguously establishing which curve follows shape (development) and size (growth) during the "pure" heterochronic processes. This can be done by plotting both a shape and a size variable and defining their onset and offset timings (Figures C.9, C.10, C.11, C.12, C.13, C.14, C.15, and C.16).

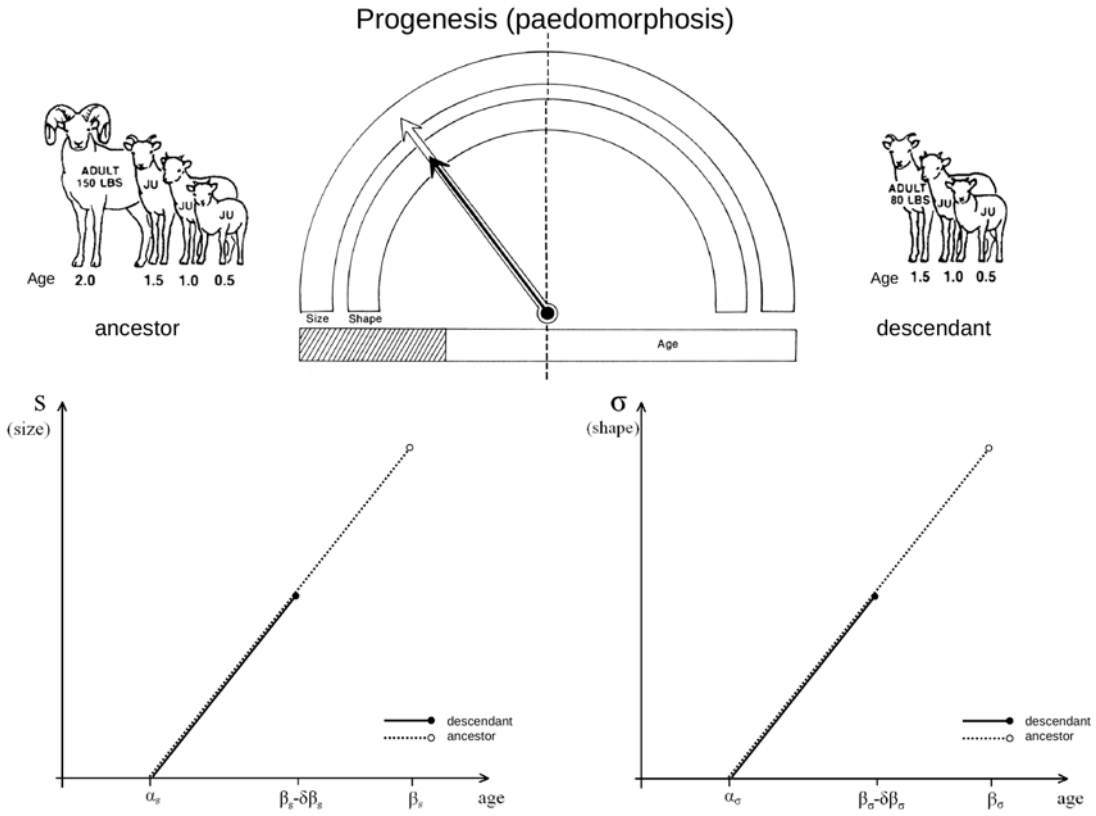

Figure C.9: **Clock model and formalism for progenesis.** Left to the clock, an example of ancestor; right to the clock, the hypothetic descendant. Two plots are done for the formalism, detailing shape and size curves. The ancestor is represented by dashed lines, and the descendant by solid lines. α, time of onset; β, time of offset; δ, time displacement of onset or offset. Bighorn sheep drawings from Figure 2 from Vrba (1996).

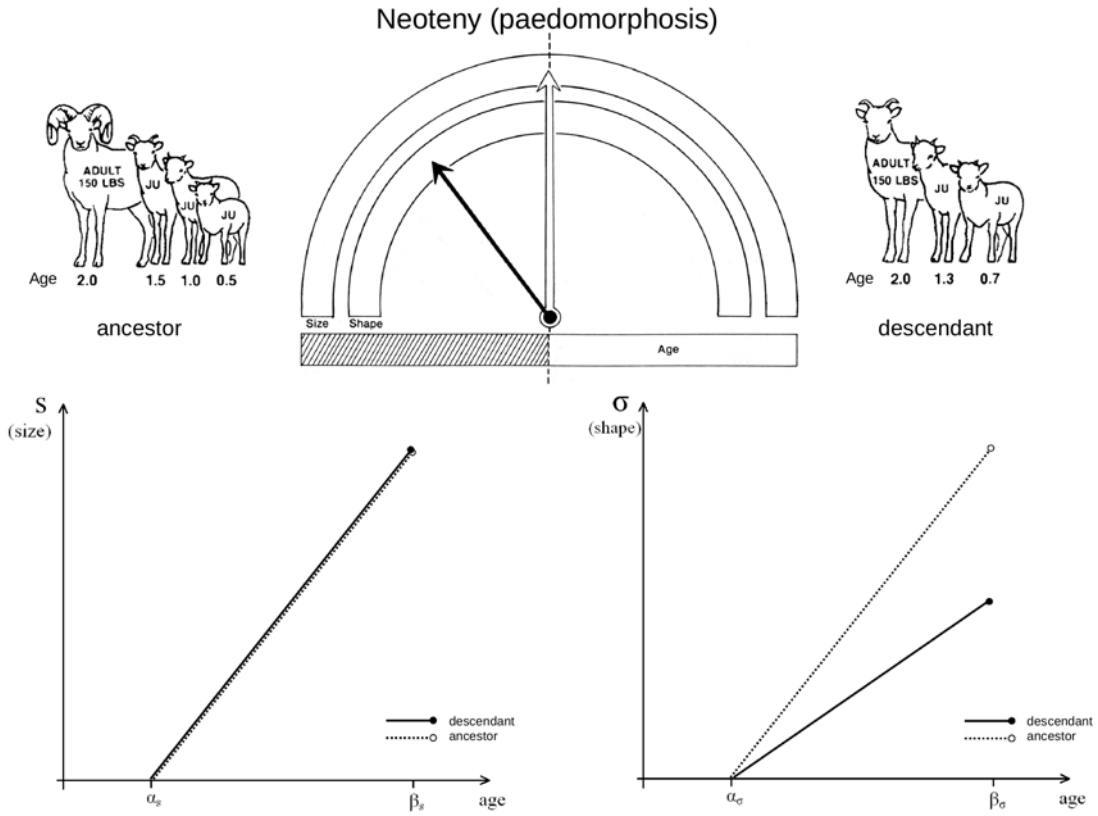

Figure C.10: **Clock model and formalism for neoteny.** Left to the clock, an example of ancestor; right to the clock the hypothetic descendant. Two plots are done for the formalism, detailing shape and size curves. The ancestor is represented by dashed lines, and the descendant by solid lines. α, time of onset; β, time of offset; δ, time displacement of onset or offset. Bighorn sheep drawings from Figure 2 from Vrba (1996).

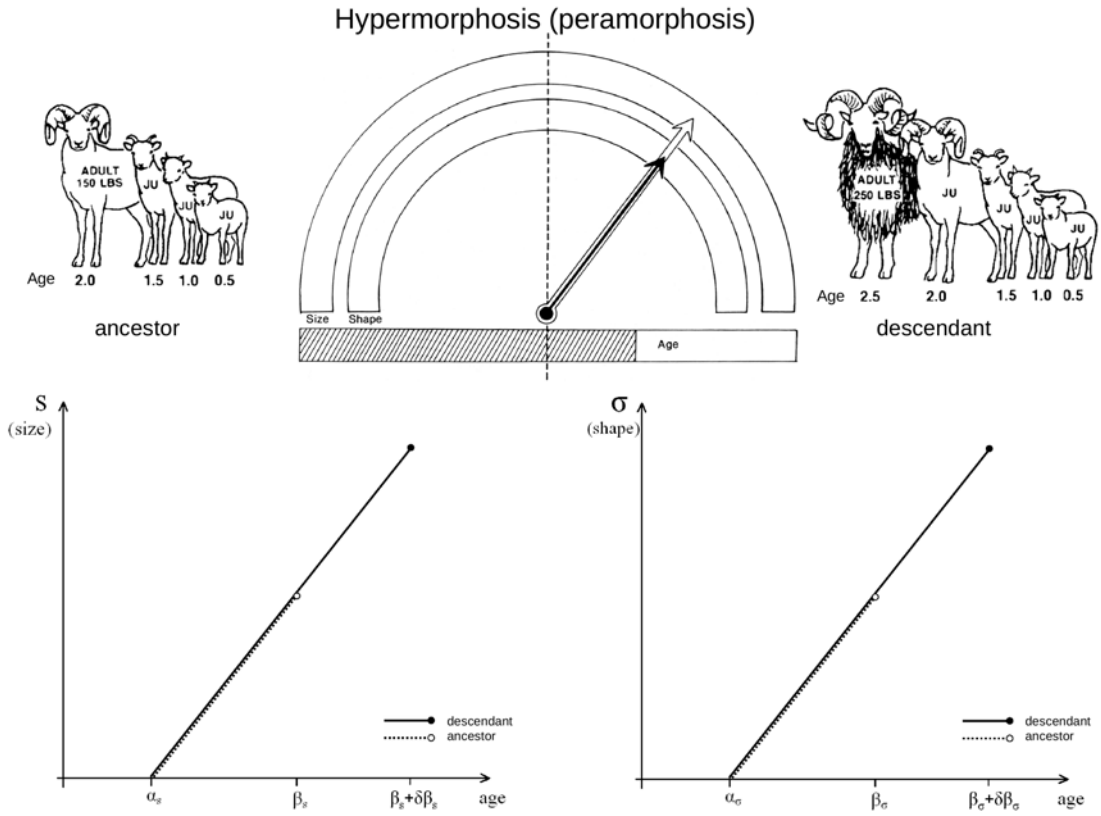

Figure C.11: **Clock model and formalism for hypermorphosis.** Left to the clock, an example of ancestor; right to the clock the hypothetic descendant. Two plots are done for the formalism, detailing shape and size curves. The ancestor is represented by dashed lines, and the descendant by solid lines. α, time of onset; β, time of offset; δ, time displacement of onset or offset. Bighorn sheep drawings from Figure 2 from Vrba (1996).

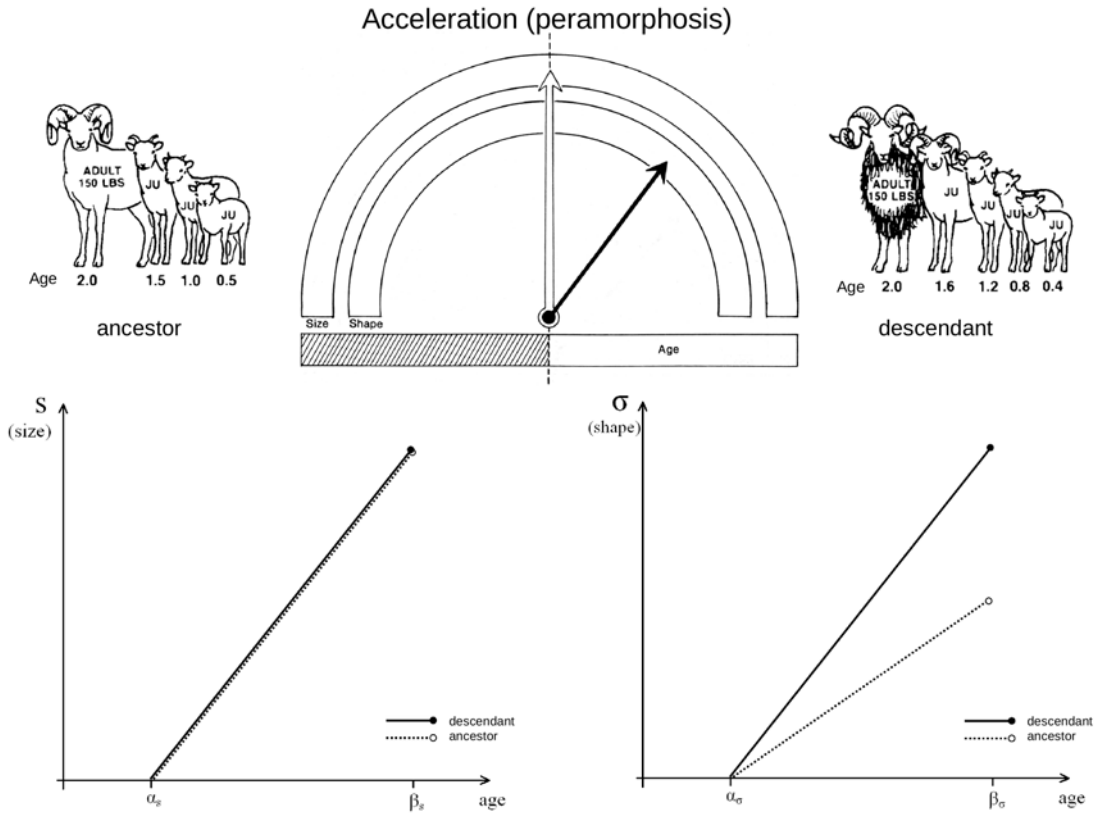

Figure C.12: **Clock model and formalism for acceleration.** Left to the clock, an example of ancestor; right to the clock the hypothetic descendant. Two plots are done for the formalism, detailing shape and size curves. The ancestor is represented by dashed lines, and the descendant by solid lines. α, time of onset; β, time of offset; δ, time displacement of onset or offset. Bighorn sheep drawings from Figure 2 from Vrba (1996).

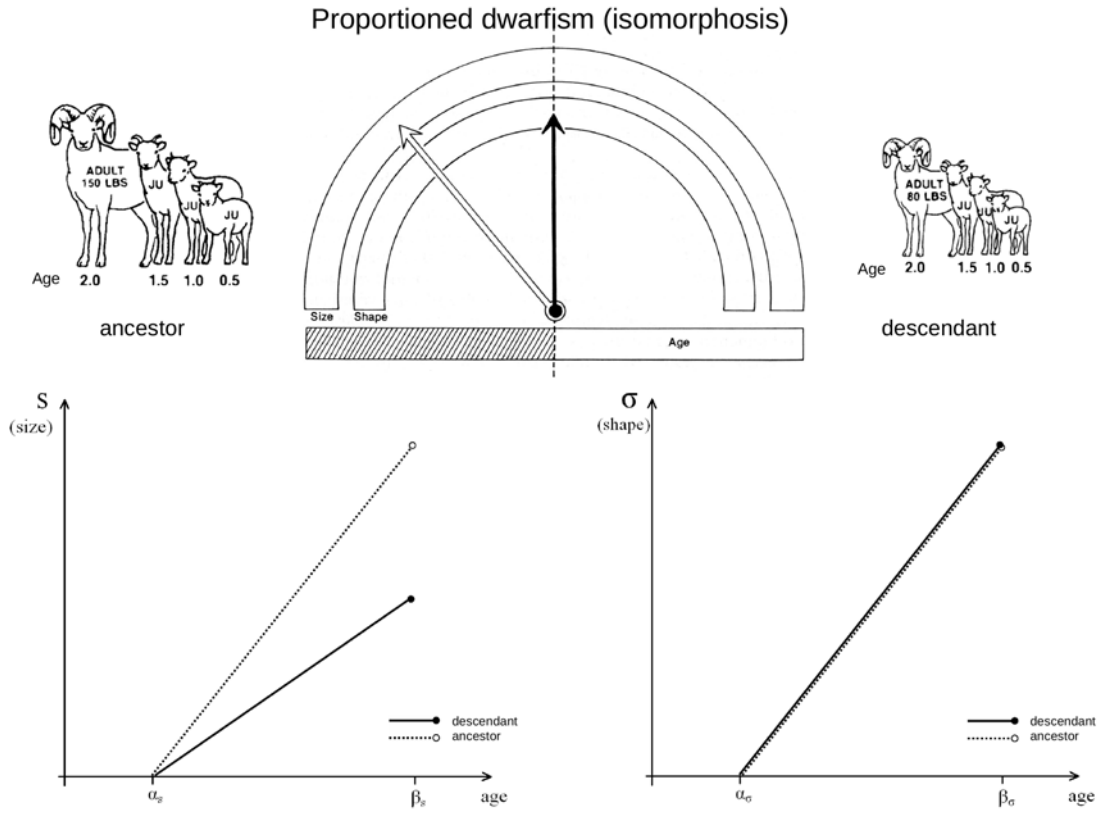

Figure C.13: **Clock model and formalism for proportioned dwarfism.** Left to the clock, an example of ancestor; right to the clock the hypothetic descendant. Two plots are done for the formalism, detailing shape and size curves. The ancestor is represented by dashed lines, and the descendant by solid lines. α, time of onset; β, time of offset; δ, time displacement of onset or offset. Bighorn sheep drawings from Figure 2 from Vrba (1996).

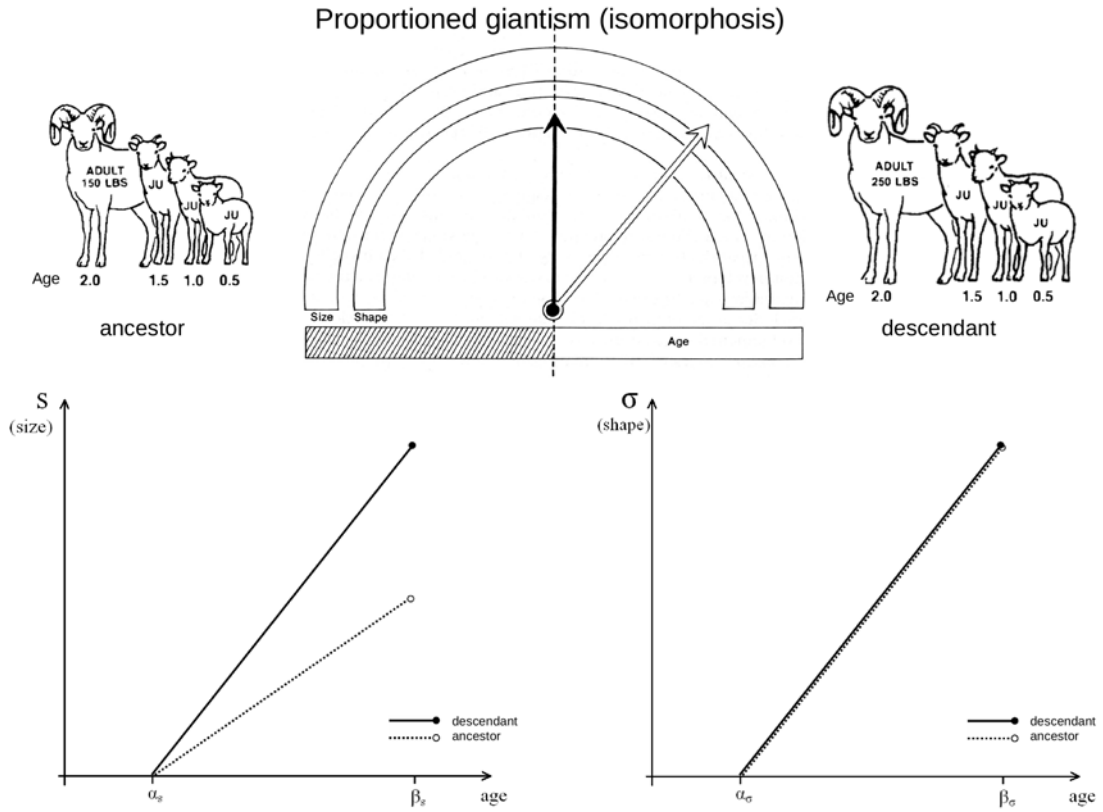

Figure C.14: **Clock model and formalism for proportioned giantism.** Left to the clock, an example of ancestor; right to the clock the hypothetic descendant. Two plots are done for the formalism, detailing shape and size curves. The ancestor is represented by dashed lines, and the descendant by solid lines. α, time of onset; β, time of offset; δ, time displacement of onset or offset. Bighorn sheep drawings from Figure 2 from Vrba (1996).

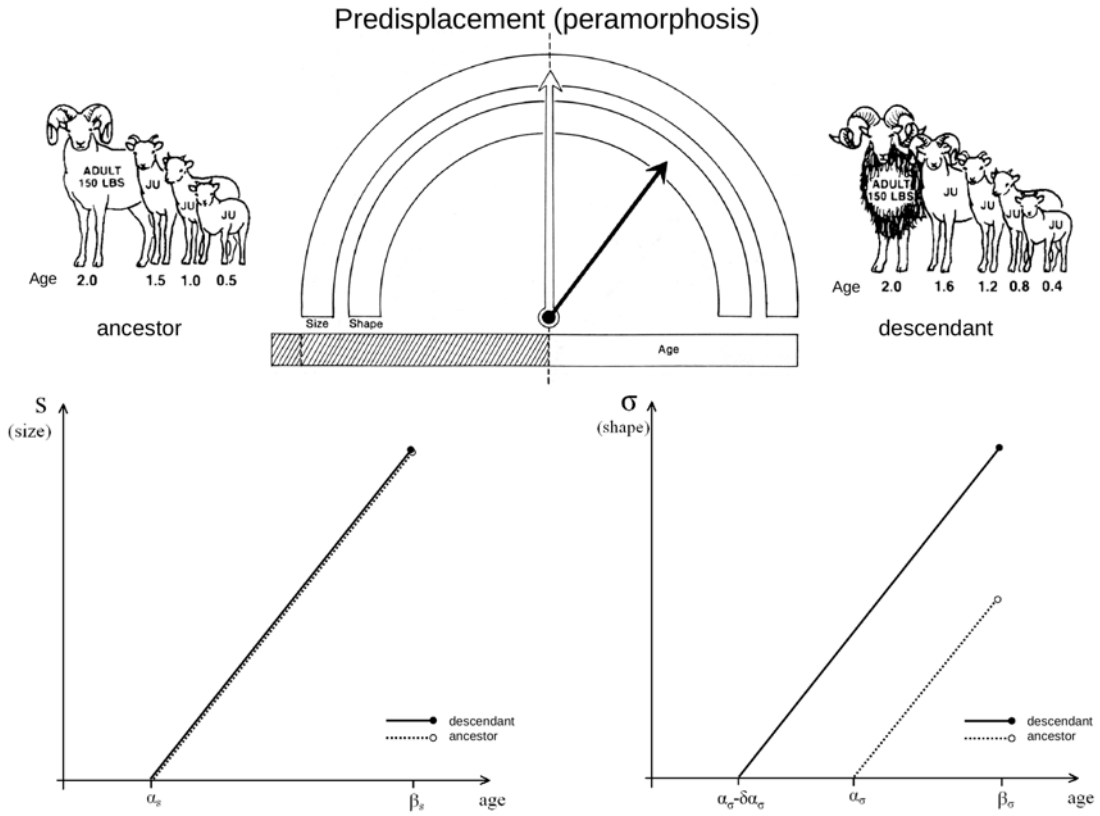

Figure C.15: **Clock model and formalism for predisplacement.** Left to the clock, an example of ancestor; right to the clock the hypothetic descendant. Two plots are done for the formalism, detailing shape and size curves. The ancestor is represented by dashed lines, and the descendant by solid lines. α, time of onset; β, time of offset; δ, time displacement of onset or offset. Bighorn sheep drawings from Figure 2 from Vrba (1996).

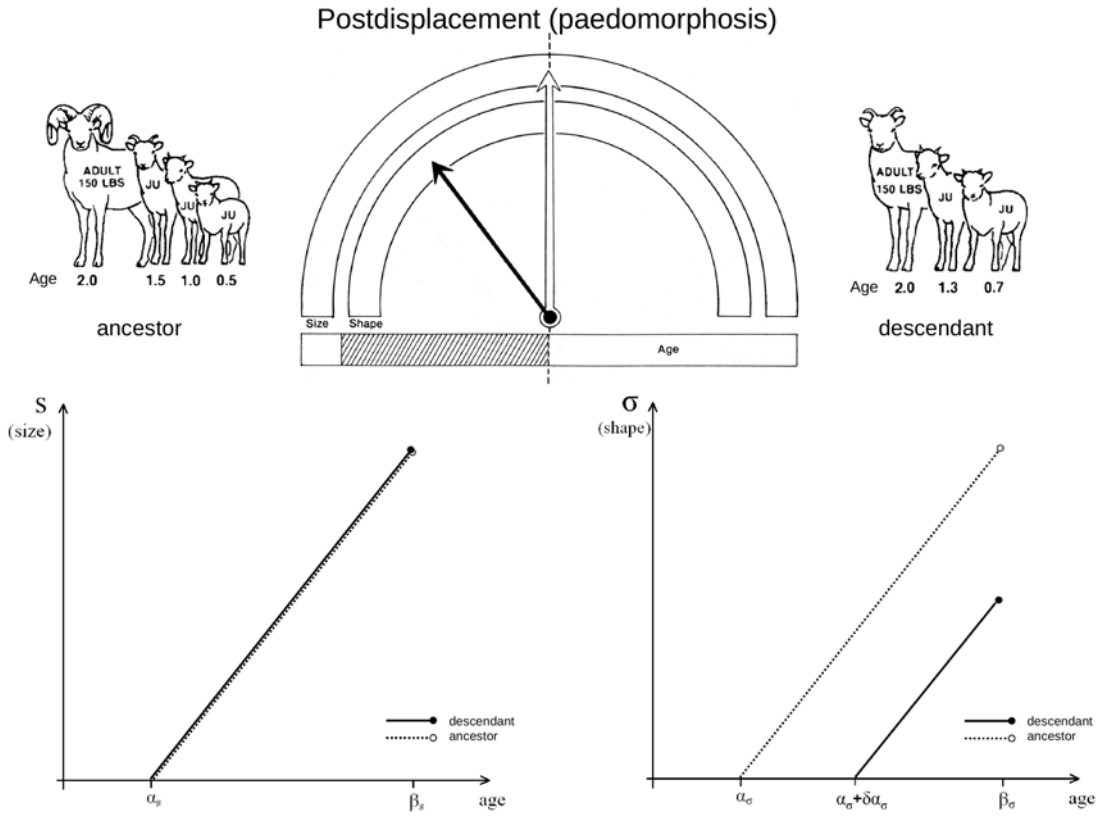

Figure C.16: **Clock model and formalism for postdisplacement.** Left to the clock, an example of ancestor; right to the clock the hypothetic descendant. Two plots are done for the formalism, detailing shape and size curves. The ancestor is represented by dashed lines, and the descendant by solid lines. α, time of onset; β, time of offset; δ, time displacement of onset or offset. Bighorn sheep drawings from Figure 2 from Vrba (1996).